Systems analysis of INTOR-like designs based on a simplified rescaling method

Albert F. Knobloch

IPP 4/235 April 1988

MAX-PLANCK-INSTITUT FÜR PLASMAPHYSIK

8046 GARCHING BEI MÜNCHEN

MAX-PLANCK-INSTITUT FÜR PLASMAPHYSIK

GARCHING BEI MÜNCHEN

Systems analysis of INTOR-like designs based on a simplified rescaling method

Albert F. Knobloch

IPP 4/235 April 1988

Die nachstehende Arbeit wurde im Rahmen des Vertrages zwischen dem Max-Planck-Institut für Plasmaphysik und der Europäischen Atomgemeinschaft über die Zusammenarbeit auf dem Gebiete der Plasmaphysik durchgeführt.

Abstract

On the basis of a simplified non-optimizing rescaling method the INTOR-like next-step tokamak reactor designs, NET-DN, FER, TIBER II and OTR (as of March 1987), are analysed and compared with each other and with INTOR, as of Phase Two A Part 2, on a common basis in order to understand their characteristic differences deriving from the respective input assumptions. Always on the basis of a certain confinement scaling, this is done with different approaches. It is generally seen that the physics input assumptions and their respective combination play a major role, with the maximum toroidal field and the central solenoid radius also being influential. Depending on the set of physics/engineering input assumptions in combination with the set of design parameters required, a certain domain in multiparameter space becomes accessible from which a choice could be made (e.g. to optimize cost for a certain fusion power). The results referring to typical INTOR assumptions and requirements were also contributed to the INTOR Phase Two A Part 3 workshop. An outlook is added on what a next-step parameter set could look like on the basis of modified physics input assumptions as adopted towards the end of the INTOR studies and no longer taken into account by them.

IPP 4/235

Systems analysis of INTOR-like designs based on a simplified rescaling method.

A. F. Knobloch

April 1988

Contents

		page
1.	Introduction	1
2.	Major features and parameters	1
3.	Description of systems analysis process	1
4.	Representation of INTOR-like designs	3
5.	Sensitivity analysis	5
5.1	Design guidelines	7
5.2	Individual sensitivities	7
5.3	Global sensitivities	17
5.3.1	Global substitution analysis	17
5.3.2	Transition study	26
5.3.3	Sensitivity study of combined input parameter changes	51
5.3.4	Overall comparison of INTOR-like design points and outlook on the impact of changing the input assumptions	64
6.	Direct capital cost comparison	73
7.	Summary and conclusions	74
8.	Acknowledgements	75
	References	76
Annex I	Simplified rescaling procedure for establishing possible next-step Tokamak reactor design parameters	77
	1. Physics part of simplified rescaling	77
	2. Engineering part of simplified rescaling	83
	3. Some relations for comparing existing design parameter sets and for determining essential next-step design parameters from given input	86
Appendix I	Reduction of the confinement scaling equation	91
Appendix II	Ignition margins calculated according to different scalgs.	93
Appendix III	List of symbols	95
Appendix IV	Evaluation of some engineering design constraints	96
Appendix V	List of the values calculated (examples)	97

1. Introduction

In parallel with evaluations based on elaborate, detailed codes that incorporate optimization routines, a number of studies have been conducted on the basis of simplified systems of equations representing present understanding of tokamak design physics and engineering dependences. These studies are based on existing INTOR and national designs as characterized in Section 2. Also described is an INTOR-like case "S" as used for sensitivity analysis.

The simplified non-optimizing rescaling approach treats only the most essential input and design parameters and is briefly described in Section 3. Its ability to represent the designs characterized in Section 2 is demonstrated in Section 4. This inspires confidence that design variations about these design points can be carried out with good approximation.

Section 5 describes a number of studies aimed at showing the impact of individual and multiple input parameter changes without optimizing adjustment of other parameters and gives the observations made in these systems analysis studies. Consideration is also given to an overall comparison of INTOR-like design points and to the outlook for alternatives.

Section 6 gives the direct capital cost comparison.
Section 7 gives the summary and conclusions.
This report is an augmented version of contributions made to the INTOR workshop in Phase IIA Part 3.

2. Major features and parameters

Table 2.1 summarizes some characteristic features and parameters of INTOR, as of Phase IIA Part 2, and of the four national designs as well as of one INTOR-like design, "S", that was used for sensitivity studies.

3. Description of systems analysis process

The simplified non-optimizing rescaling approach uses relative quantities throughout, with INTOR as of Phase IIA Part 1 as the reference case. The

Table 2-1 Major features and parameters

	INTOR IIA-2	NET-DN	FER	TIBER II	OTR	"S"
Ignited or Q	ignited	ignited	Q >20	Q >5	Q >5	ignited
Current drive	inductive	inductive	hybrid	non-inductive	inductive	inductive
Major radius (m)	5.00	5.18	4.42	3.00	6.30	5.09
Minor radius (m)	1.20	1.35	1.25	0.83	1.50	1.21
Elongation	∿1.6	∿2.0	∿1.7	2.4	∿1.5	2.08
Tor. field (axis) (T)	5.5	5.0	4.6	5.6	5.8	5.5
Plasma current (MA)	8.0	10.8	8.7	10.0	8.0	10.1
Fusion power (MW)	620	648	407	314	500	660

plasma is described by average quantities and the usual relations for total and fuel beta, safety factor (current-q), Murakami density limit, and ignition margin during burn with different possible confinement scaling laws. The latter are expressed in power product form. The plasma power balance does not include radiation. Profile effects can be taken into account. The engineering components are included to the extent essential for determining the major plasma radius. Hence, the central solenoid radius, the toroidal field magnet and the inner blanket/shield thickness are represented by characteristic geometry factors and simplified scaling functions that ensure consistent variation of the magnet dimensions while keeping the average stresses and current densities - which are checked afterwards - approximately constant. On the basis of a certain maximum toroidal field consistently scaled design points are found by iteration using the respective input data. Since no optimization and no constraints are involved and since some intrinsic decoupling between the physics and the engineering parts of the parameters exists, the method can be used to study the impact of individual or combined input parameter changes over a relatively wide range. From that range those cases may be selected that correspond to certain constraints. Since the computing procedure is very short, a large number of cases may be run for selection according to various rules. Coupled to the short computer program applying the simplified rescaling method is an equally simple costing program, which was previously used to generate the EC INTOR cost figures in Phase IIA Part 1. For a more detailed description see /1/ and Annex I.

4. Representation of INTOR-like designs

The rescaling method was used to recalculate INTOR IIA-2 /2/ and the four national designs, NET-DN, FER, TIBER II, and OTR /3/, on the basis of the input data listed in Table 4-1. For comparison, the data for the design point "S" (used later on for sensitivity studies) are also shown, as also are the physics guidelines for INTOR (as of December 1986). The latter indicate that, in comparison with INTOR as of Phase IIA Part 2, some of the recommended input parameters have since changed. The INTOR-like design point "S" attempts to comply with more recent guidelines.

Table 4-1

Input assumptions for mutual comparison of 5 next-step designs and "S"

	INTOR IIA-2	NET-DN	FER	TIBER II	OTR	"S"	+Guidelines Dec. 1986
Physics							
g/g_o	0.700	0.606	0.606	0.479	0.603	0.550	0.606
q/q_o	0.848	1.020	0.874	1.037	1.014	1.000	1.000
k/k_o	1.000	1.281	1.063	1.500	0.938	1.300	1 - 1.375
C_f	1.000	0.923	1.249	1.328	0.859	0.897	0.897
C	1.143	1.024	1.110	0.888	1.154	1.130	1.130
C_n	1.000	1.000	0.915	1.023	0.923	0.923	0.923
$C_p = C'_p$	0.847	0.910	0.832	0.877	0.917	0.900	
M_{iAX}	2.768	2.904	2.354	2.142	2.395	3.234	> 2.5
m_i	1.143	1.200	0.972	0.885	0.989	1.336	
$\int \mathcal{S}$	1.394	1.533	1.013	0.976	1.187	1.627	
$\mathcal{S}$	1.000	1.000	1.200	1.940	0.800	1.000	1 - 2
m	1.115	1.000	0.674	0.327	1.040	0.957	0.855
Engineering							
F_1	0.403	0.337	0.304	0.272	0.476	0.380	
F_2	0.241	0.255	0.236	0.137	0.269	0.240	
F_3	0.264	0.258	0.262	0.251	0.272	0.250	
F_4	0.062	0.036	0.079	0.039	0.090	0.060	
B_{max}/B_{maxo}	0.991	0.997	0.909	1.019	0.983	0.950	

+ see EURFUBRU/XII-52/86/EDV24 Brussels/Vienna December 1986

For all five designs that were recalculated, the ignition margin based on ASDEX H-mode scaling was evaluated as part of the physics input parameters. (Alternatively, each individual parameter set could have been treated with the ignition margin based on its respective assumed confinement scaling.) The differences observed in the input assumptions reveal differences in the degree of extrapolation from existing physics results, differences in the operating mode (see FER and TIBER II) as well as differences in the predicted advancement of engineering (see TIBER II). The maximum toroidal field (taken here at the innermost toroidal field coil circumference) is naturally a powerful tool for optimizing for a given figure of merit (e.g. minimum cost) or adjusting to certain desired operating parameters.

Table 4-2 lists the results (first column) of the recalculation together with the original data. It is seen that the limited set of essential design parameters covered in this study is represented quite well with some minor adjustments in C_f, C_p, g/g_o and m as indicated. All other input parameters have been taken as originally given. Appendix V gives a complete list of the values calculated.

The fact that the five designs can be rather well represented lends confidence for further application of the method in sensitivity analysis.

5. Sensitivity analysis

Four different studies on the sensitivity of INTOR-like designs to input parameter changes are carried out. The impact of individual input parameter changes is expressed in the form of relative sensitivities, whereas global sensitivities to multiple input parameter changes are shown in three different ways: the first method is global substitution analysis, where the entire physics and the entire engineering input parameter sets are exchanged between several existing designs; the second uses a stepwise transition between two designs, in which first the individual physics input parameters are consecutively changed and then the individual engineering parameters; the third method consists in varying several input parameters in such a way that certain constraints on the resulting design parameters remain fulfilled. In this way a typical design parameter range

Table 4-2 Recalculation of next-step reactor design parameters
Results of recalculation and comparison with original data sets (2nd row)

Name	INTOR IIA-2	NET-DN	FER	TIBER II	OTR
g/g_o	o.7oo/o.693	o.6o6/o.6o6	o.6o6/o.6o6	o.479/o.519	o.6o3/o.6o6
q/q_o	o.848/o.848	1.o2o/1.o2o	o.874/o.874	1.o37/1.o37	1.o14/1.o14
k/k_o	1.ooo/1.ooo	1.281/1.281	1.o63/1.o63	1.5oo/1.5oo	o.938/o.938
C_f	1.ooo/1.ooo	o.923/o.923	1.249/1.249	1.328/1.328	o.859/o.897
C	1.143/1.143	1.o24/1.o24	1.11o/1.11o	o.888/o.888	1.154/1.154
C_n	1.ooo/1.ooo	1.ooo/1.ooo	o.915/o.915	1.o23/1.o23	o.923/o.923
C_p	o.847/1.ooo	o.91o/O.910	o.832/o.832	o.877/o.877	o.917/o.917
M_{iAX}	2.768	2.9o4	2.354	2.142	2.395
M_{iMV}	1.3o4	1.678	1.348	1.422	1.o83
M_{iKG}	o.984	1.o27	o.853	o.925	o.893
M_{iG} (f_H = 2.2)	o.823	o.914	o.776	o.834	o.819
$\mathcal{S}$	1.ooo/1.ooo	1.ooo/1.ooo	1.2oo/1.2oo	1.94o/1.94o	o.8oo/o.8oo
m	1.115/o.943	1.ooo/o.998	o.674/o.67o	o.327/o.326	1.o4o/1.o4o
ρ	o.943/o.943	o.977/o.977	O.834/o.834	O.566/o.566	1.189/1.189
a/a_o	1.ooo/1.ooo	1.124/1.125	1.o42/1.o42	o.691/o.692	1.25o/1.25o
A/A_o	o.943/o.943	o.87o/o.868	o.8oo/o.8oo	o.819/o.818	o.951/o.951
I/I_o	1.251/1.25o	1.684/1.688	1.367/1.366	1.56o/1.563	1.249/1.25o
B/B_o	1.oo1/1.ooo	o.91o/o.9o9	o.838/o.838	1.o1o/1.oo9	1.o55/1.o55
δ	1.o75/1.ooo	o.865/o.869	o.781/o.823	1.o6o/1.ooo	o.591/o.615
η	o.945/o.944	1.o46/1.o48	o.657/o.655	o.5o6/o.5o6	o.8o7/o.8o6
β/β_o	o.876/o.875	o.998/1.ooo	o.948/o.948	1.o7o/1.o71	o.571/o.571
$\beta DT/\beta DT_o$	1.oo1/1.ooo	1.o22/1.o24	1.o52/1.o51	o.951/o.951	o.659/o.659
$\beta pol/\beta pol_o$	o.56o/o.566	o.538/o.547	o.424/o.566	o.4o7/o.377	o.582/
$\beta-\beta_{DT}$ (%)	o.8oo/o.8oo	1.399/1.4oo	o.995/1.ooo	2.o97/2.1oo	o.496/o.5oo

can be identified which is based on a range of input parameter variations together with a certain range of constraints. Observations made in these studies are described.

5.1 Design guidelines

The sensitivity studies described below were carried out using the method described in Section 3. No optimization is involved.
Essential values that may encounter a limit are checked, such as average tensile stress, average current density in the TF coils and poloidal flux capability. Different confinement scalings are considered in order to identify their impact as well. For evaluation of single sensitivities the INTOR-like design point "S" is used (see Tables 4-1 and 5.3.1-1) with all its input parameters fixed except the one changed. Design point "S" is also used to study the global sensitivity to combined input parameter changes and the impact of imposing constraints on the design parameters.

For the substitution and transition analysis INTOR IIA-2 and the four national design points are used. They are characterized for that purpose as described in Section 4.

5.2 Individual sensitivities

The data of consistent design points resulting from single input parameter changes is used to evaluate relative sensitivities with "S" as the reference point. The range for single input parameter variations is chosen such that it covers the possible or likely variation according to guidelines and for inductive current drive around the respective value for "S". Thus, in general, two sensitivity values are shown, one for the lower limit and the other for the upper limit in input parameter variation. A total of eleven essential input parameters are varied individually, and the sensitivities are given for ten design parameters including cost. Tables 5-1 through 5-3 list the results for ASDEX H-mode scaling, Mirnov scaling and Kaye-Goldston scaling (enhancement factor 2, eq. 21a). Physics input parameters are the Troyon factor, the plasma elongation, the safety factor (current-q), the useful β-fraction (related to Z_{eff}), the power density profile factor and the performance parameter. Engineering input parameters are the maximum toroidal field at the innermost circumference of the

toroidal field coil bores and the geometry factors that determine (according to the respective plasma current and major radius) the central solenoid radius (mainly determined by F_1), the toroidal field coil thickness (mainly determined by F_4), the inner blanket/shield thickness (determined by F_2-F_4) and the inner horizontal wall radius (determined by $F_3 * a/a_o$).

Tables 5-1 through 5-3 show sensitivities in a rather large range (absolute values of up to 2.5 for ASDEX H-mode and Mirnov scalings, even larger for Kaye-Goldston scaling). The distribution of low and high, negative and positive sensitivities over the relationships between the impacted quantity and modified input is notably dependent on the confinement scaling used. A remarkable similarity is generally seen when the sensitivities for Mirnov scaling are compared with those for ASDEX H-mode scaling, apart from a number of single differences. For Mirnov scaling the impact of changes in the safety factor is lower, except for the impact on the wall loading. The impact of changes in maximum toroidal field on cost is also lower, the impact on fusion power is even of opposite sign, whereas the impact of changes in central solenoid radius on fusion power, wall load and cost is stronger. When the sensitivities obtained for Kaye-Goldston scaling (H-mode enhancement factor 2, $P = W_{th}/\tau_E$; see Appendix I) are compared with those for ASDEX H-mode scaling, much less similarity is seen. The impact of the Troyon factor, elongation, safety factor and useful beta fraction is for many cases much stronger or much weaker and sometimes of opposite sign. In a similar way, highly different sensitivities are seen for changes of maximum toroidal field and of the central solenoid radius. Taking the sums of the absolute sensitivities for columns and rows in Tables 5-1 through 5-3 helps to provide an overall view. From the vertical sums that refer to the input parameters one sees that single sensitivities are particularly strong for the physics input parameters and the maximum toroidal field, while the constituents of the radial build accumulate much less in sensitivity, with the exception of the central solenoid radius, whose impact appears about as strong as that of one of the physics input parameters. For Kaye-Goldston scaling the sensitivities to changes of elongation, safety factor and maximum toroidal field are particularly strong.

Table 5-1 Sensitivity of INTOR-like reactor parameter sets to single input parameter changes
(Reference point "S", constant performance parameter $\gamma\vartheta$, except for changing $\gamma\vartheta$, ASDEX H-mode scaling)

Input para.	g/g_o	k/k_o	q/q_o	C	C_f	$\gamma\vartheta$	$\frac{B_{max}}{B_{maxo}}$	T_{OH}/R_o	T_{TF}/R_o	T_{BS}/R_o	R_v/R_o	$\sum$ absol.sens.
lower lim.	0.500	1.000		0.850	0.850	1.464	0.900	0.297	0.151			
reference	0.550	1.300	1.000	1.130	0.897	1.627	0.950	0.342	0.186	0.180	0.252	
upper lim.	0.600	1.375	1.200	1.150	0.950	1.790	1.050	0.360	0.217	0.210	0.282	
η	0.581	-0.300		0.602	1.000	1.398	-0.244	0.112	0.026			4.676 + 0.702
	0.560	-0.300	0.795	0.568	1.000	1.461	-0.213	0.117	0.032	0.121	0.199	
ρ	-0.311	-0.864		-0.357	0.000	0.300	-0.740	0.330	0.077			2.236 + 1.879
	-0.274	-0.623	0.404	-0.288	0.000	0.283	-0.625	0.352	0.092	0.369	0.363	
δ	1.217	1.089		1.197	1.000	1.002	1.710	0.153	0.025			5.966 + 3.499
	1.238	0.983	-0.461	1.232	1.000	0.760	1.770	0.070	0.021	-0.510	-1.101	
I/I_o	-0.544	-0.555		-0.626	0.000	0.521	-0.841	-0.630	-0.130			2.523 + 1.712
	-0.475	-0.461	0.277	-0.501	0.000	0.495	-0.732	-0.527	-0.139	0.056	0.055	
A/A_o	0.079	0.765		0.084	0.000	-0.037	0.571	0.685	0.152			1.390 + 1.537
	0.075	0.786	-0.425	0.077	0.000	-0.071	0.562	0.663	0.174	0.065	0.064	
β/β_o	0.927	0.816		-0.086	0.000	0.081	-0.591	-0.752	-0.157			2.356 + 1.628
	0.920	0.828	-0.446	-0.078	0.000	0.073	-0.531	-0.639	-0.170	-0.064	-0.064	
M_{iAX}	0.000	0.000		1.000	1.000	1.000	0.000	0.000	0.000			3.000 + 0.000
	0.000	0.000	0.000	1.000	1.000	1.000	0.000	0.000	0.000	0.000	0.000	
M_{iKG}	-0.637	1.790		1.613	1.000	0.836	0.971	0.507	0.109			7.262 + 1.864
	-0.551	2.263	-1.386	1.803	1.000	0.821	0.961	0.457	0.122	-0.139	-0.138	
M_{iG}	-0.799	1.233		1.218	1.000	0.743	0.120	0.646	0.146			5.707 + 1.317
	-0.680	1.432	-0.714	1.266	1.000	0.726	0.128	0.641	0.169	0.204	0.201	
$\frac{cost}{cost_o}$	-0.436	-1.433		-0.546	0.212	0.809	-1.050	-0.001	0.008			4.177 + 1.765
	-0.350	-0.913	0.741	-0.379	0.214	0.820	-0.836	0.067	0.017	0.402	0.304	
$\sum$abs.sens.	5.531	8.845	5.649	7.329	5.212	6.727	6.838	3.816	0.830	1.930	2.489	55.196

Table 5-2 Sensitivity of INTOR-like reactor parameter sets to single input parameter changes

(Reference point "S", constant performance parameter $\gamma^{\mathcal{S}}$, except for changing $\gamma^{\mathcal{S}}$, MIRNOV scaling)

Input parameter	g/g_o	k/k_o	q/q_o	C	C_f	$\gamma^{\mathcal{S}}$	$\frac{B_{max}}{B_{maxo}}$	T_{OH}/R_o	T_{TF}/R_o	T_{BS}/R_o	R_V/R_o	Σ absol.sens.
lower lim.	0.500	1.000		0.850	0.850	1.755	0.900	0.287	0.150			
reference	0.550	1.300	1.000	1.130	0.897	1.949	0.950	0.342	0.186	0.180	0.252	
upper lim.	0.600	1.375	1.200	1.150	0.950	2.144	1.050	0.365	0.218	0.210	0.283	
η	0.680	0.077		0.698	1.000	1.304	0.525	0.808	0.221			3.905 + 1.963
	0.663	0.186	0.146	0.669	1.000	1.352	0.519	0.804	0.250	0.208	0.201	
ρ	-0.290	-0.786		-0.331	0.000	0.278	-0.576	0.414	0.115			1.956 + 1.865
	-0.253	-0.545	0.271	-0.265	0.000	0.263	-0.491	0.427	0.132	0.387	0.373	
δ	1.269	1.227		1.239	1.000	0.729	2.083	0.527	0.131			6.201 + 4.244
	1.298	1.212	-0.737	1.288	1.000	0.705	2.248	0.430	0.136	-0.467	-1.036	
I/I_o	-0.506	-0.411		-0.580	0.000	0.484	-0.556	-0.222	-0.055			2.041 + 1.002
	-0.442	-0.322	0.060	-0.466	0.000	0.459	-0.491	-0.180	-0.057	0.086	0.083	
A/A_o	0.074	0.750		0.079	0.000	-0.076	0.533	0.519	0.139			1.377 + 1.307
	0.068	0.781	-0.398	0.065	0.000	-0.067	0.518	0.488	0.152	0.059	0.057	
β/β_o	0.932	0.831		-0.080	0.000	0.075	-0.547	-0.566	-0.142			2.392 + 1.371
	0.925	0.850	-0.474	-0.072	0.000	0.067	-0.492	-0.473	-0.149	-0.059	-0.057	
M_{iMV}	0.000	0.000		1.000	1.000	1.000	0.000	0.000	0.000			3.000 + 0.000
	0.000	0.000	0.000	1.000	1.000	1.000	0.000	0.000	0.000	0.000	0.000	
M_{iKG}	-0.572	1.910		1.652	1.000	0.778	1.390	0.819	0.219			7.536 + 2.606
	-0.497	2.528	-1.624	1.862	1.000	0.761	1.432	0.777	0.243	-0.090	-0.088	
M_{iG}	-0.740	1.367		1.259	1.000	0.691	0.511	0.877	0.241			6.027 + 2.118
	-0.633	1.655	-0.970	1.322	1.000	0.673	0.508	0.881	0.274	0.249	0.240	
$cost/cost_o$	-0.374	-1.038		-0.473	0.210	0.754	-0.586	0.423	0.120			3.209 + 1.929
	-0.296	-0.697	0.360	-0.325	0.212	0.759	-0.458	0.454	0.140	0.453	0.347	
Σabs.sens.	5.437	8.397	5.040	7.391	5.210	6.169	7.307	5.175	1.383	2.058	2.482	56.049

Table 5-3 Sensitivity of INTOR-like reactor parameter sets to single input parameter changes

(Reference point "S", constant performance parameter $\gamma\vartheta$, except for changing $\gamma\vartheta$, KAYE-GOLDSTON scaling)

Input parameter	g/g_o	k/k_o	q/q_o	C	C_f	$\gamma\vartheta$	$\frac{B_{max}}{B_{maxo}}$	T_{OH}/R_o	T_{TF}/R_o	T_{BS}/R_o	R_V/R_o	Σ absol.sens.
lower lim.	0.500	1.000		0.850	0.850	3.313	0.900	0.307	0.152			
reference	0.550	1.300	1.000	1.130	0.897	3.681	0.950	0.342	0.186	0.180	0.252	
upper lim.	0.600	1.375	1.200	1.150	0.950	4.050	1.050	0.356	0.216	0.210	0.284	
η	1.546	-7.511		-1.047	1.000	1.662	-2.073	-1.078	-0.170			17.965 + 4.039
	1.631	-3.542	5.199	-0.785	1.000	1.790	-1.627	-0.845	-0.183	0.371	0.347	
ρ	-0.088	-2.117		-0.745	0.000	0.359	-1.118	0.199	0.040			4.418 + 2.167
	-0.079	-1.306	1.109	-0.559	0.000	0.344	-0.906	0.237	0.052	0.419	0.391	
δ	1.715	-0.839		0.555	1.000	0.938	0.853	-0.444	-0.080			6.131 + 2.694
	1.841	-1.020	1.084	0.488	1.000	0.924	0.786	-0.446	-0.096	-0.387	-0.930	
I/I_o	-0.153	-2.458		-1.316	0.000	0.625	-1.488	-1.271	-0.204			5.992 + 3.238
	-0.139	-1.681	1.440	-0.974	0.000	0.601	-1.233	-1.028	-0.221	0.142	0.133	
A/A_o	0.023	0.905		0.157	0.000	-0.100	0.657	0.942	0.166			1.733 + 1.866
	0.022	1.026	-0.548	0.148	0.000	-0.086	0.658	0.913	0.196	0.052	0.049	
β/β_o	0.979	0.672		-0.164	0.000	0.098	-0.681	-1.042	-0.171			2.234 + 1.993
	0.977	0.613	-0.321	-0.144	0.000	0.088	-0.614	-0.879	-0.190	-0.051	-0.048	
M_{iKG}	0.000	0.000		1.000	1.000	1.000	0.000	0.000	0.000			3.000 + 0.000
	0.000	0.000	0.000	1.000	1.000	1.000	0.000	0.000	0.000	0.000	0.000	
M_{iAX}	0.722	-3.967		0.047	1.000	1.194	-1.244	-0.994	-0.138			9.340 + 2.707
	0.703	-2.382	2.410	0.046	1.000	1.220	-1.039	-0.696	-0.151	0.171	0.160	
M_{iG}	-0.224	-0.758		0.579	1.000	0.888	0.788	0.269	0.051			4.203 + 1.751
	-0.200	-0.482	-0.754	0.569	1.000	0.884	0.646	0.300	0.064	0.332	0.311	
$cost/cost_o$	0.174	-5.962		-1.748	0.213	0.965	-2.133	-0.706	-0.104			12.206 + 3.912
	0.208	-2.717	3.144	-1.141	0.212	1.001	-1.586	-0.483	-0.105	0.547	0.422	
Σabs.sens.	5.624	25.189	16.009	7.358	5.213	7.829	11.035	6.945	1.124	2.472	2.791	91.589

Taking the horizontal sums permits one to identify those design parameters that are particularly succeptible to impact from input parameter changes.

For ASDEX H-mode scaling the fusion power and neutron wall load are strongly influenced by physics input parameter changes (the neutron wall load by engineering input parameter changes as well), whereas the major radius, plasma current and beta show more moderate and comparable impact resulting from changes in physics and in engineering input parameters. Cost is strongly influenced by physics input parameters.

For Mirnov scaling the picture is similar to ASDEX H-mode scaling with a stronger impact of engineering input parameter changes on the power, neutron wall load and cost. The overall sensitivity level (as indicated by the total sum of absolute sensitivity values considered) is practically the same as for ASDEX H-mode scaling.

For Kaye-Goldston scaling the overall sensitivity level is almost twice that of the other two scalings. Particularly the impact on the fusion power and cost derives mainly from physics input parameters, but also from changes in engineering input. The overall impact of any changes on the plasma current is about twice as large as for ASDEX H-mode scaling. The impact is stronger for other design parameters as well. (Taking eq. 21 for Kaye-Goldston scaling would lead to a lower overall sensitivity level than using eq. 21a.)

The reference case "S" and the 19 alternative cases, listed in Table 5-4, which are arrived at by single input parameter changes are characterized in Figs. 5-1 through 5-3, which show the design points in the plane of fusion power vs. major radius. This representation allows direct comparison of single sensitivities among different confinement scalings.

It is clear that, for example, the sensitivity to changes of the performance parameter and the power density profile factor is the same for all three confinement scalings considered. For ASDEX H-mode and Mirnov scalings no large differences in sensitivity are seen from changes of the Troyon factor and the useful beta fraction, but the impact of changes in

Table 5-4 List of cases and input parameters as used in the study of the impact of single input parameter changes (ASDEX H-mode scaling)[+]

Case No.	g/g_o	k/k_o	q/q_o	C	C_f	$\gamma_{\mathfrak{R}}$	$\frac{B_{max}}{B_{maxo}}$	F_1	F_2	F_3	F_4
"S"	0.550	1.300	1.000	1.130	0.897	1.627	0.950	0.380	0.240	0.250	0.060
1	0.500										
2	0.600										
3			1.200								
4		1.000									
5		1.375									
6					0.850						
7					0.950						
8				0.850							
9				1.150							
10								0.330			
11								0.400			
12									0.270		
13										0.270	
14											0.040
15											0.080
16							0.900				
17							1.050				
18						- 10%					
19						+ 10%					

Only the parameters that are changed have been listed. The following numbers have been used throughout for the input parameters not mentioned in the table:

$C_p = 0.900$, $C_n = 0.923$, $\mathfrak{R} = 1.000$

[+]For Mirnov and Kaye-Goldston scaling the $\gamma_{\mathfrak{R}}$-values for "S" would be 1.949 and 3.681, respectively

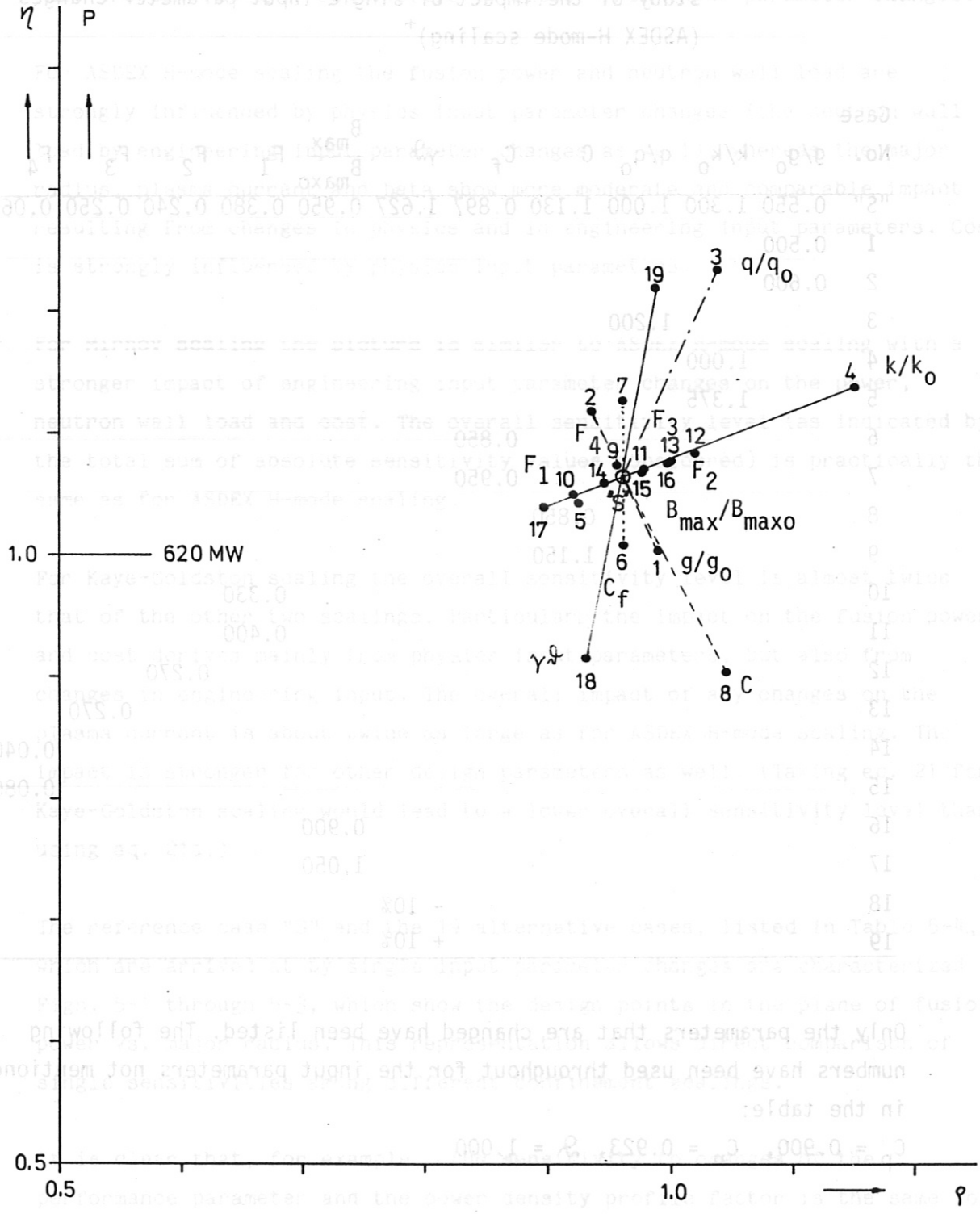

Fig. 5-1 Fusion power vs. major radius - ASDEX H-mode scaling. Sensitivity to single input parameter changes (for cases see Table 5-4, Reference INTOR IIA-1).

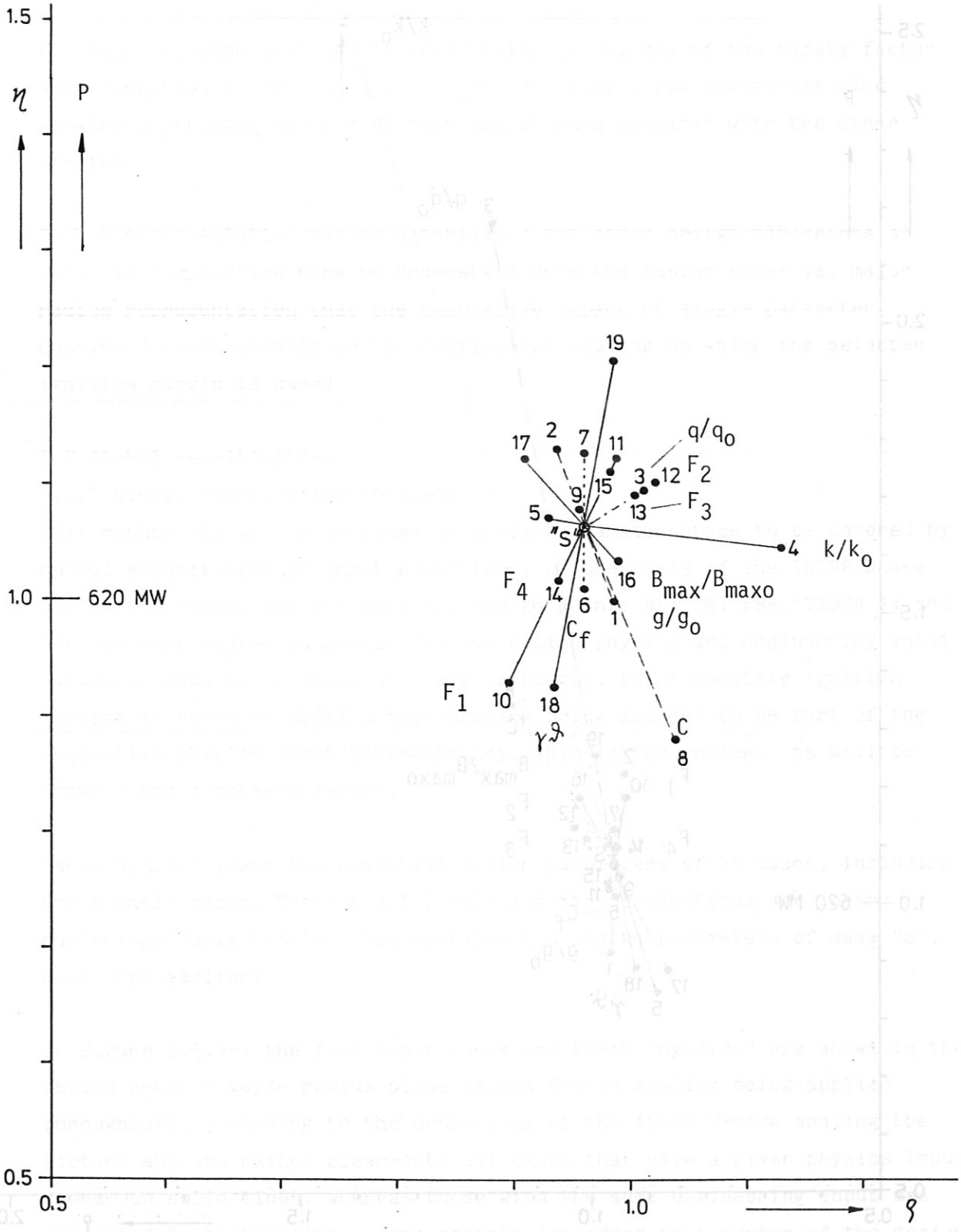

Fig. 5-2 Fusion power vs. major radius - MIRNOV scaling. Sensitivity to single input parameter changes (for cases see Table 5-4, Reference INTOR IIA-1).

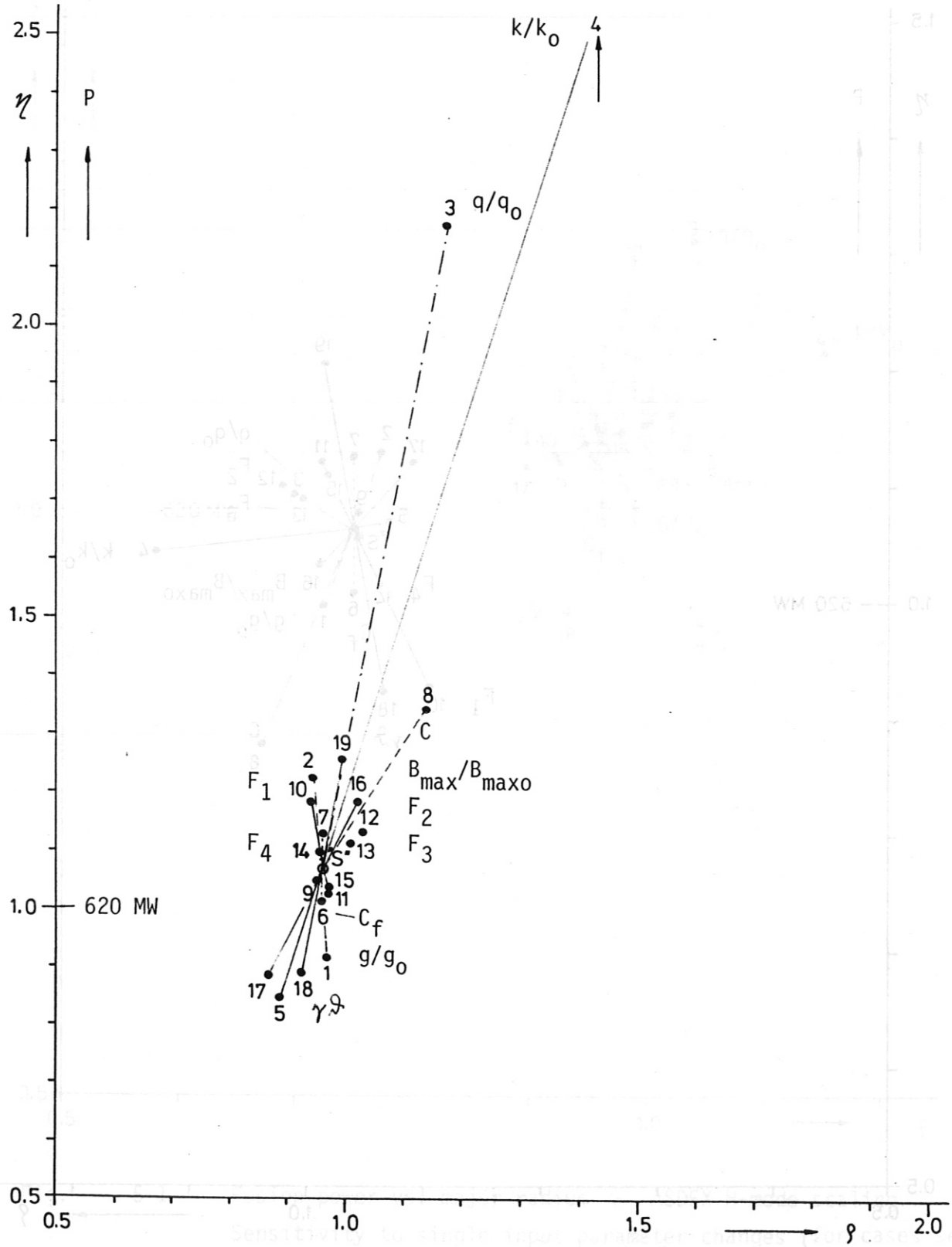

Fig. 5-3 Fusion power vs. major radius - KAYE-GOLDSTON scaling. Sensitivity to single input parameter changes (for cases see Table 5-4, Reference INTOR IIA-1).

the safety factor and elongation is definitely different, as is the impact of changes in the maximum field and central solenoid radius.

For Kaye-Goldston scaling the sensitivity to changes of the safety factor and elongation is very large, some of the other input parameters also showing a stronger and a different impact when compared with the other scalings.

Such a representation can be established for other design parameters as well. It may suffice here to understand from the fusion power vs. major radius representation that the cumulative impact of single parameter changes depends notably on the confinement scaling on which the selected ignition margin is based.

5.3 Global sensitivities

5.3.1 Global substitution analysis

This method allows a wide range in design parameter space to be covered by mutual substitution of input parameters. On the basis of the INTOR Phase IIA Part 2 design and the national design points NET-DN, FER, TIBER II and OTR (as represented in Section 4) the entire physics and engineering input parameter sets as of Table 4-1 were exchanged, the respective ignition margins in terms of ASDEX H-mode scaling being assumed to be part of the respective physics input parameter set. This latter choice - as will be shown - has a notable impact.

Table 5.3.1-1 lists the essential design parameters of 25 cases, including the 5 basic cases. Table 5.3.1-2 explains the combinations and their numbering. Table 5.3.1-1 also contains the design parameters of case "S", mentioned earlier.

In Figure 5.3.1-1 the five basic cases and their "hybrids" are shown in the fusion power - major radius plane (ASDEX H-mode scaling being applied throughout). According to the properties of the ASDEX H-mode scaling the picture appears rather clear-cut: all cases that have a given physics input appear on solid lines, whereas those with the same engineering input are connected by broken lines. Some remarks are added to a number of the design

Table 5.3.1-1 25 design points for comparative analysis, one "suggested" design point (ASEDEX H-mode scaling)

Case	A/A_o	I/I_o	δ	ρ	B/B_o	η	β/β_o	$\frac{\beta pol}{\beta pol_o}$	$\beta-\beta_{DT}$ (%)	m	$\frac{cost}{cost_o}$	M_{iAX}	M_{iMV}	M_{iKG}+
2	o.817	1.448	o.939	o.951	o.862	o.948	1.o11	o.485	o.923	1.117	1.o97	2.768	1.5o5	o.925
4	o.764	1.52o	o.948	o.9oo	o.836	o.931	1.o8o	o.454	o.987	1.o97	1.o48	2.768	1.61o	o.911
6	o.681	1.527	1.537	o.645	o.93o	o.833	1.213	o.4o4	1.1o8	o.981	o.786	2.768	1.8o6	o.94o
8	1.o92	1.116	1.o23	1.o42	1.o84	o.977	o.756	o.648	o.698	1.152	1.o64	2.768	1.127	1.o22
1	1.oo4	1.462	o.968	o.982	1.o47	1.o49	o.864	o.621	1.212	1.oo1	1.137	2.9o4	1.456	1.o89
10	o.8o9	1.78o	o.865	o.927	o.877	1.o29	1.o73	o.5oo	1.5o5	o.981	1.183	2.9o4	1.8o6	1.oo9
12	o.723	1.782	1.411	o.663	o.98o	o.92o	1.2o1	o.447	1.684	o.878	o.88o	2.9o4	2.o21	1.o42
14	1.163	1.3o9	o.9o8	1.o95	1.128	1.o87	o.746	o.719	1.o46	1.o37	1.2o1	2.9o4	1.257	1.137
3	o.984	1.131	o.876	o.878	o.996	o.67o	o.77o	o.521	o.8o8	o.686	o.849	2.354	1.o97	o.919
9	o.851	1.313	o.76o	o.888	o.855	o.672	o.891	o.451	o.935	o.689	o.922	2.354	1.268	o.863
16	o.7o9	1.377	1.277	o.593	o.932	o.587	1.o7o	o.375	1.122	o.6o2	o.644	2.354	1.522	o.881
18	1.142	1.oo7	o.834	o.971	1.o81	o.692	o.664	o.6o5	o.696	o.7o9	o.896	2.354	o.944	o.956
5	1.144	1.287	o.692	o.866	1.o62	o.583	o.767	o.568	1.5o2	o.376	o.851	2.142	1.o2o	o.961
11	o.988	1.488	o.616	o.862	o.92o	o.582	o.888	o.491	1.74o	o.376	o.9o3	2.142	1.181	o.9o5
15	o.924	1.554	o.638	o.8o4	o.9o2	o.569	o.949	o.459	1.86o	o.367	o.86o	2.142	1.263	o.895
20	1.329	1.15o	o.645	o.971	1.144	o.6o6	o.66o	o.66o	1.293	o.758	o.9o7	2.142	o.878	o.996
7	o.824	1.398	o.613	1.o85	o.971	o.78o	o.659	o.5o4	o.573	1.oo9	1.188	2.395	1.252	o.859
13	o.717	1.614	o.533	1.1oo	o.837	o.784	o.758	o.438	o.658	1.o13	1.3o8	2.395	1.439	o.8o8
17	o.667	1.716	o.515	1.o65	o.796	o.776	o.814	o.4o8	o.7o7	1.oo2	1.288	2.395	1.546	o.79o
19	o.599	1.719	o.82o	o.776	o.883	o.698	o.9o6	o.376	o.787	o.9o2	o.952	2.395	1.722	o.815
I	o.943	1.251	1.o75	o.943	1.oo1	o.945	o.876	o.56o	o.8oo	1.115	1.o12	2.768	1.3o4	o.984
II	o.87o	1.684	o.865	o.977	o.91o	1.o46	o.998	o.538	1.399	1.ooo	1.225	2.9o4	1.678	1.o26
III	o.8oo	1.367	o.781	o.834	o.838	o.657	o.948	o.424	o.995	o.674	o.868	2.354	1.348	o.854
IV	o.819	1.56o	1.o6o	o.566	1.o1o	o.5o6	1.o7o	o.4o7	2.o97	o.327	o.627	2.142	1.422	o.925
V	o.951	1.249	o.591	1.189	1.o55	o.8o7	o.571	o.582	o.496	1.o4o	1.24o	2.395	1.o83	o.893
"S"	o.952	1.578	1.o18	o.96o	o.995	1.o65	o.865	o.523	o.836	o.957	1.164	3.234	1.721	1.176

+for M_{iKG}: $f_H = 2$, $P = P_\alpha$ (eq.21)

Table 5.3.1-2

Cases for mutual comparison of 5 next-step designs

	INTOR IIA-2		NET-DN		FER		TIBER II		OTR	
Case	P	E	P	E	P	E	P	E	P	E
1		X	X							
2	X			X						
3		X			X					
4	X					X				
5		X					X			
6	X							X		
7		X							X	
8	X									X
9				X	X					
10			X			X				
11				X			X			
12			X					X		
13				X					X	
14			X							X
15						X	X			
16					X			X		
17						X			X	
18					X					X
19								X	X	
20							X			X

Sequence of the cases in Table 5.3.1-1

2 , 4 , 6 , 8 (INTOR IIA-2 physics + 4 other cases' eng.)
1 ,10 ,12 ,14 (NET-DN physics + 4 other cases' eng.)
3 , 9 ,16 ,18 (FER physics + 4 other cases' eng.)
5 ,11 ,15 ,20 (TIBER II physics + 4 other cases' eng.)
7 ,13 ,17, 19 (OTR physics + 4 other cases' eng.)

I = INTOR IIA-2
II = NET-DN
III = FER
IV = TIBER II
V = OTR

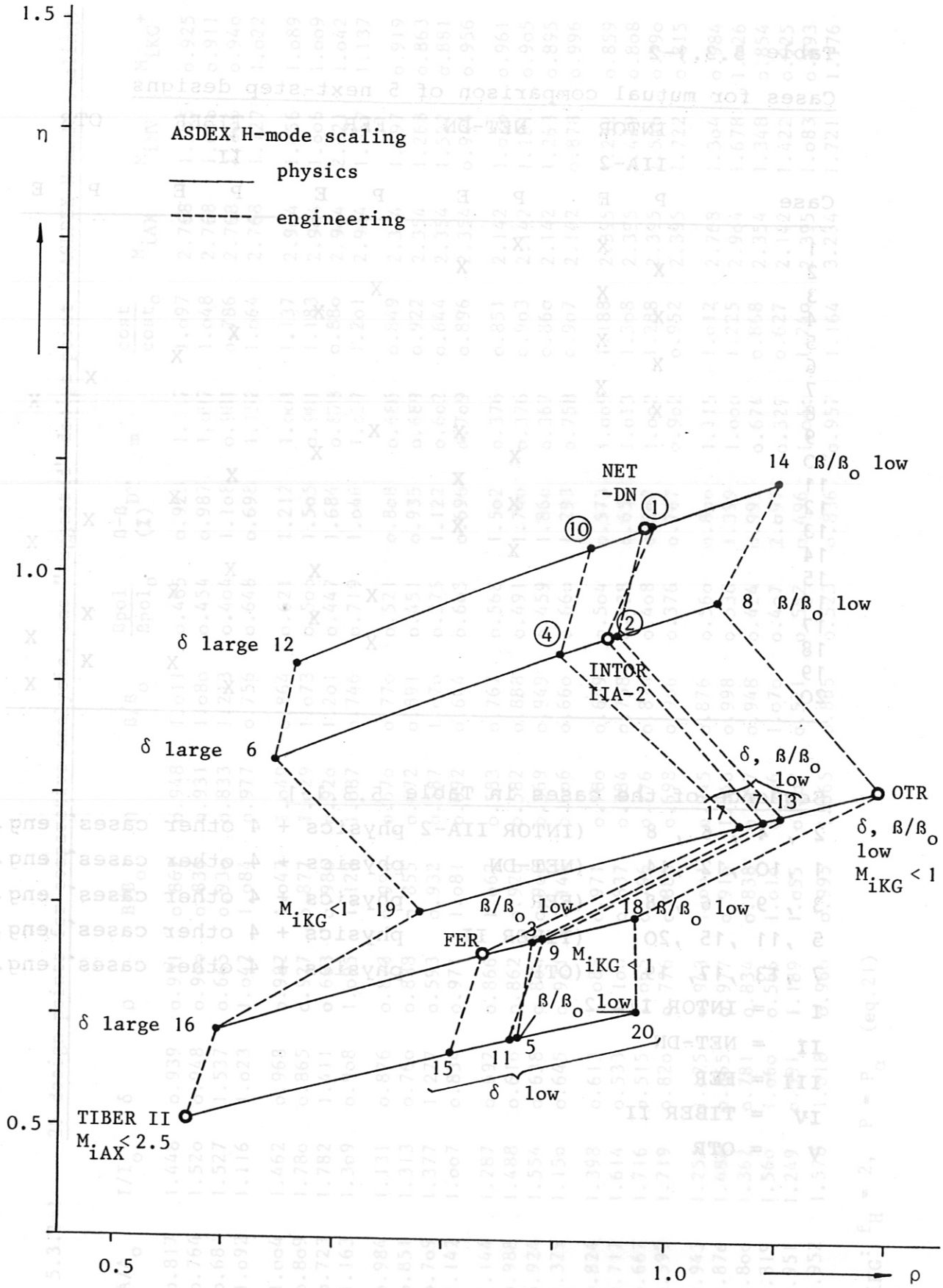

Fig. 5.3.1-1 Comparison of 5 original designs with alternatives. Fusion power vs. major radius (see Table 5.3.1-1). Remaining alternative data points: ◯

points that characterize them as "low" or "large" in the parameter indicated with respect to the INTOR values. Hence parameter combinations (wall load, beta, ignition margin) typical of INTOR are found in a limited domain around INTOR IIA-2 and NET-DN.

On the basis of the ASDEX H-mode confinement scaling the fusion power level is obviously strongly determined by the physics input parameter combination, while - for given physics input - the engineering parameter combination mainly impacts on the major radius. Figures 5.3.1-2 and 5.3.1-3 show the wall load and the plasma current vs. major radius for the same cases. Here, obviously, the combination of the physics and engineering input parameter sets is important and the ordering of the (now broken) solid lines for cases with equal physics input is changed. The domain for INTOR-like cases in terms of plasma current appears particularly large.

For comparison, power vs. radius diagrams are shown in Figs. 5.3.1-4 and 5.3.1-5 for Mirnov and Kaye-Goldston scalings. Since these scalings involve an aspect ratio dependence different from that of the ASDEX H-mode scaling, the lines connecting cases for a certain physics input are now broken, and the sequence of design data points for different engineering assumptions differs from that in Fig. 5.3.1-1. Comparing data points in Figs. 5.3.1-1, 5.3.1-4 and 5.3.1-5 with the same number (= same combination physics/engineering input) for the average tensile stress and average current density in the inner toroidal field coil leg gives about the same values independently of the confinement scaling. This proves that the simplified rescaling model can indeed be used for such a substitution analysis with fair approximation. As indicated further in Figs. 5.3.1-4 and 5.3.1-5, the parameter combinations (wall load, beta, ignition margin) typical of INTOR are again found in a limited domain (somewhat different in shape) around the INTOR IIA-2 and NET-DN data points.

Comparison of Figs. 5.3.1-1, 5.3.1-4 and 5.3.1-5 shows that for all three confinement scalings used certain design points can be found from substitution analysis that comply with the usual INTOR-like conditions on neutron wall load, beta and ignition margin. The remaining design data points, however, differ somewhat depending on the confinement scaling. For

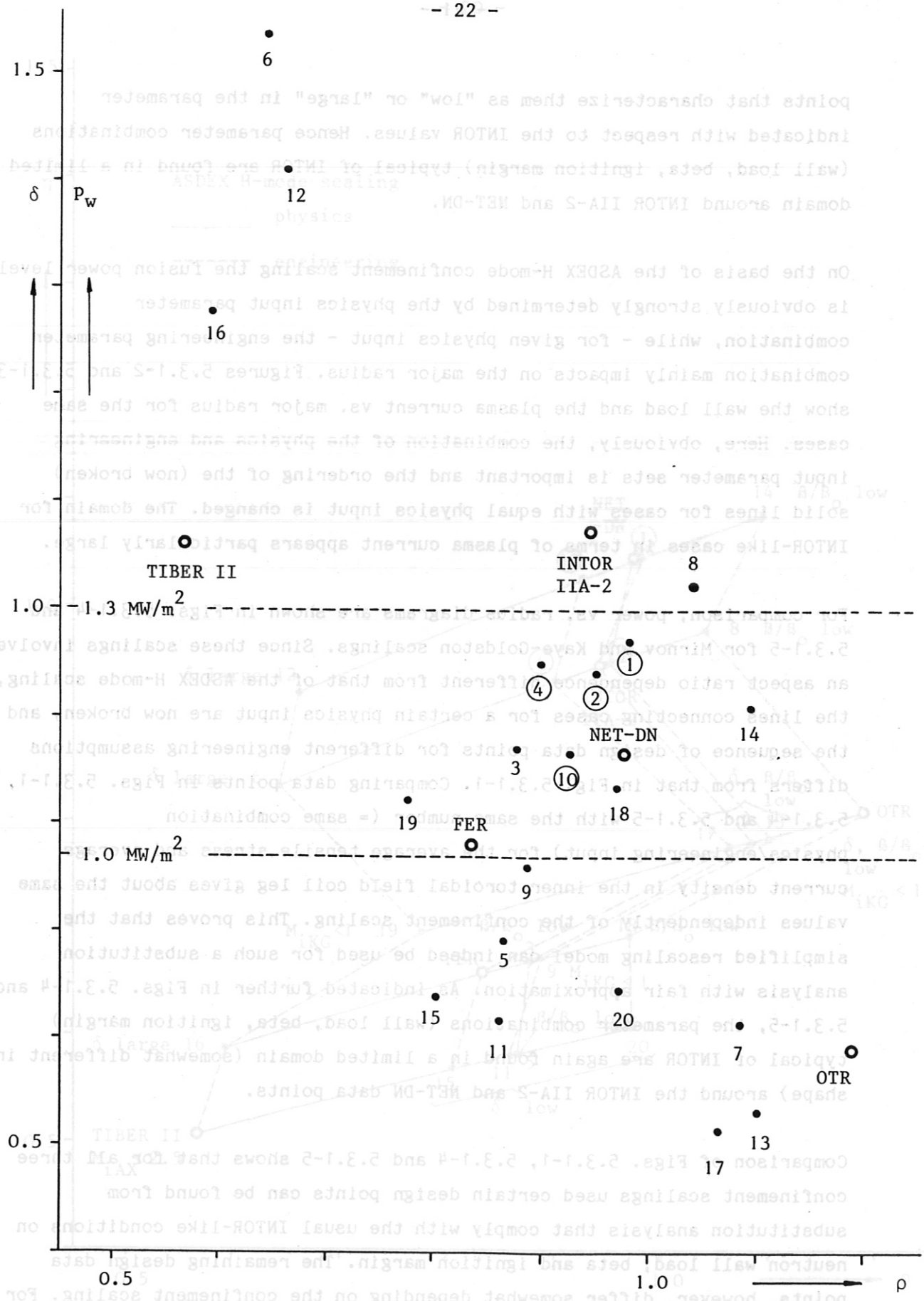

Fig. 5.3.1-2 Comparison of 5 original designs with alternatives. Neutron wall load vs. major radius (see Table 5.3.1-1). Remaining alternative data points: ◯

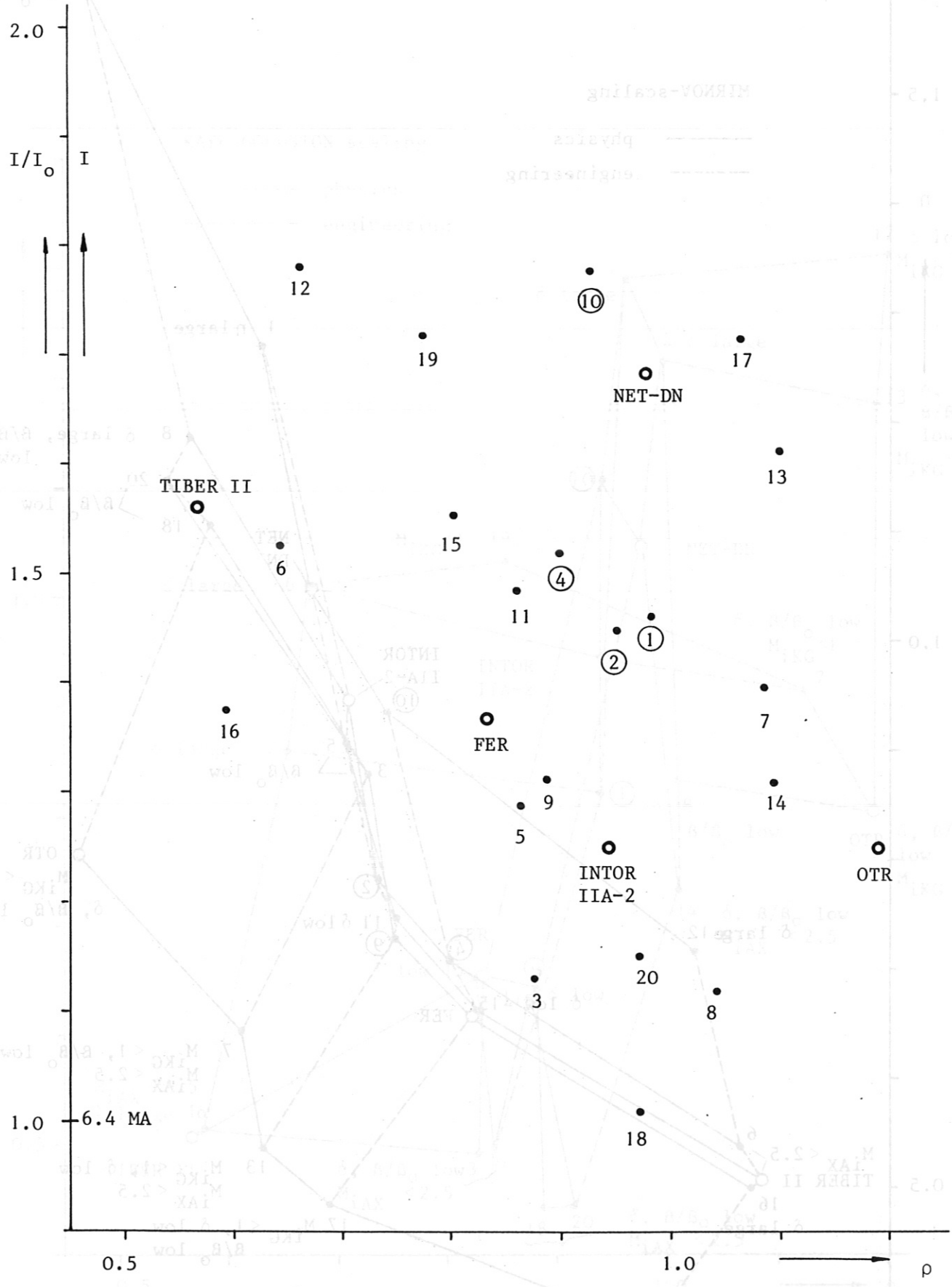

Fig. 5.3.1-3 Comparison of 5 original designs with alternatives. Plasma current vs. major radius (see Table 5.3.1-1). Remaining alternative data points: ◯

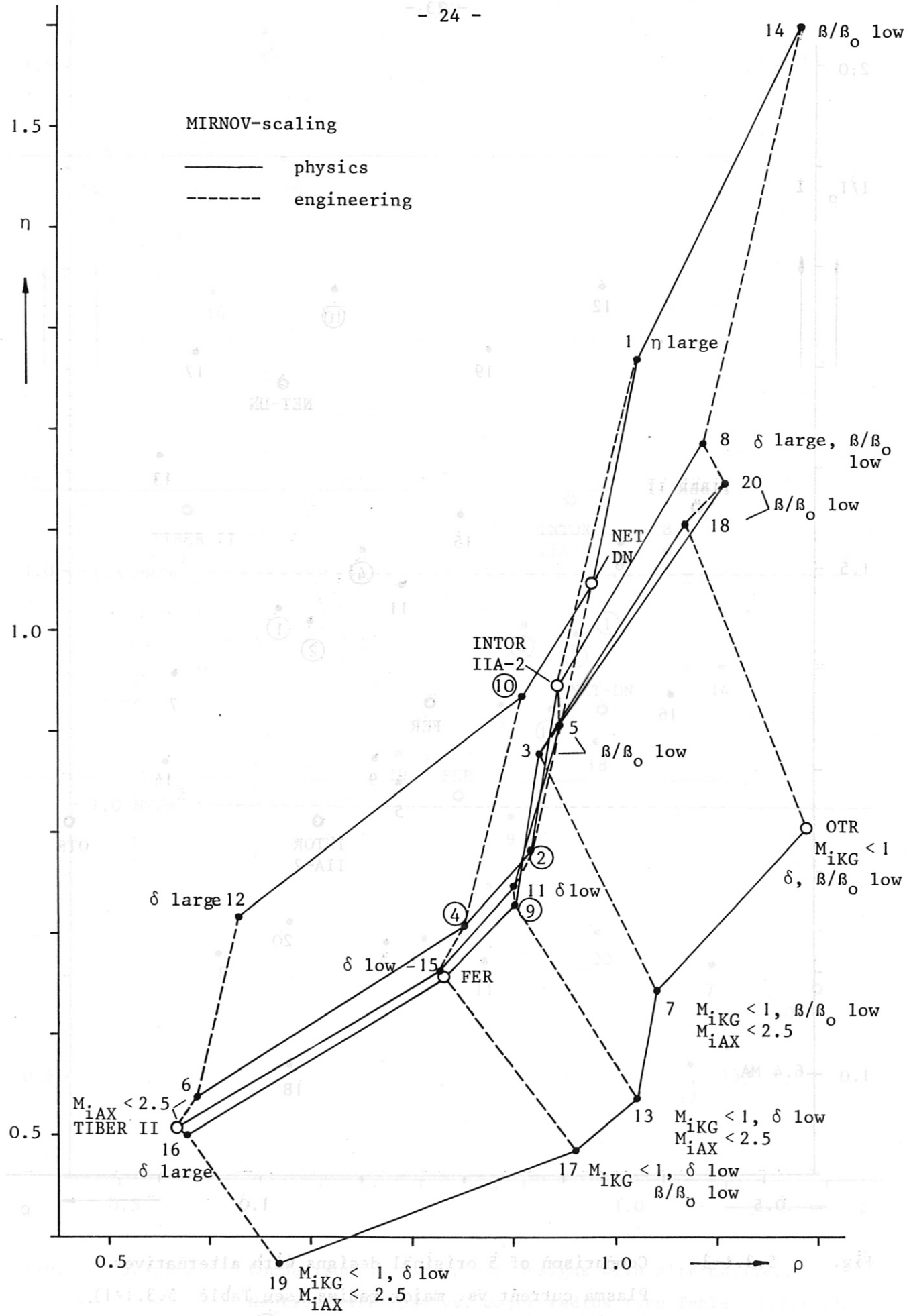

Fig. 5.3.1-4 Comparison of 5 original designs with alternatives.
Fusion power vs. major radius.
Remaining alternative data points: ○

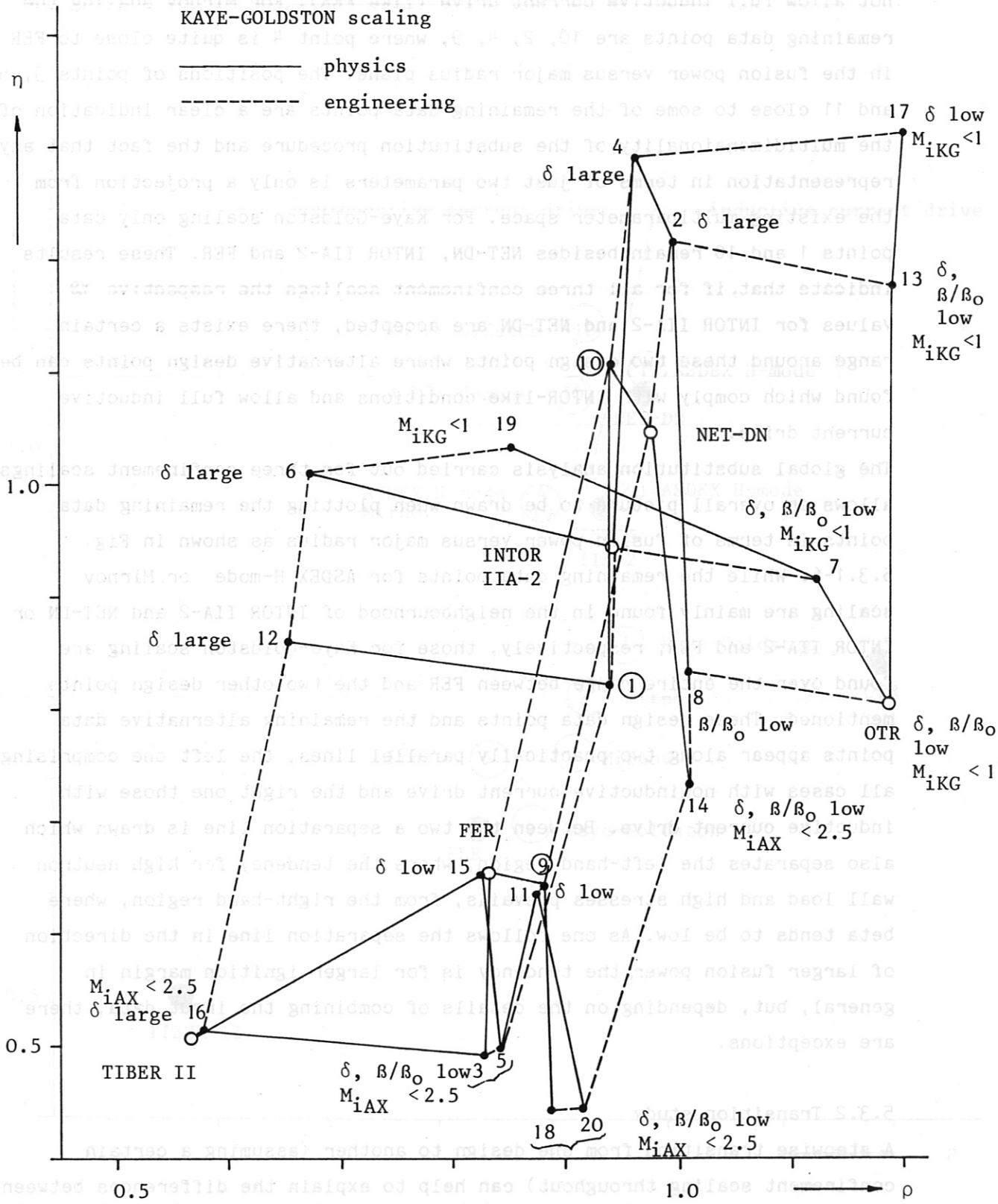

Fig. 5.3.1-5 Comparison of 5 original designs with alternatives. Fusion power vs. major radius. Remaining alternative data points: ◯

ASDEX H-mode scaling in addition to NET-DN, INTOR IIA-2 and FER the data points 1, 10 and 2, 4 comply with INTOR-like conditions, where 4 and 10 do not allow full inductive current drive (like FER). For Mirnov scaling the remaining data points are 10, 2, 4, 9, where point 4 is quite close to FER in the fusion power versus major radius plane. The positions of points 3, 5 and 11 close to some of the remaining data points are a clear indication of the multidimensionality of the substitution procedure and the fact that any representation in terms of just two parameters is only a projection from the existing multiparameter space. For Kaye-Goldston scaling only data points 1 and 10 remain besides NET-DN, INTOR IIA-2 and FER. These results indicate that, if for all three confinement scalings the respective $n\tau_E$-values for INTOR IIA-2 and NET-DN are accepted, there exists a certain range around these two design points where alternative design points can be found which comply with INTOR-like conditions and allow full inductive current drive.

The global substitution analysis carried out for three confinement scalings allows an overall picture to be drawn when plotting the remaining data points in terms of fusion power versus major radius as shown in Fig. 5.3.1-6. While the remaining data points for ASDEX H-mode or Mirnov scaling are mainly found in the neighbourhood of INTOR IIA-2 and NET-DN or INTOR IIA-2 and FER, respectively, those for Kaye-Goldston scaling are found over the entire range between FER and the two other design points mentioned. These design data points and the remaining alternative data points appear along two practically parallel lines, the left one comprising all cases with noninductive current drive and the right one those with inductive current drive. Between the two a separation line is drawn which also separates the left-hand region, where the tendency for high neutron wall load and high stresses prevails, from the right-hand region, where beta tends to be low. As one follows the separation line in the direction of larger fusion power, the tendency is for larger ignition margin in general, but, depending on the details of combining the input data, there are exceptions.

5.3.2 Transition study

A stepwise transition from one design to another (assuming a certain confinement scaling throughout) can help to explain the differences between

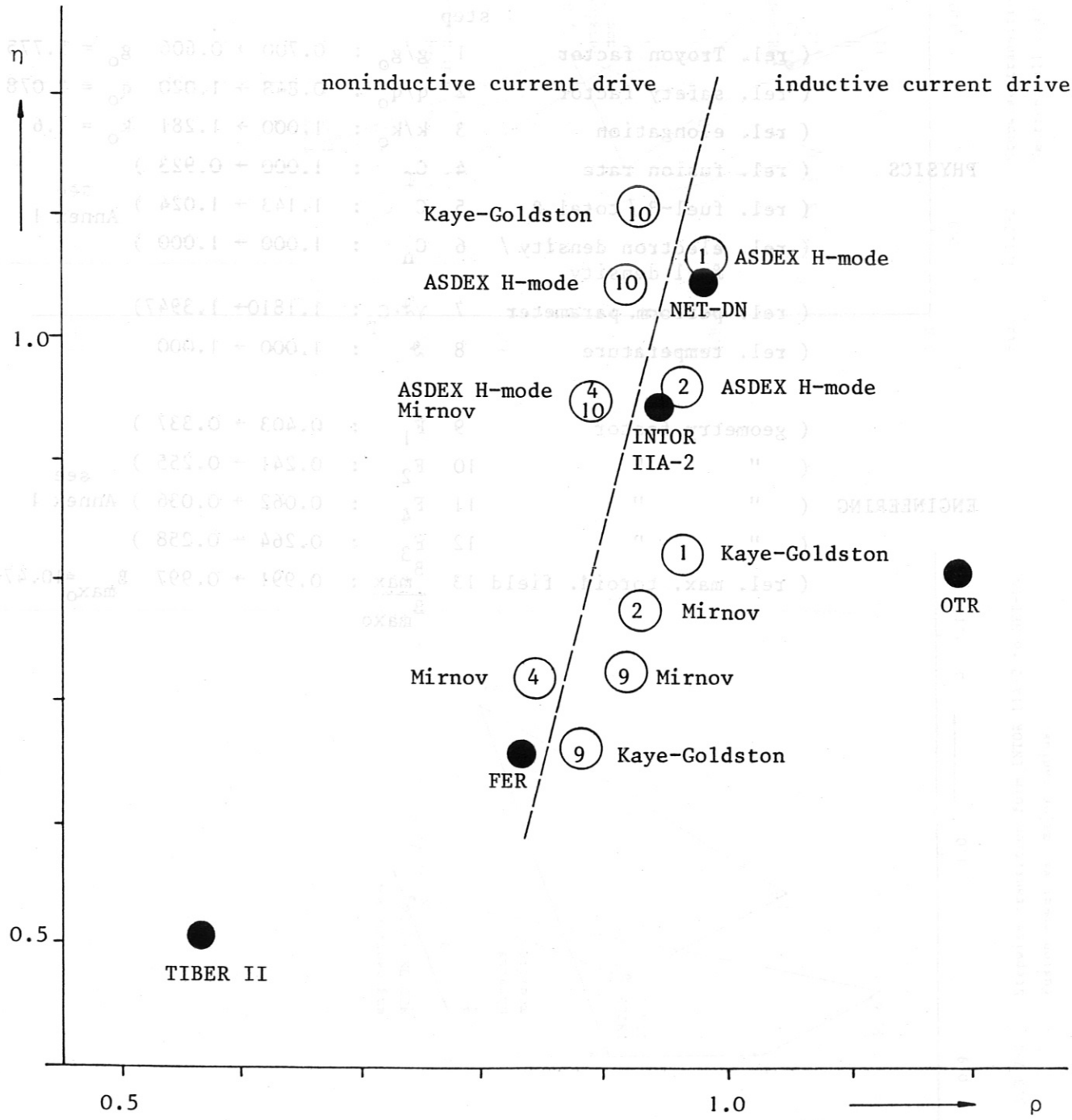

Fig. 5.3.1-6 Comparison of remaining alternative data points for three confinement scalings.
Fusion power vs. major radius.

Table 5.3.2-1

Sequence of stepwise modification of input parameters

ASDEX H-mode scaling: INTOR IIA-2 to NET-DN

		step			
	(rel. Troyon factor	1	g/g_o :	0.700 → 0.606	g_o = 5.775
	(rel. safety factor	2	q/q_o :	0.848 → 1.020	q_o = 2.078
	(rel. elongation	3	k/k_o :	1.000 → 1.281	k_o = 1.6
PHYSICS	(rel. fusion rate	4	C_f :	1.000 → 0.923)	
	(rel. fuel-ß / total ß	5	C :	1.143 → 1.024)	see Annex 1
	(rel. electron density / fuel density	6	C_n :	1.000 → 1.000)	
	(rel. perform. parameter	7	$\gamma \vartheta \cdot C_p$:	1.1810→ 1.3947)	
	(rel. temperature	8	ϑ :	1.000 → 1.000	
	(geometry factor	9	F_1 :	0.403 → 0.337)	
	(" "	10	F_2 :	0.241 → 0.255)	see
ENGINEERING	(" "	11	F_4 :	0.062 → 0.036)	Annex 1
	(" "	12	F_3 :	0.264 → 0.258)	
	(rel. max. toroid. field	13	$\frac{B_{max}}{B_{maxo}}$:	0.991 → 0.997	B_{max_o}=10.474 T

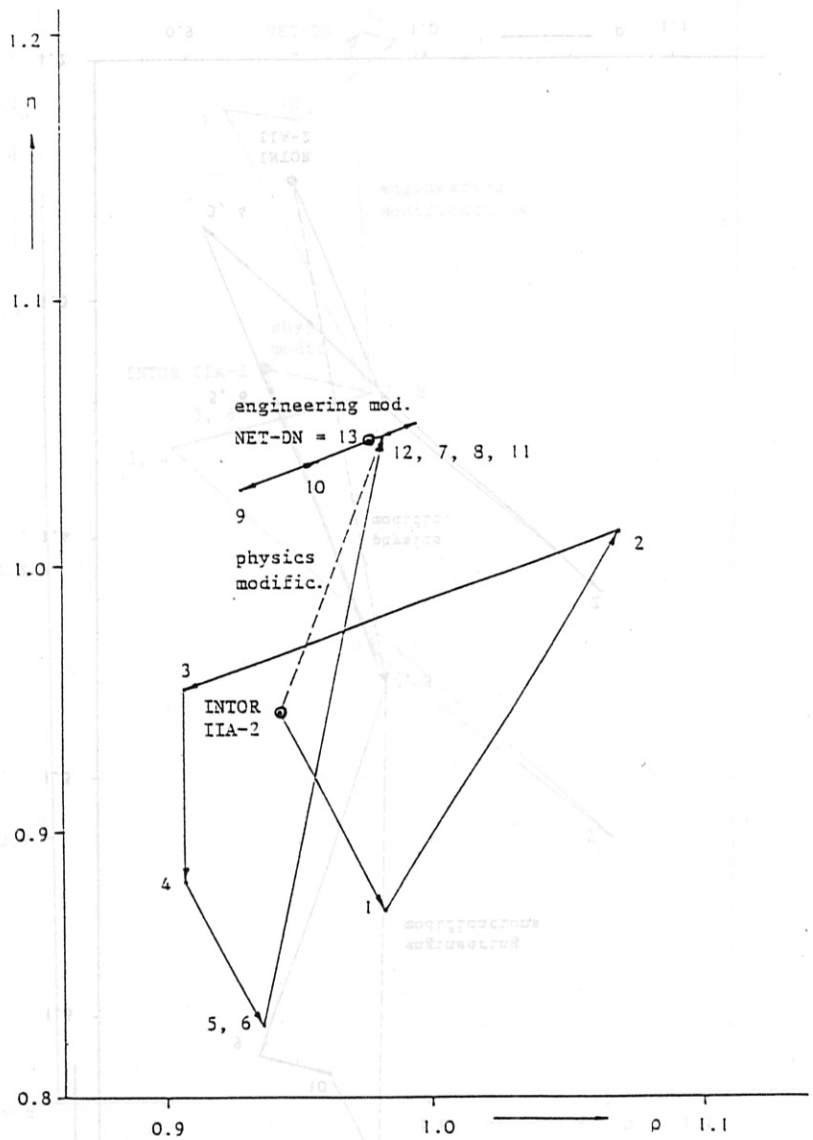

Fig. 5.3.2-1 Stepwise transition form INTOR IIA-2 to NET-DN. Fusion power vs. major radius.

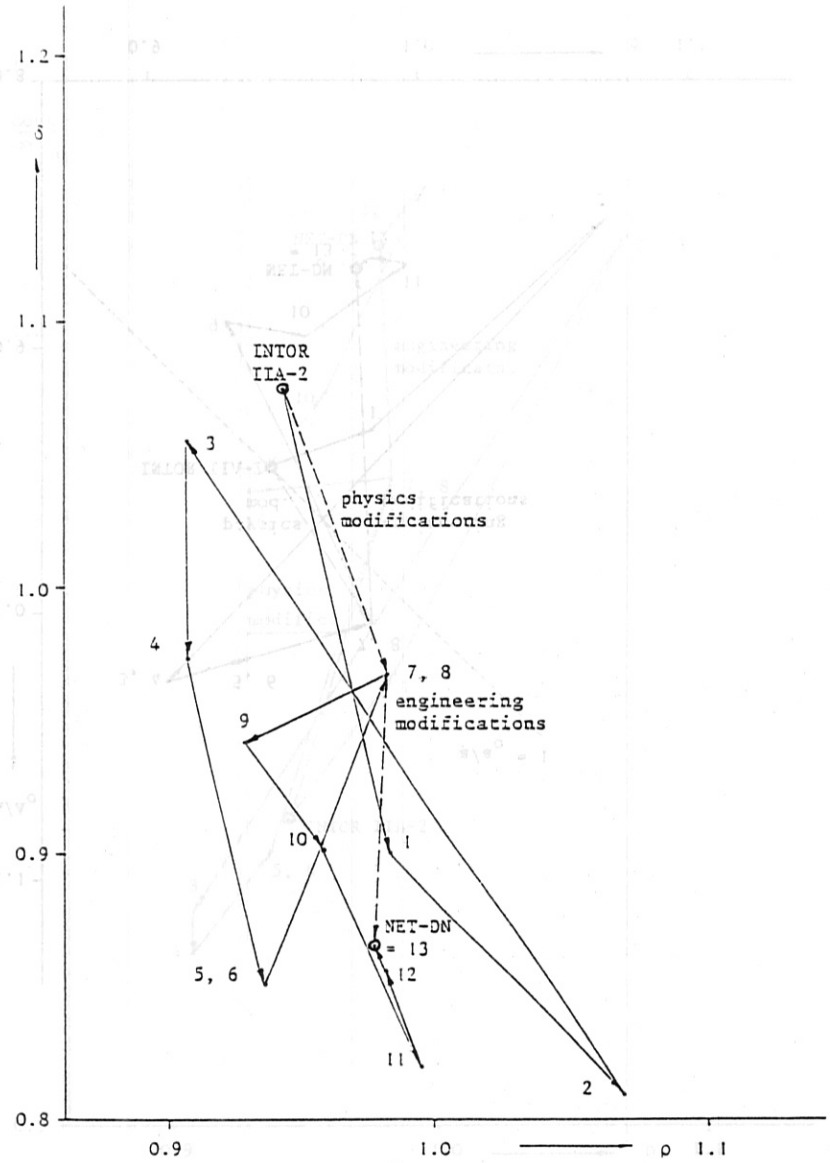

Fig. 5.3.2-2 Stepwise transition from INTOR IIA-2 to NET-DN. Neutron wall load vs. major radius.

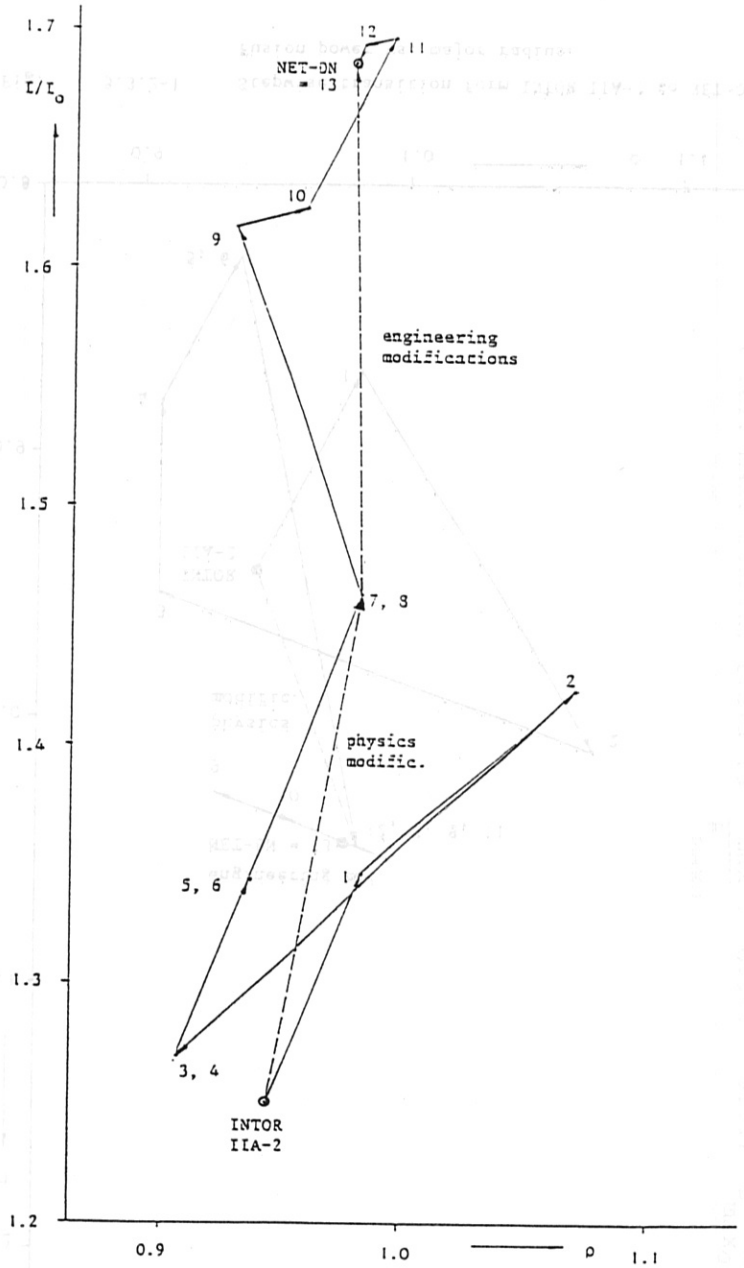

Fig. 5.3.2-3 Stepwise transition from INTOR IIA-2 to NET-DN. Plasma current vs. major radius.

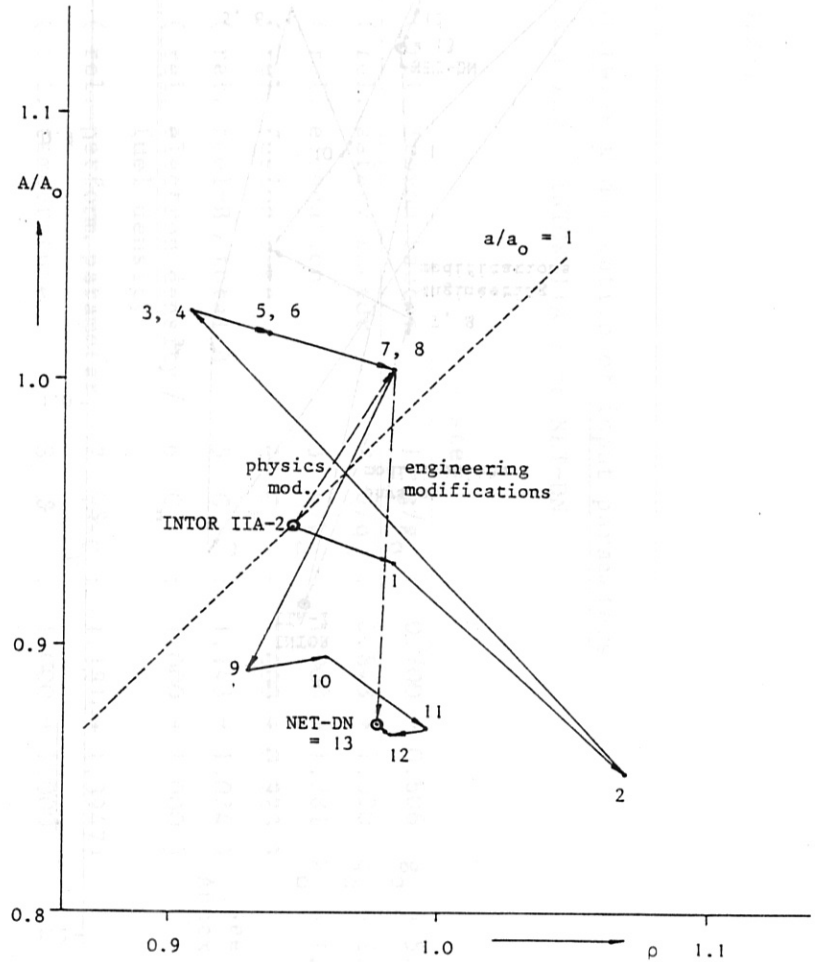

Fig. 5.3.2-4 Stepwise transition from INTOR IIA-2 to NET-DN. Aspect ratio vs. major radius.

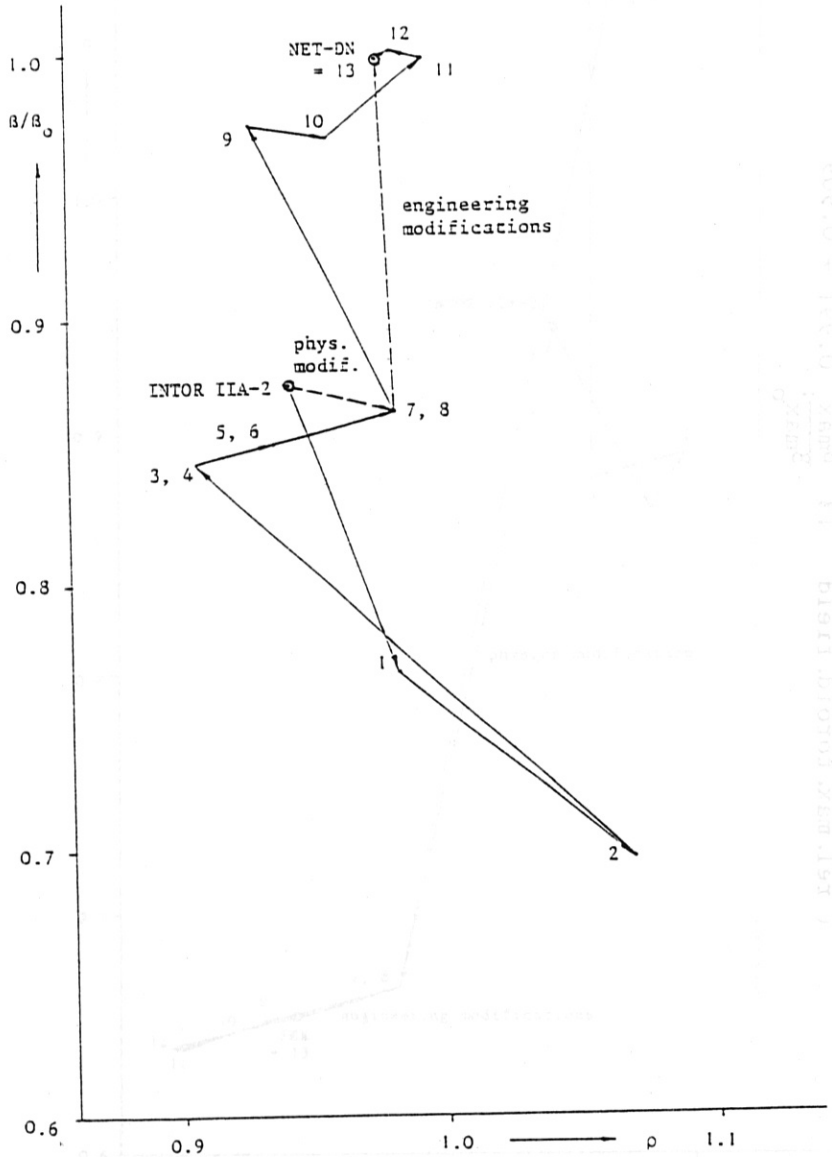

Fig. 5.3.2-5 Stepwise transition form INTOR IIA-2 to NET-DN.
Beta vs. major radius.

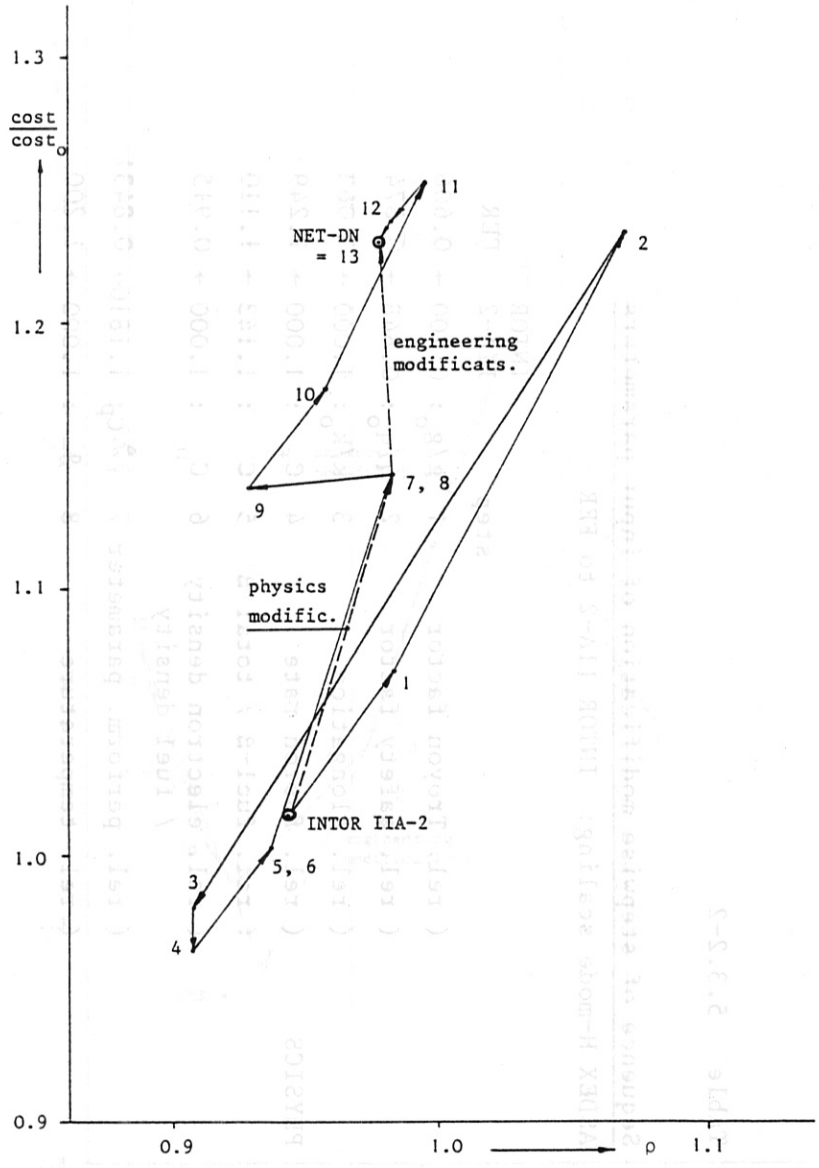

Fig. 5.3.2-6 Stepwise transition from INTOR IIA-2 to NET-DN.
Cost vs. major radius.

Table 5.3.2-2

Sequence of stepwise modification of input parameters

ASDEX H-mode scaling: INTOR IIA-2 to FER

		step		INTOR IIA-2	FER
	(rel. Troyon factor	1	g/g_o :	0.700 →	0.606
	(rel. safety factor	2	q/q_o :	0.848 →	0.874
	(rel. elongation	3	k/k_o :	1.000 →	1.063
PHYSICS	(rel. fusion rate	4	C_f :	1.000 →	1.249
	(rel. fuel-ß / total ß	5	C :	1.143 →	1.110
	(rel. electron density / fuel density	6	C_n :	1.000 →	0.915
	(rel. perform. parameter	7	$\gamma \beta \cdot C_p$:	1.1810→	0.8431
	(rel. temperature	8	β :	1.000 →	1.200
	(geometry factor	9	F_1 :	0.403 →	0.304
	(geometry factor	10	F_2 :	0.241 →	0.236
ENGINEERING	(geometry factor	11	F_4 :	0.062 →	0.079
	(geometry factor	12	F_3 :	0.264 →	0.262
	(rel. max. toroid. field	13	$\frac{B_{max}}{B_{max_o}}$:	0.991 →	0.909

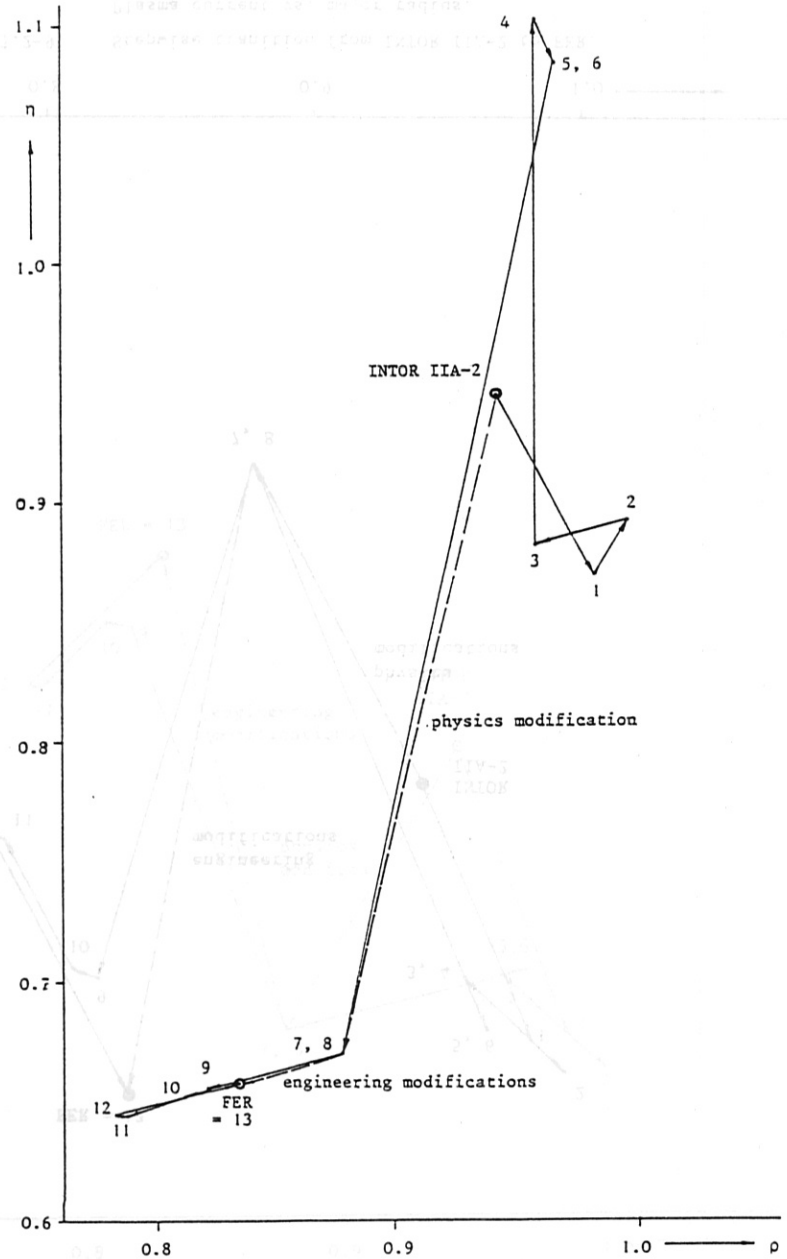

Fig. 5.3.2-7 Stepwise transition from INTOR IIA-2 to FER. Fusion power vs. major radius.

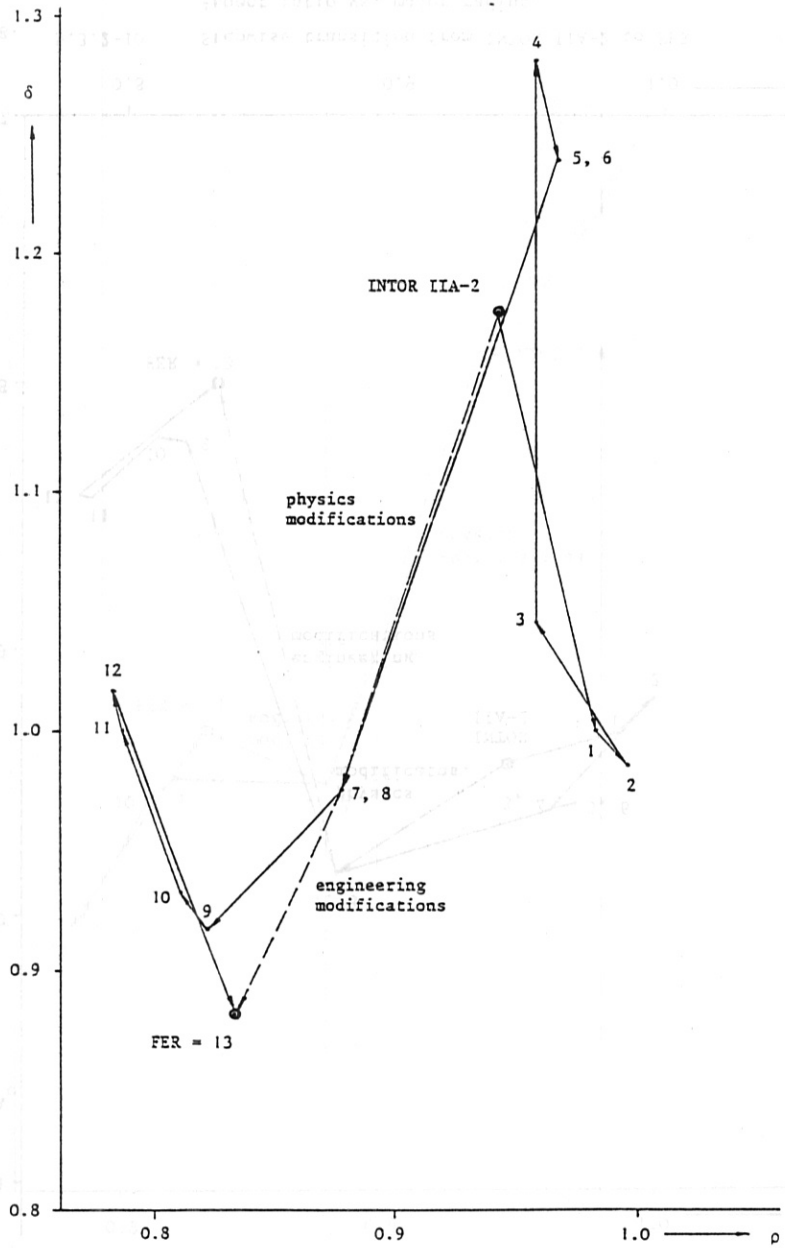

Fig. 5.3.2-8 Stepwise transition from INTOR IIA-2 to FER. Neutron wall load vs. major radius.

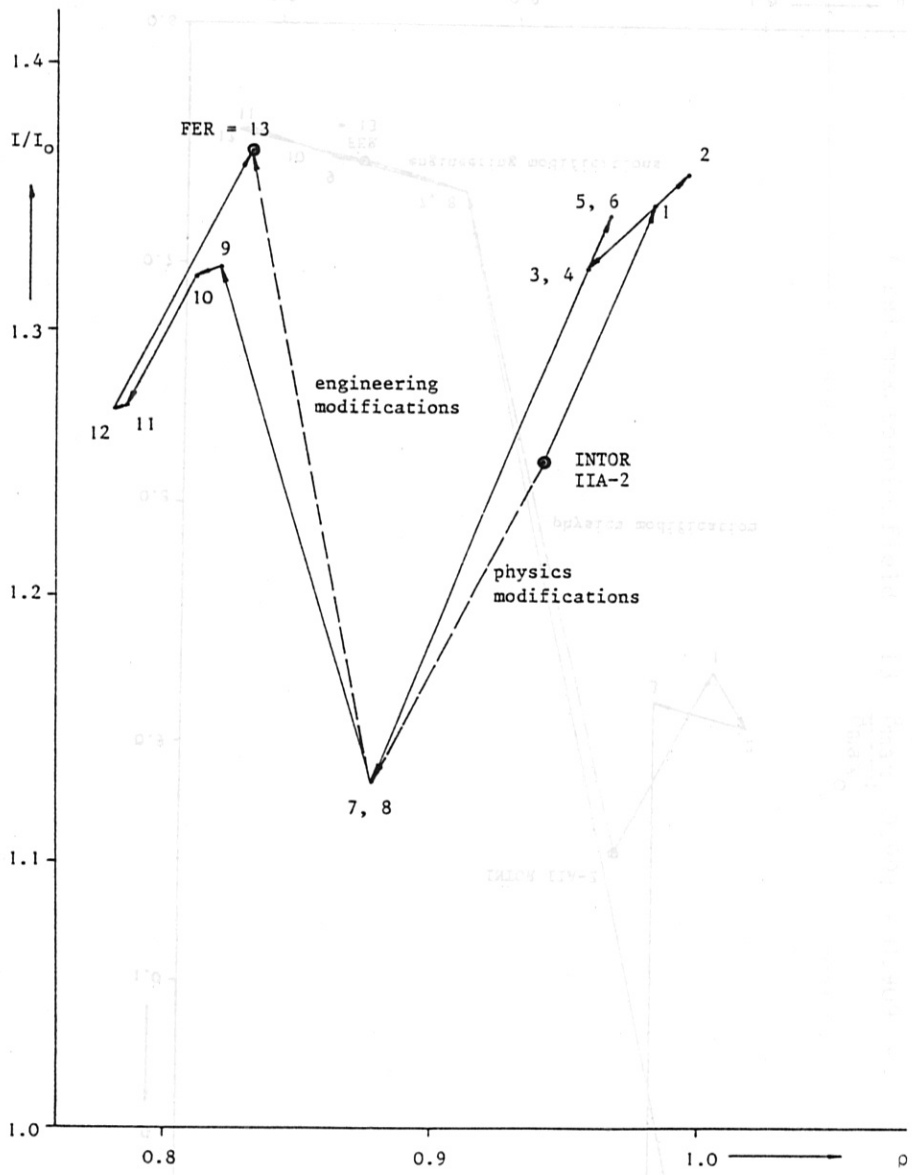

Fig. 5.3.2-9 Stepwise tranition from INTOR IIA-2 to FER.
Plasma current vs. major radius.

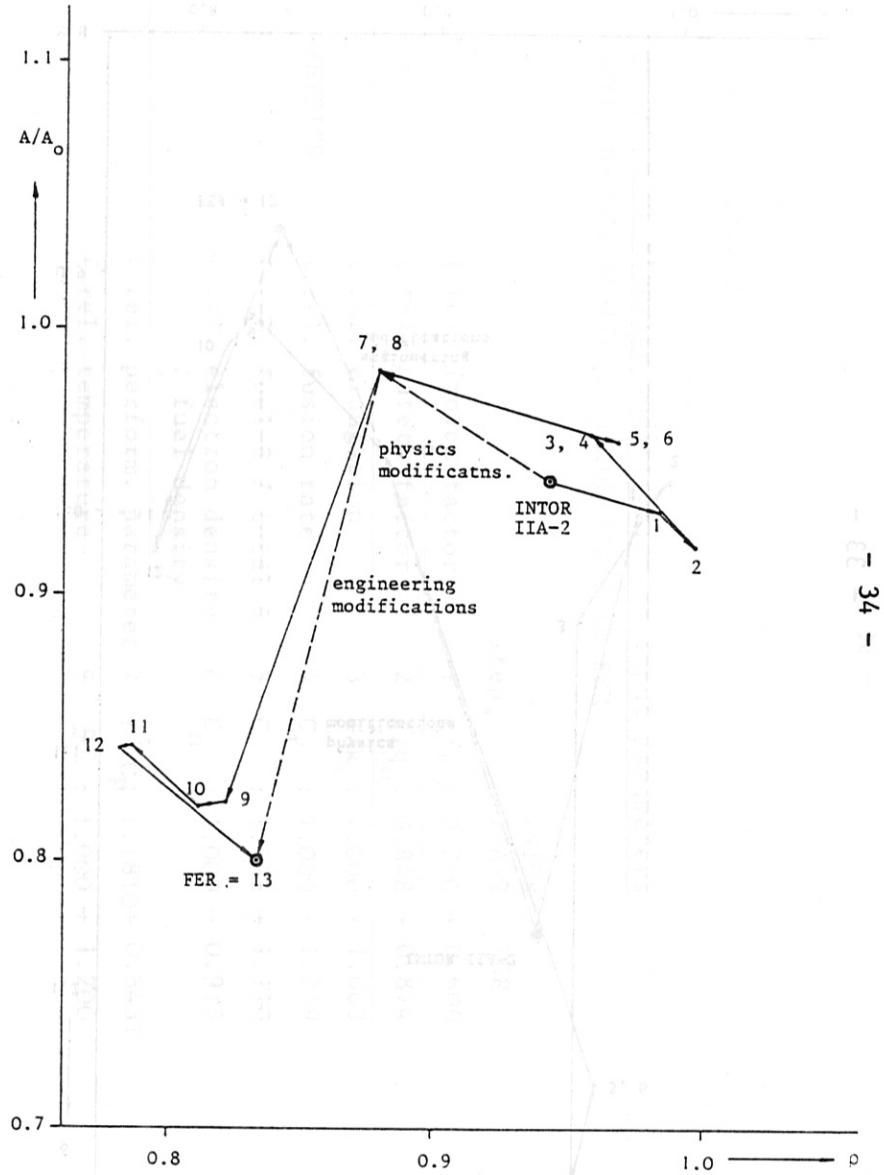

Fig. 5.3.2-10 Stepwise transition from INTOR IIA-2 to FER.
Aspect ratio vs. major radius.

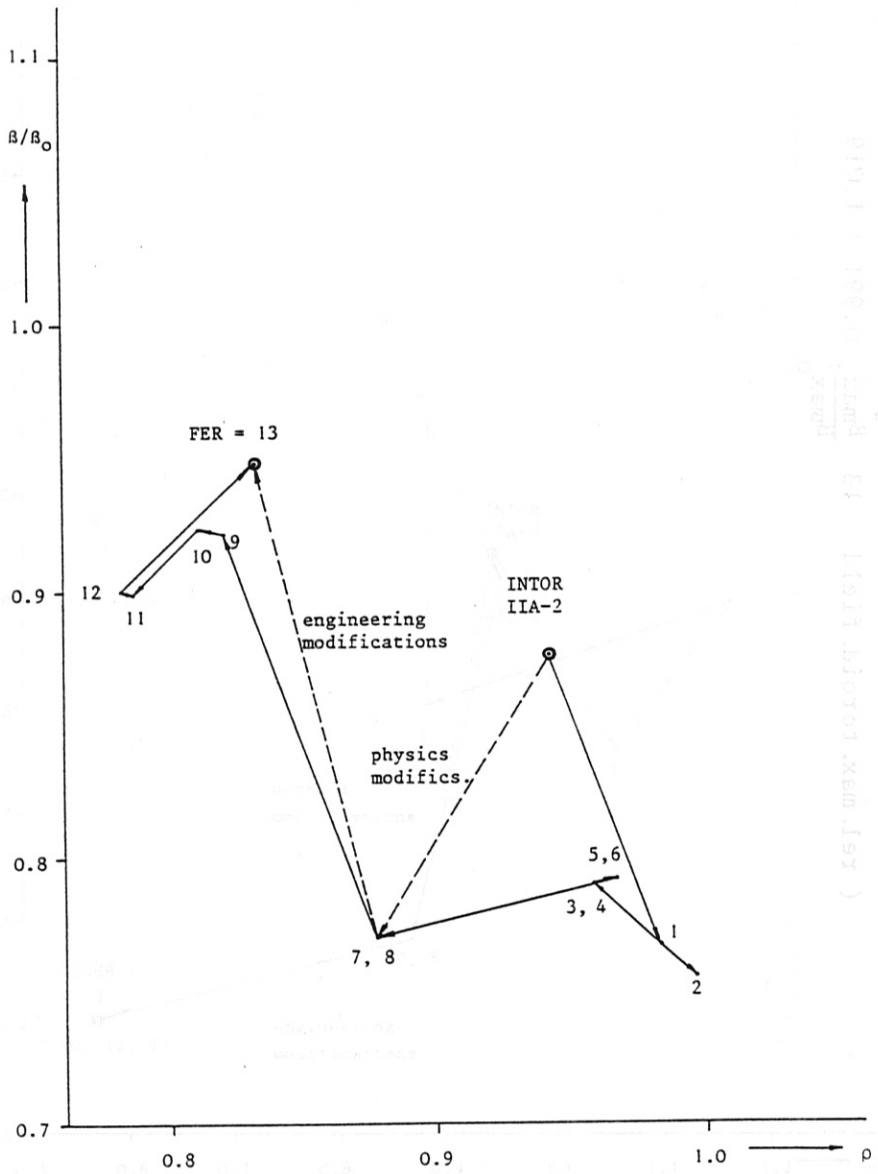

Fig. 5.3.2-11 Stepwise transition from INTOR IIA-2 to FER.
Beta vs. major radius.

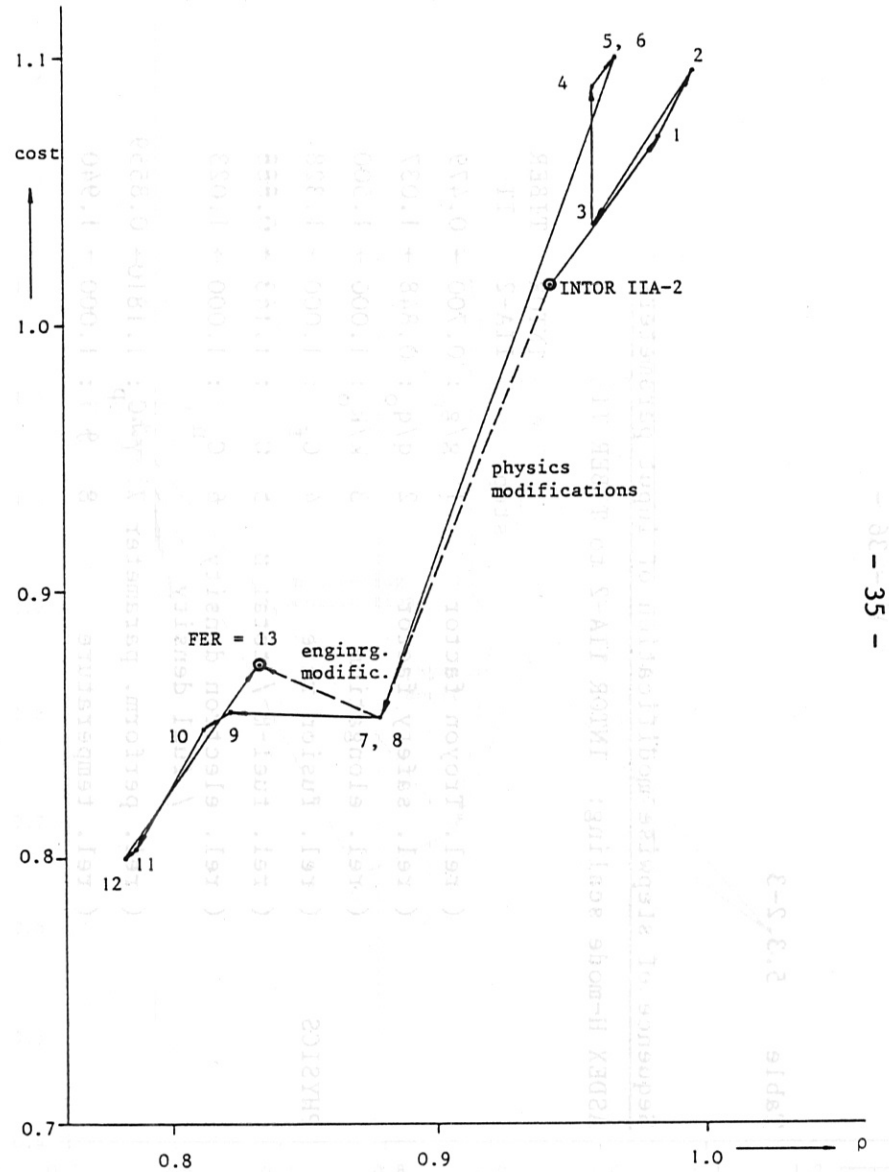

Fig. 5.3.2-12 Stepwise transition from INTOR IIA-2 to FER.
Cost vs. major radius.

Table 5.3.2-3

Sequence of stepwise modification of input parameters

ASDEX H-mode scaling: INTOR IIA-2 to TIBER II

		step		INTOR IIA-2 → TIBER II
PHYSICS	(rel. Troyon factor	1	g/g_o :	0.700 → 0.479
	(rel. safety factor	2	q/q_o :	0.848 → 1.037
	(rel. elongation	3	k/k_o :	1.000 → 1.500
	(rel. fusion rate	4	C_f :	1.000 → 1.328
	(rel. fuel-ß / total ß	5	C :	1.143 → 0.888
	(rel. electron density / fuel density	6	C_n :	1.000 → 1.023
	(rel. perform. parameter	7	$\gamma \mathfrak{H} C_p$:	1.1810 → 0.8559
	(rel. temperature	8	$\mathfrak{H}$:	1.000 → 1.940
ENGINEERING	(geometry factor	9	F_1 :	0.403 → 0.272
	(geometry factor	10	F_2 :	0.241 → 0.137
	(geometry factor	11	F_4 :	0.062 → 0.039
	(geometry factor	12	F_3 :	0.264 → 0.251
	(rel. max. toroid. field	13	$\frac{B_{max}}{B_{max_o}}$:	0.991 → 1.019

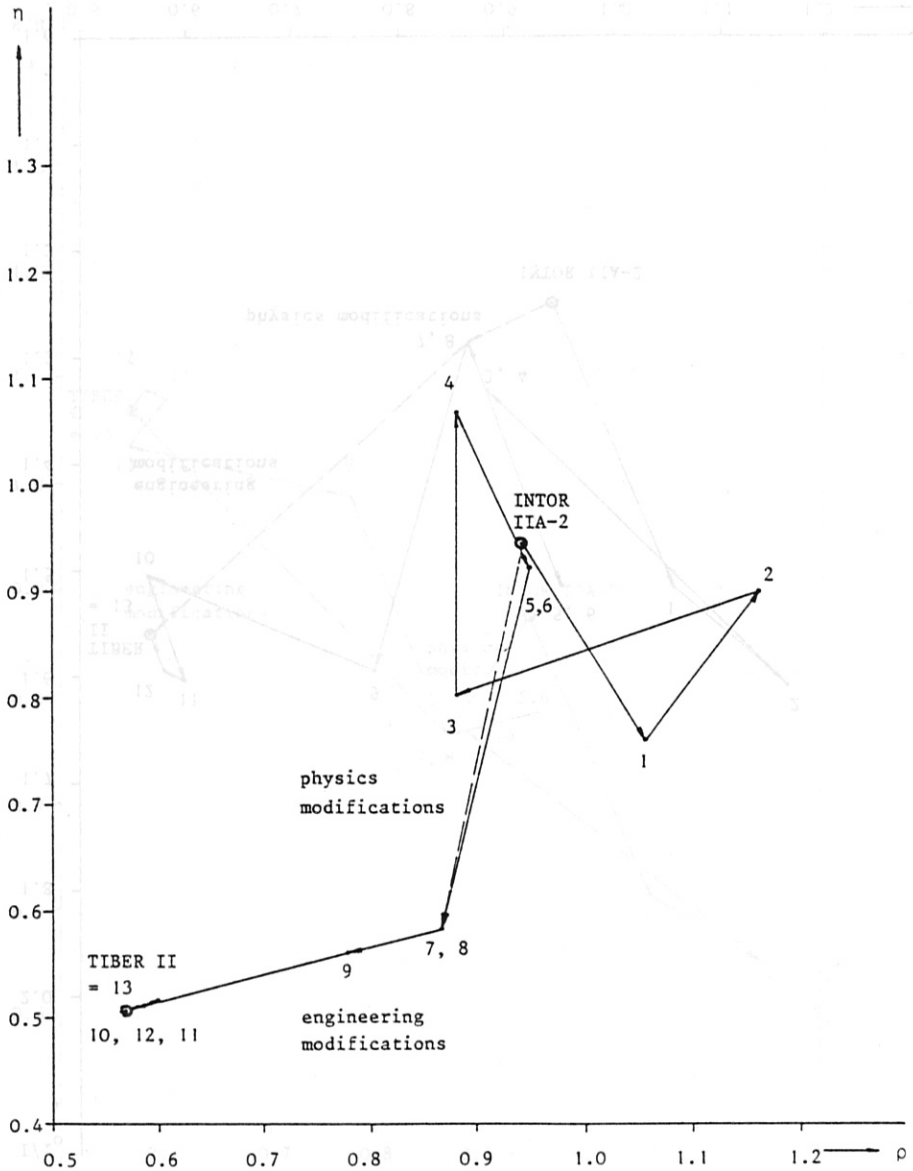

Fig. 5.3.2-13 Stepwise transition from INTOR IIA-2 to TIBER II.
Fusion power vs. major radius.

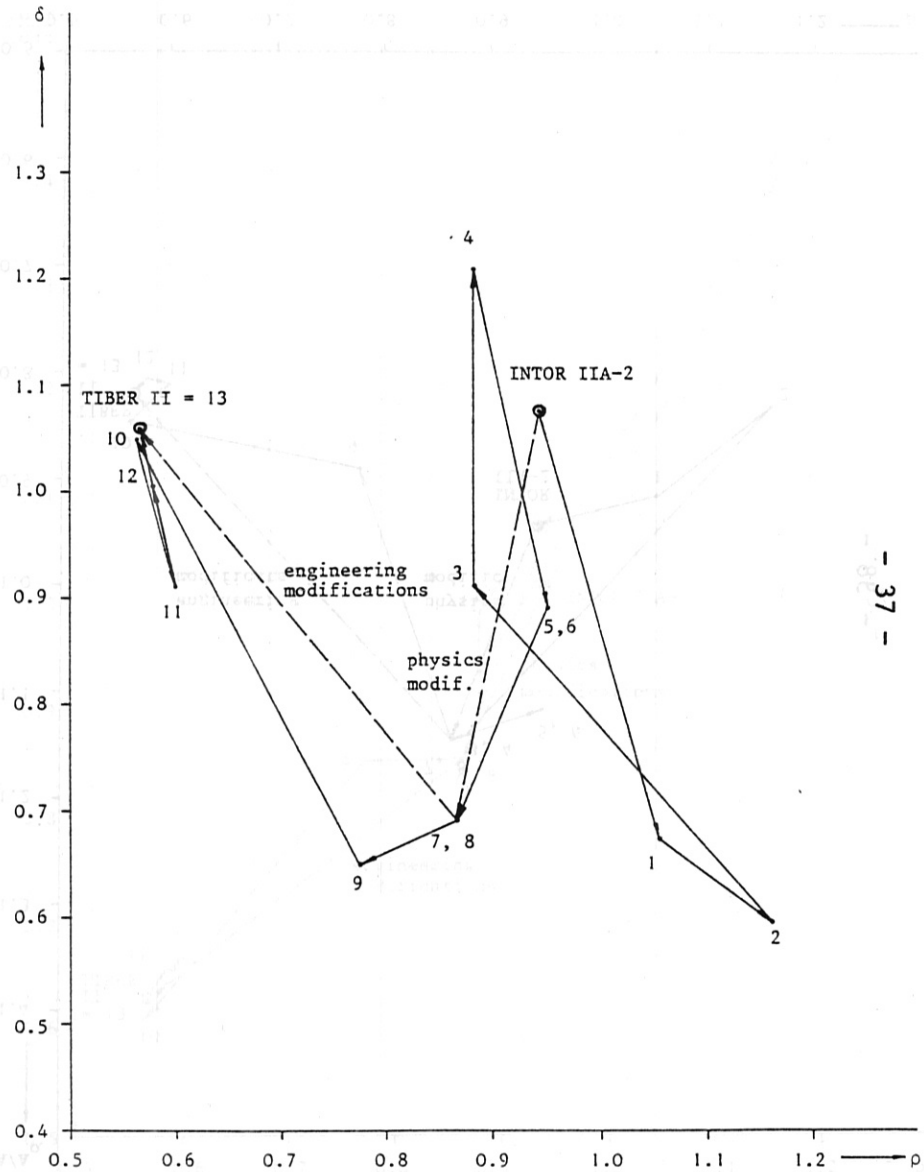

Fig. 5.3.2-14 Stepwise transition from INTOR IIA-2 to TIBER II.
Neutron wall load vs. major radius.

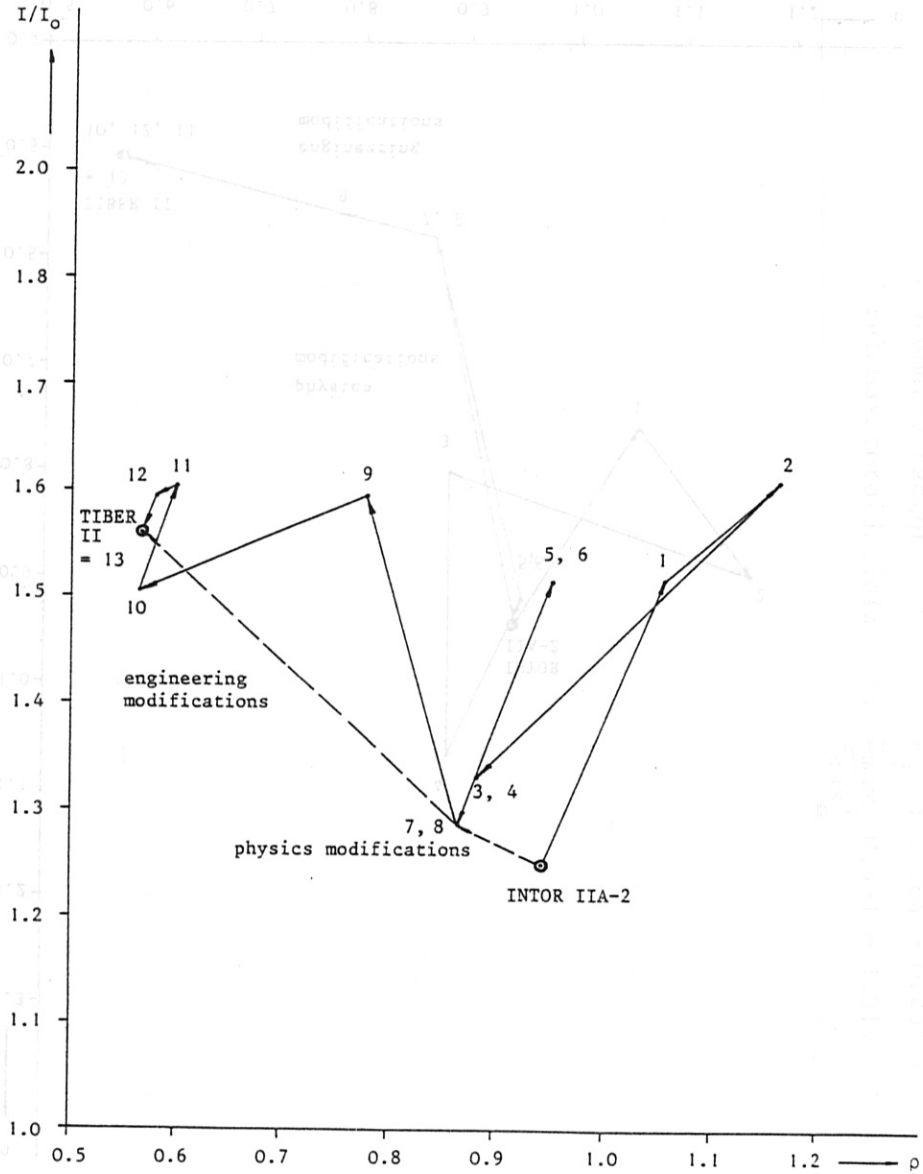

Fig. 5.3.2-15 Stepwise transition from INTOR IIA-2 to TIBER II. Plasma current vs. major radius.

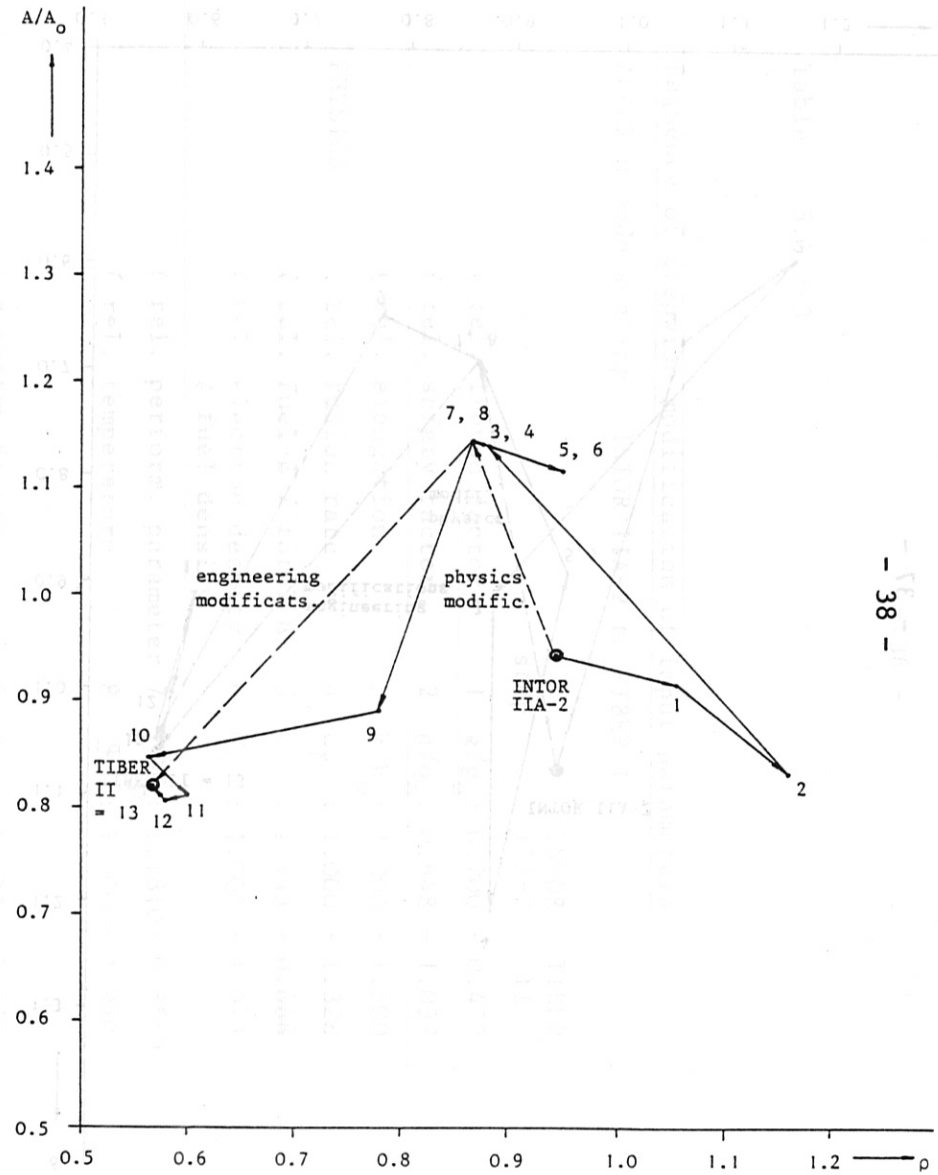

Fig. 5.3.2-16 Stepwise transition from INTOR IIA-2 to TIBER II. Aspect ratio vs. major radius.

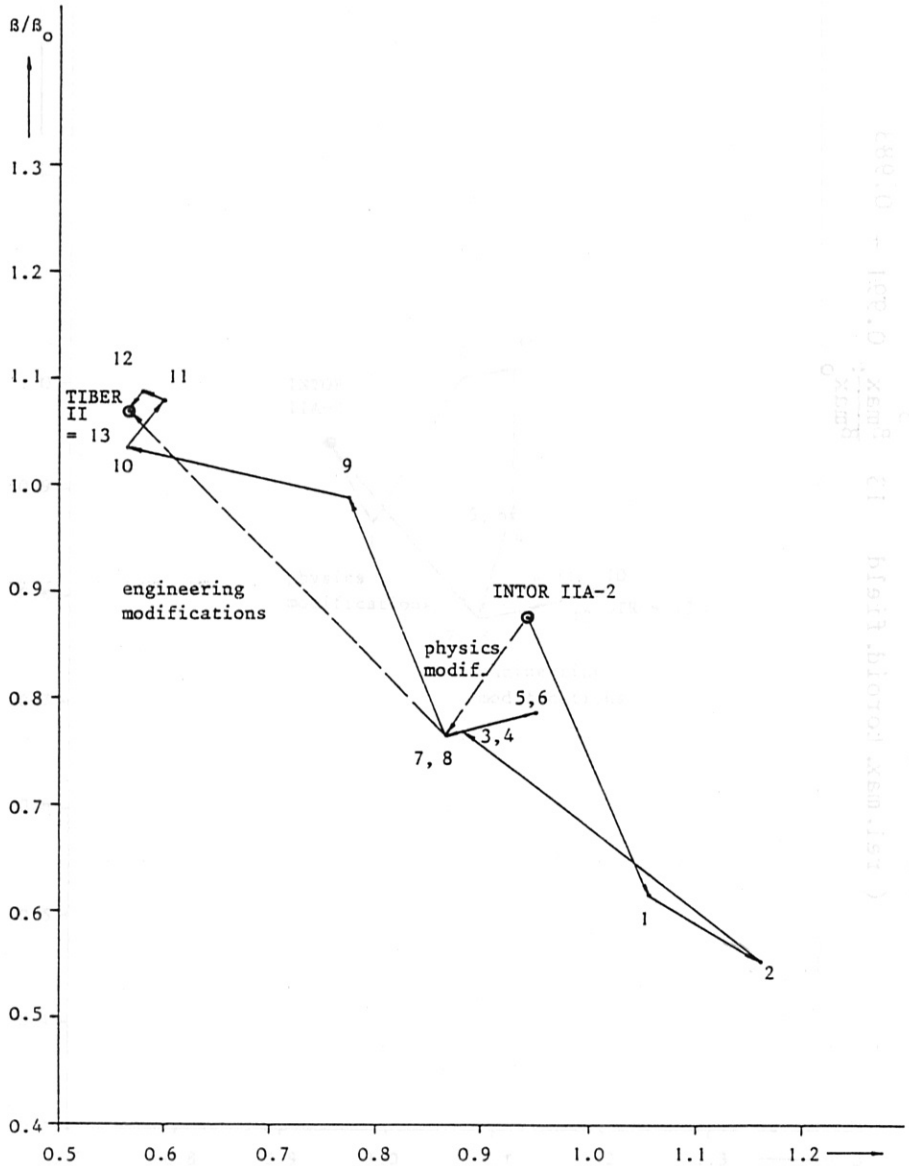

Fig. 5.3.2-17 Stepwise transition from INTOR IIA-2 to TIBER II.
Beta vs. major radius.

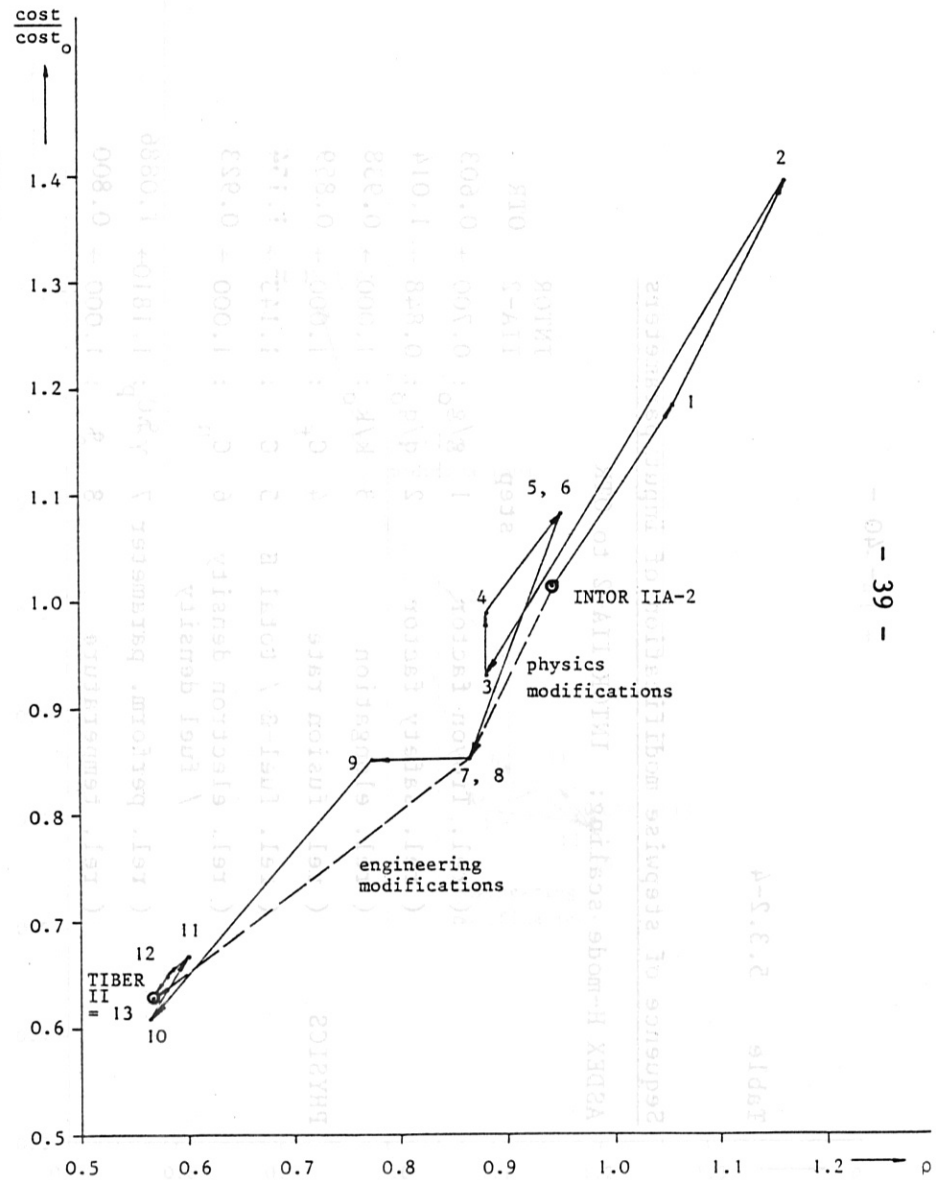

Fig. 5.3.2-18 Stepwise transition from INTOR IIA-2 to TIBER II.
Cost vs. major radius.

Table 5.3.2-4

Sequence of stepwise modification of input parameters

ASDEX H-mode scaling: INTOR IIA-2 to OTR

		step		INTOR IIA-2		OTR
	(rel. Troyon factor	1	g/g_o :	0.700	→	0.603
	(rel. safety factor	2	q/q_o :	0.848	→	1.014
	(rel. elongation	3	k/k_o :	1.000	→	0.938
PHYSICS	(rel. fusion rate	4	C_f :	1.000	→	0.859
	(rel. fuel-ß / total ß	5	C :	1.143	→	1.154
	(rel. electron density / fuel density	6	C_n :	1.000	→	0.923
	(rel. perform. parameter	7	$\gamma \beta C_p$:	1.1810	→	1.0886
	(rel. temperature	8	β :	1.000	→	0.800
	(geometry factor	9	F_1 :	0.403	→	0.476
	(geometry factor	10	F_2 :	0.241	→	0.269
ENGINEERING	(geometry factor	11	F_4 :	0.062	→	0.090
	(geometry factor	12	F_3 :	0.264	→	0.272
	(rel. max. toroid. field	13	$\frac{B_{max}}{B_{max_o}}$:	0.991	→	0.983

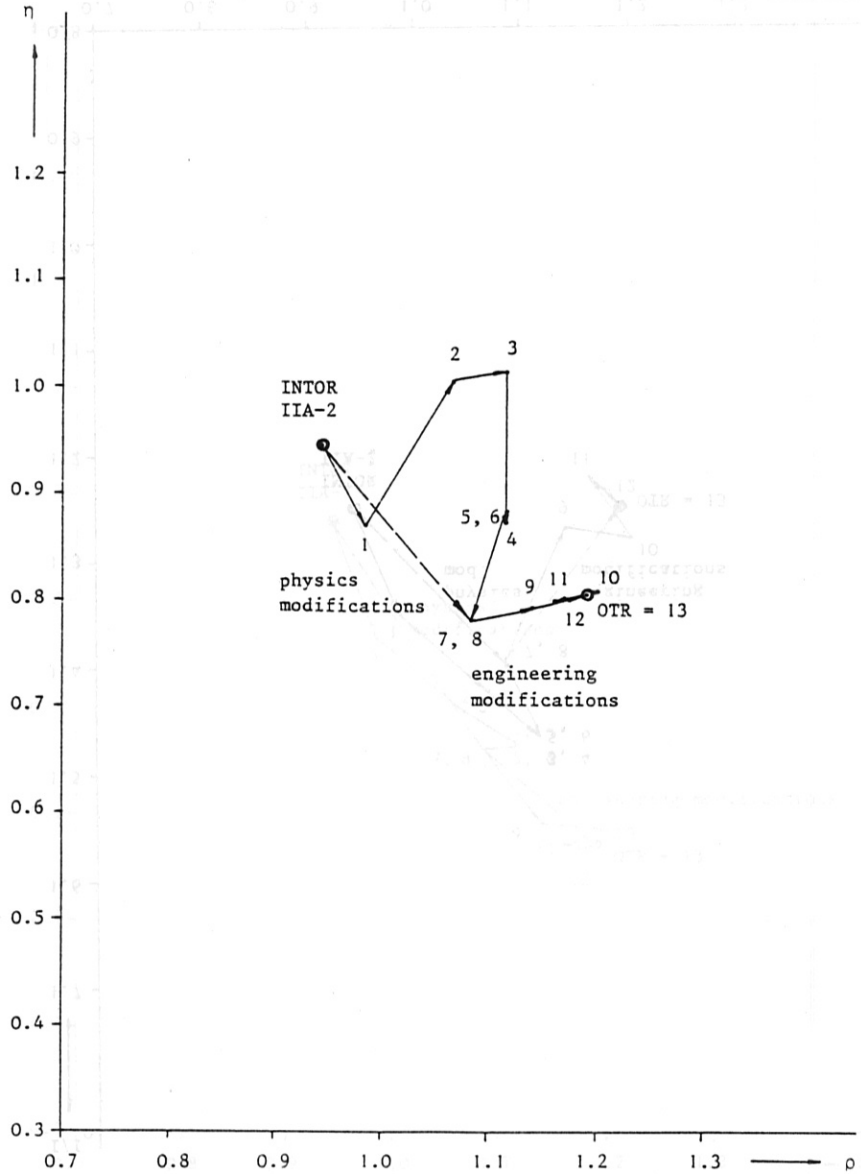

Fig. 5.3.2-19 Stepwise transition from INTOR IIA-2 to OTR. Fusion power vs. major radius.

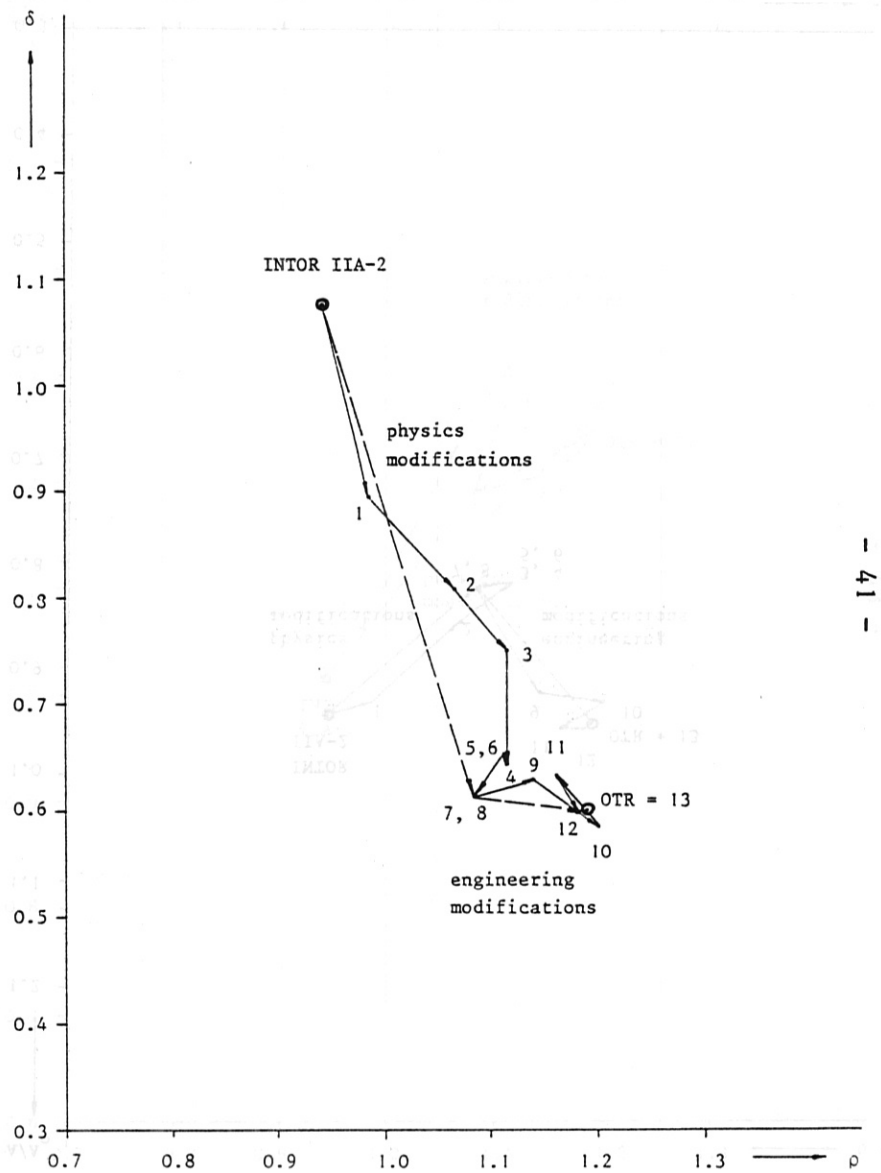

Fig. 5.3.2-20 Stepwise transition from INTOR IIA-2 to OTR. Neutron wall load vs. major radius.

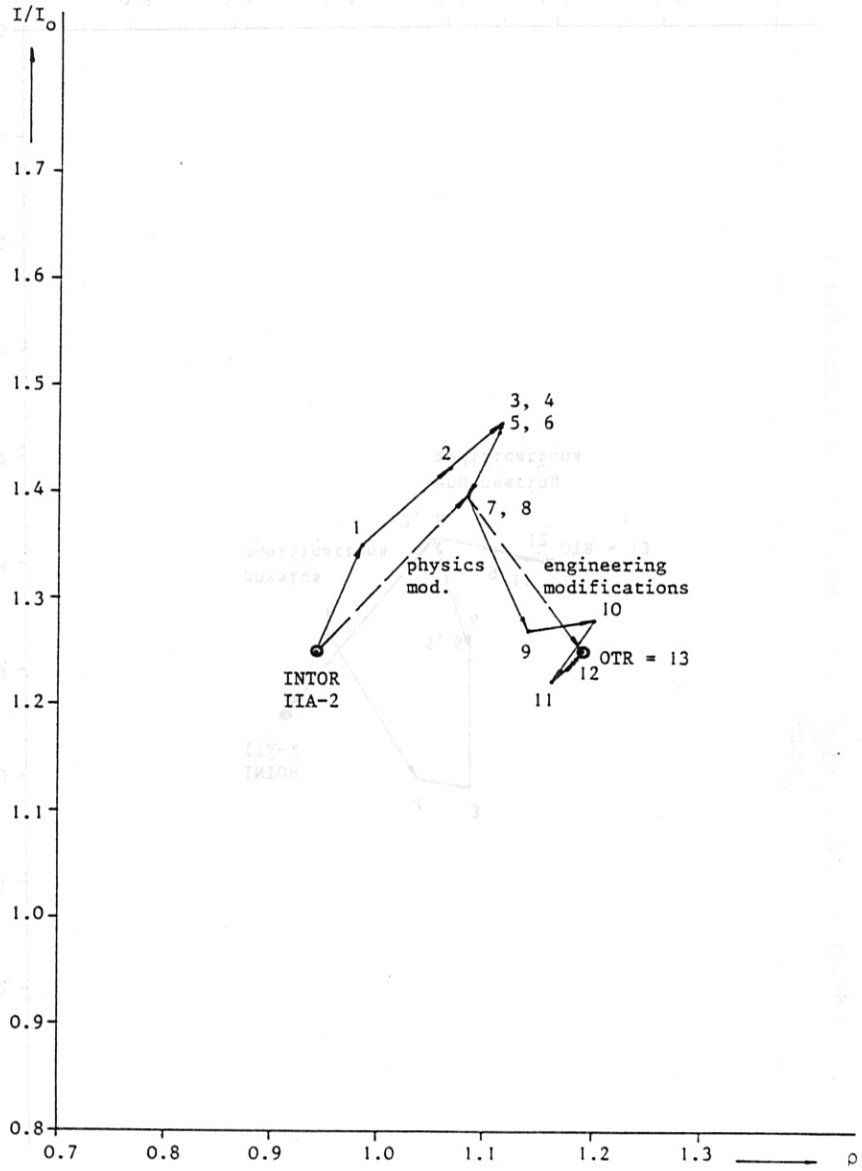

Fig. 5.3.2-21 Stepwise transition from INTOR IIA-2 to OTR.
Plasma current vs. major radius.

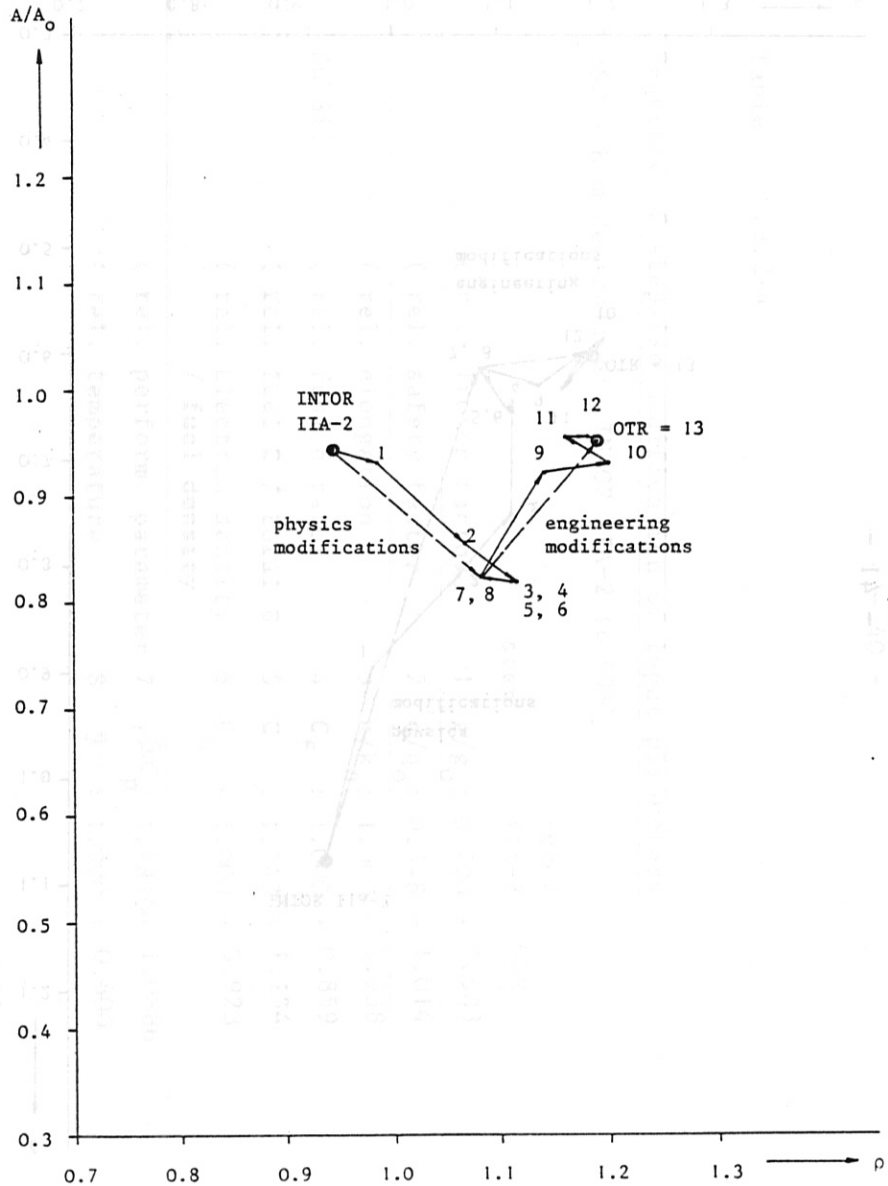

Fig. 5.3.2-22 Stepwise transititon from INTOR IIA-2 to OTR.
Aspect ratio vs. major radius.

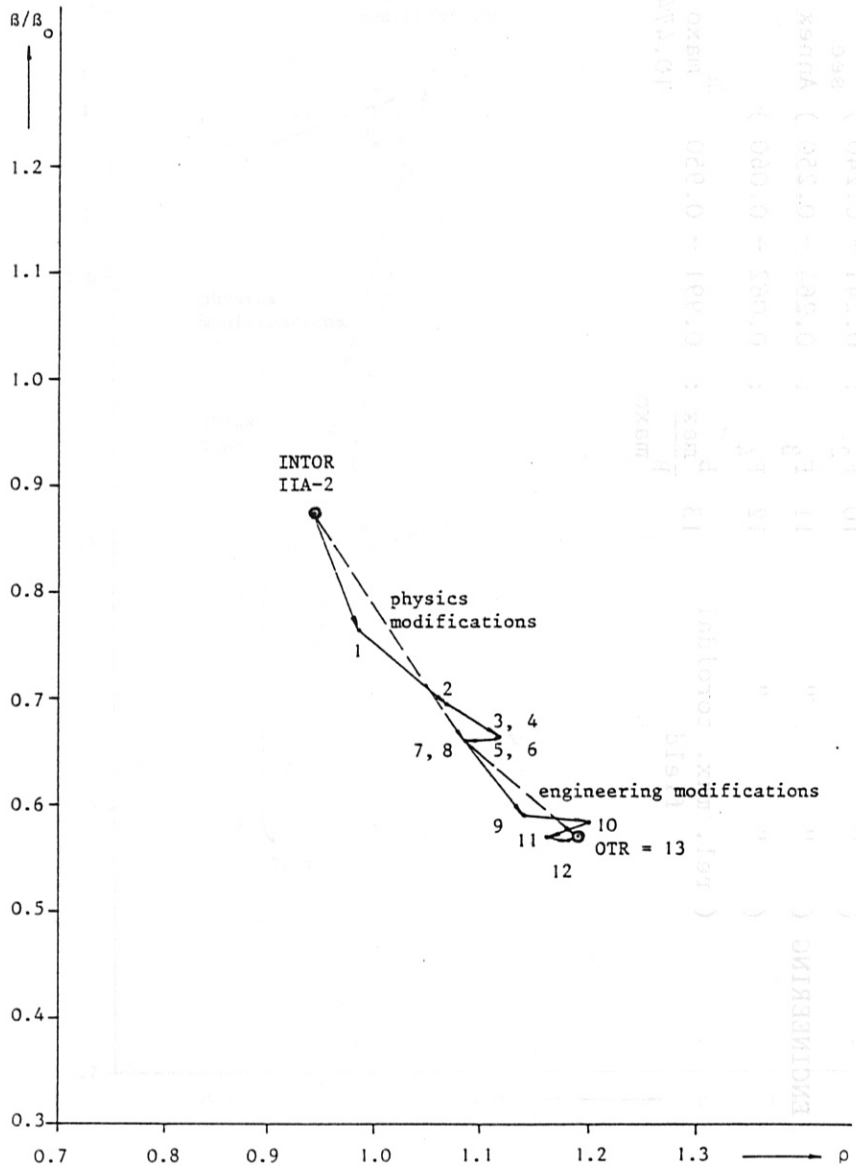

Fig. 5.3.2-23 Stepwise transition from INTOR IIA-2 to OTR.
Beta vs. major radius.

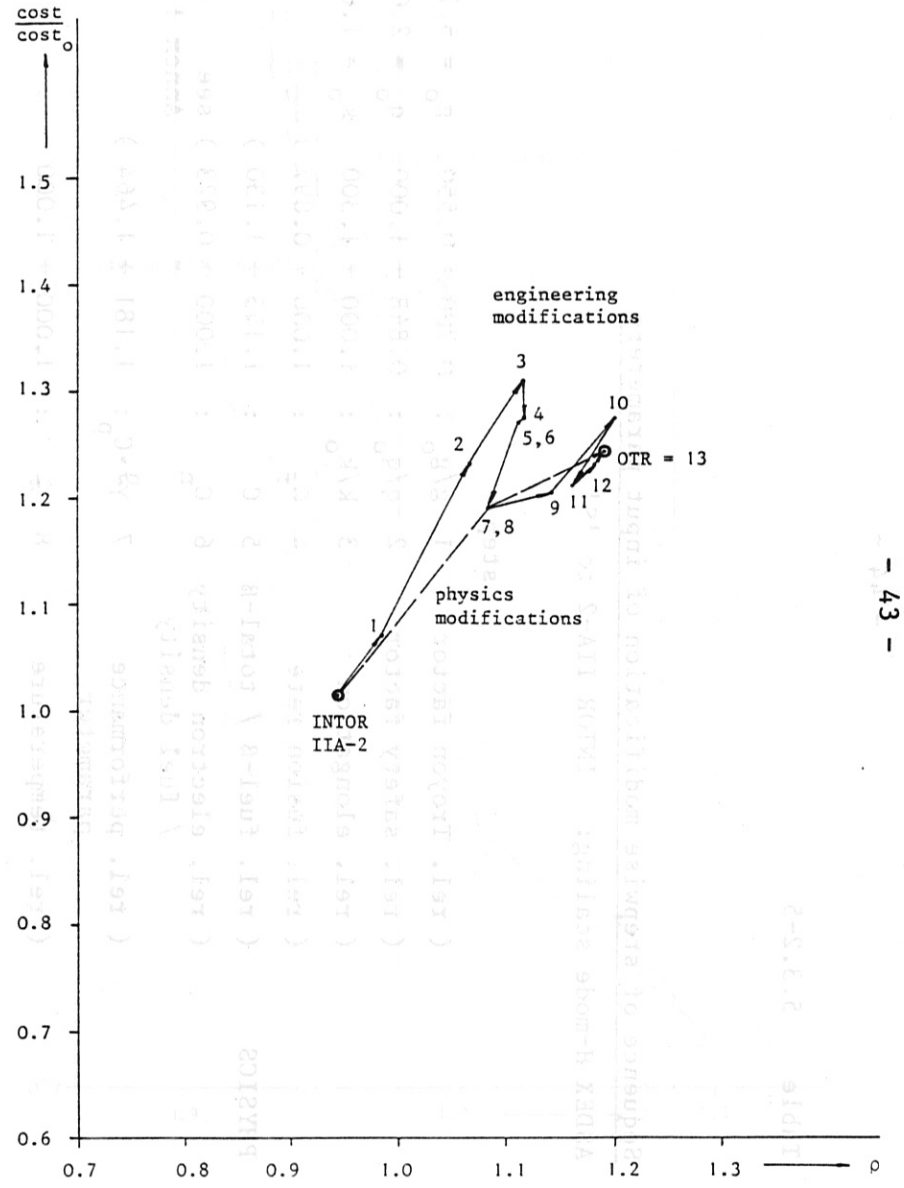

Fig. 5.3.2-24 Stepwise transition from INTOR IIA-2 to OTR.
Cost vs. major radius.

Table 5.3.2-5

Sequence of stepwise modification of input parameters

ASDEX H-mode scaling: INTOR IIA-2 to 'S'

		step			
PHYSICS	(rel. Troyon factor	1	g/g_o :	0.700 → 0.550	g_o = 5.775
	(rel. safety factor	2	q/q_o :	0.848 → 1.000	q_o = 2.078
	(rel. elongation	3	k/k_o :	1.000 → 1.300	k_o = 1.600
	(rel. fusion rate	4	C_f :	1.000 → 0.897)	
	(rel. fuel-ß / total-ß	5	C :	1.143 → 1.130)	
	(rel. electron density / fuel density	6	C_n :	1.000 → 0.923)	see Annex 1
	(rel. performance parameter	7	$\gamma\vartheta \cdot C_p$:	1.181 → 1.464)	
	(rel. temperature	8	ϑ :	1.000 → 1.000	
ENGINEERING	(geometry factor	9	F_1 :	0.403 → 0.380)	
	(" "	10	F_2 :	0.241 → 0.240)	see
	(" "	11	F_3 :	0.264 → 0.250)	Annex 1
	(" "	12	F_4 :	0.062 → 0.060)	
	(rel. max. toroidal field	13	$\frac{B_{max}}{B_{maxo}}$:	0.991 → 0.950	B_{maxo} = 10.474 T

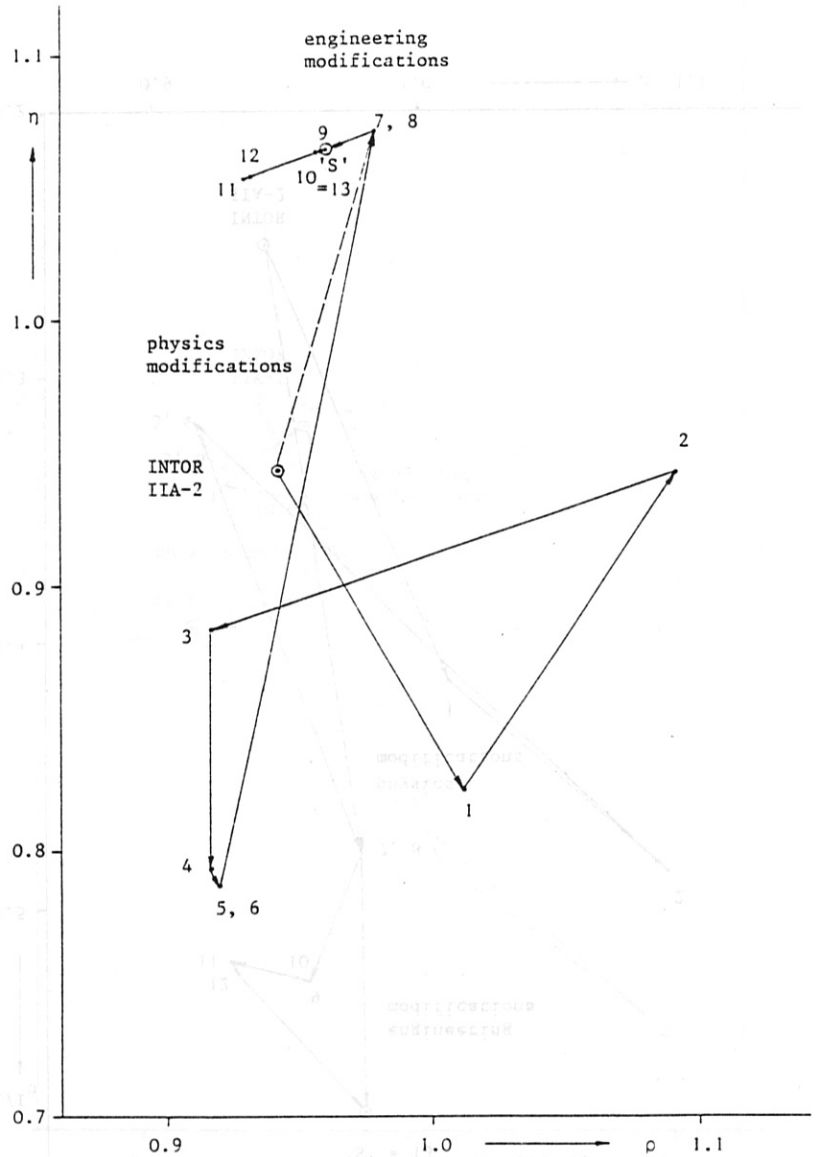

Fig. 5.3.2-25 Stepwise transition from INTOR IIA-2 to 'S'. Fusion power vs. major radius.

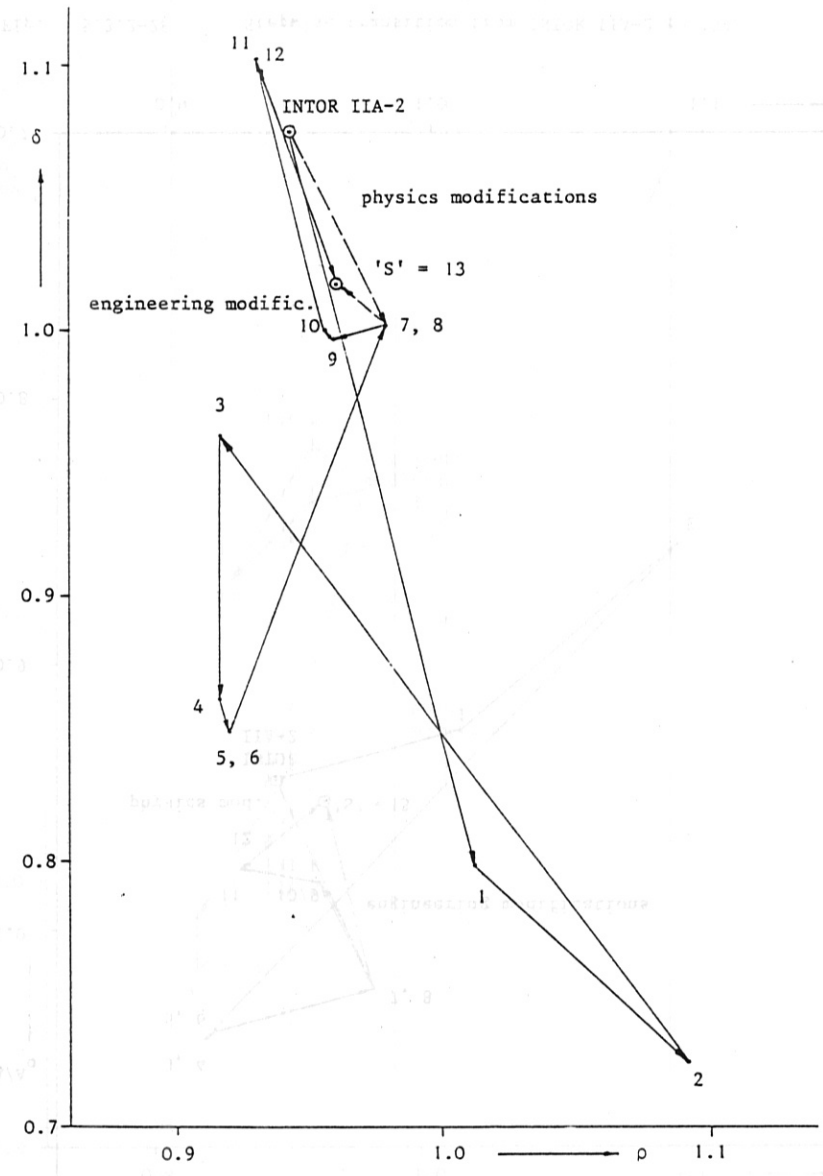

Fig. 5.3.2-26 Stepwise transition from INTOR IIA-2 to 'S'. Neutron wall load vs. major radius.

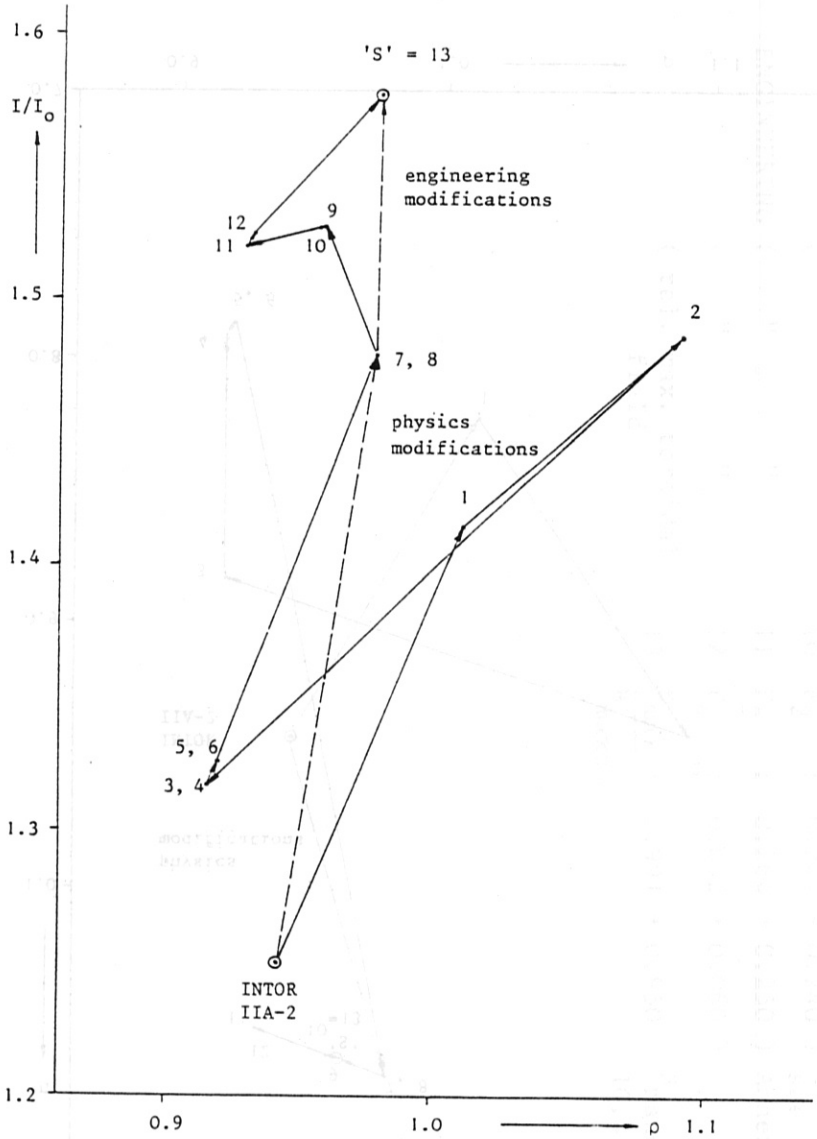

Fig. 5.3.2-27 Stepwise transition from INTOR IIA-2 to 'S'.
Plasma current vs. major radius.

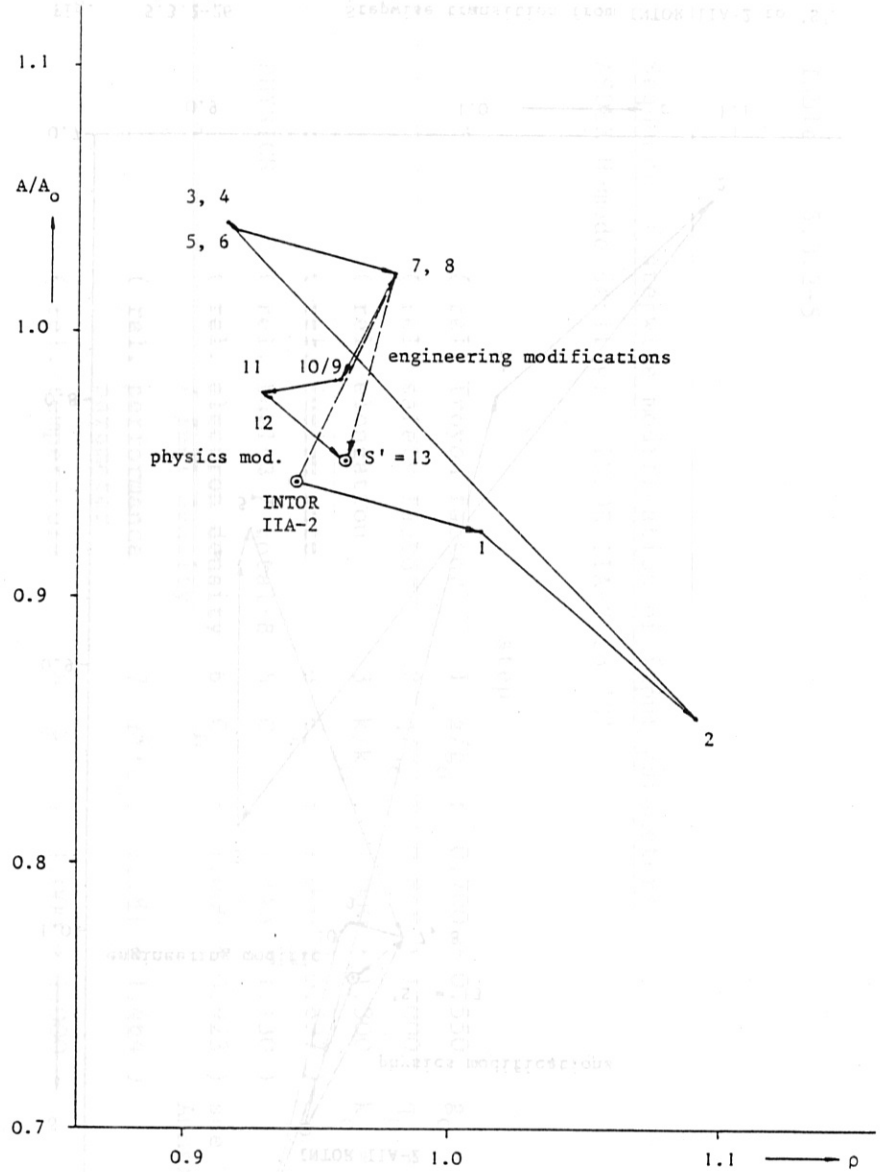

Fig. 5.3.2-28 Stepwise transition from INTOR IIA-2 to 'S'.
Aspect ratio vs. major radius.

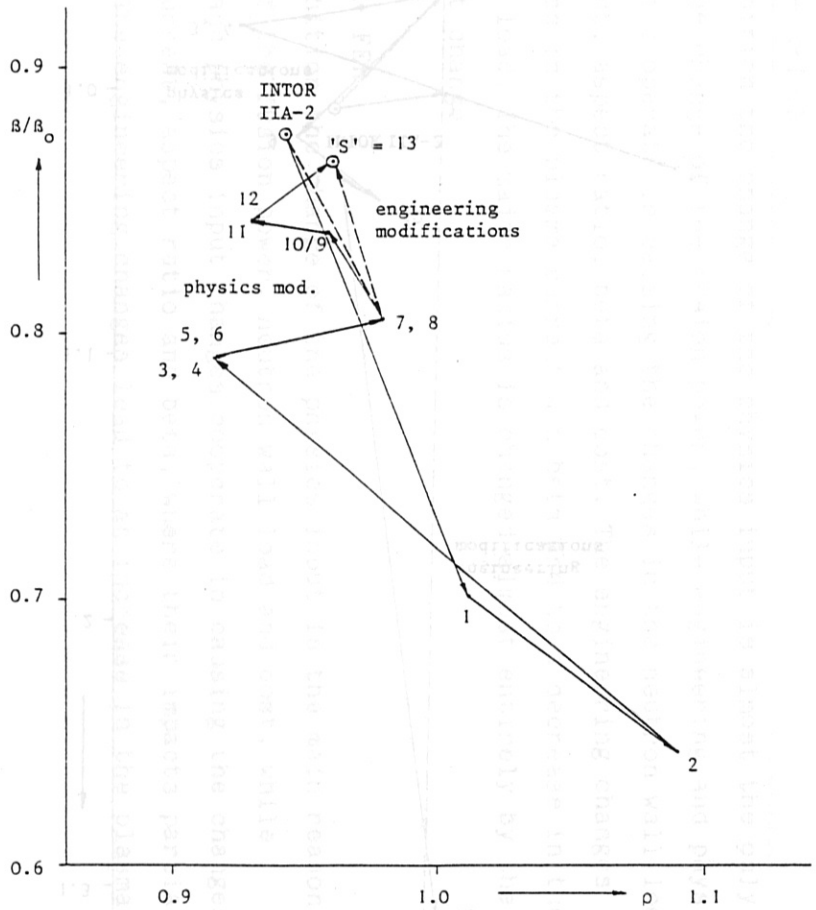

Fig. 5.3.2-29 Stepwise transition from INTOR IIA-2 to 'S'.
Beta vs. major radius.

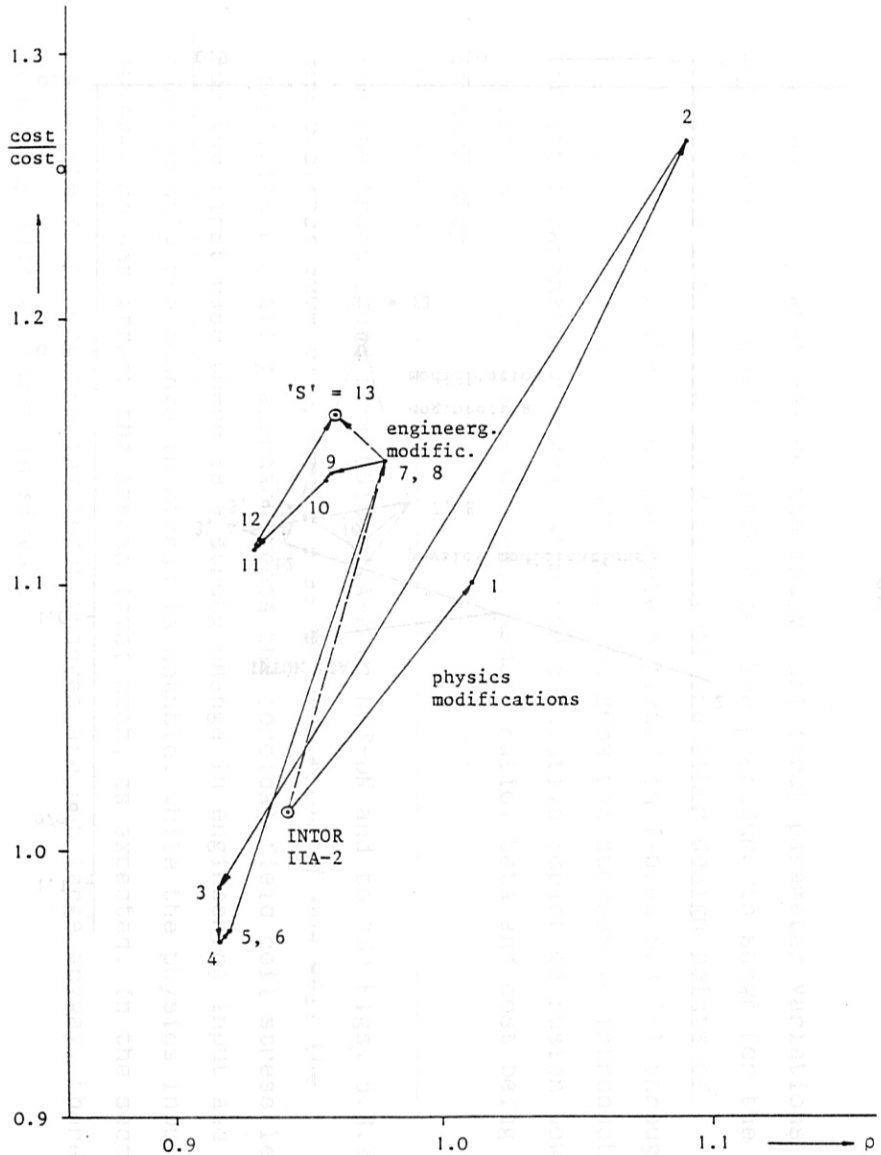

Fig. 5.3.2-30 Stepwise transition from INTOR IIA-2 to 'S'.
Cost vs. major radius.

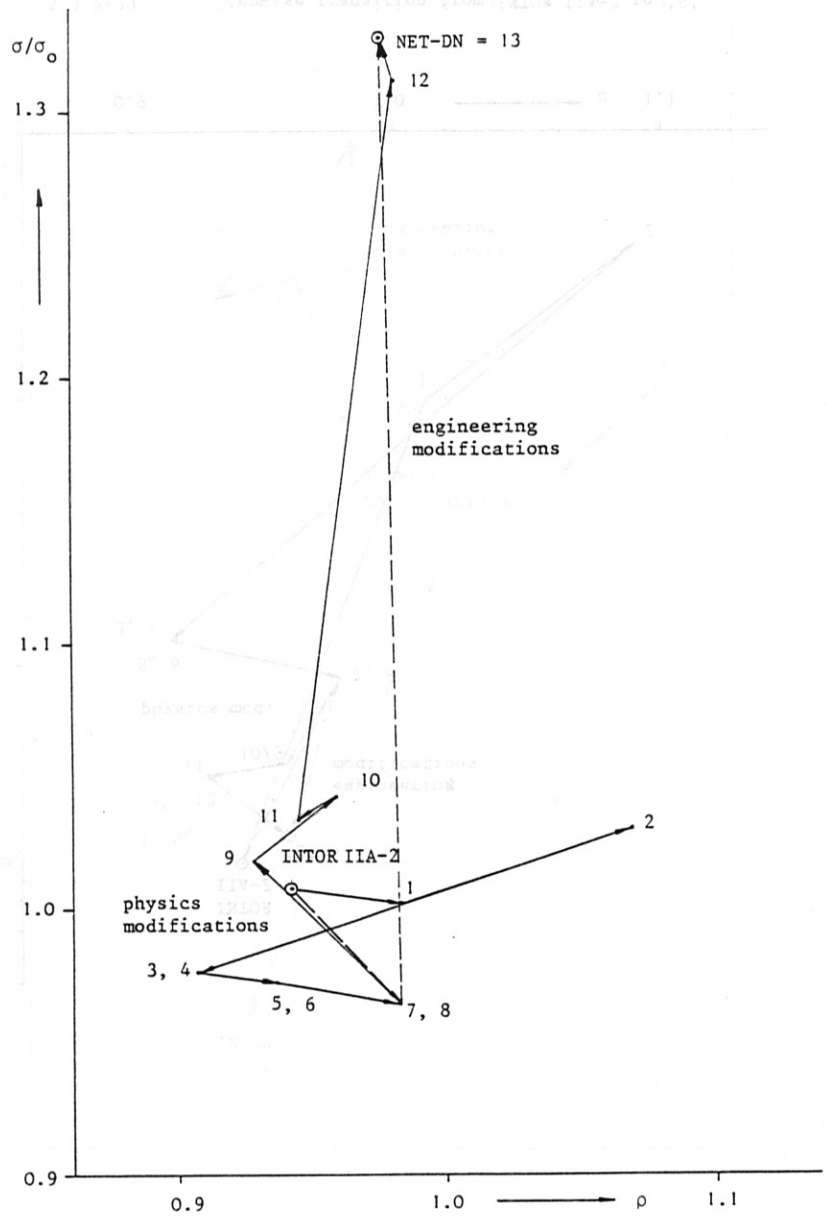

Fig. 5.3.2-31 Stepwise transition from INTOR IIA-2 to NET-DN. Average toroidal field coil tensile stress vs. major radius.

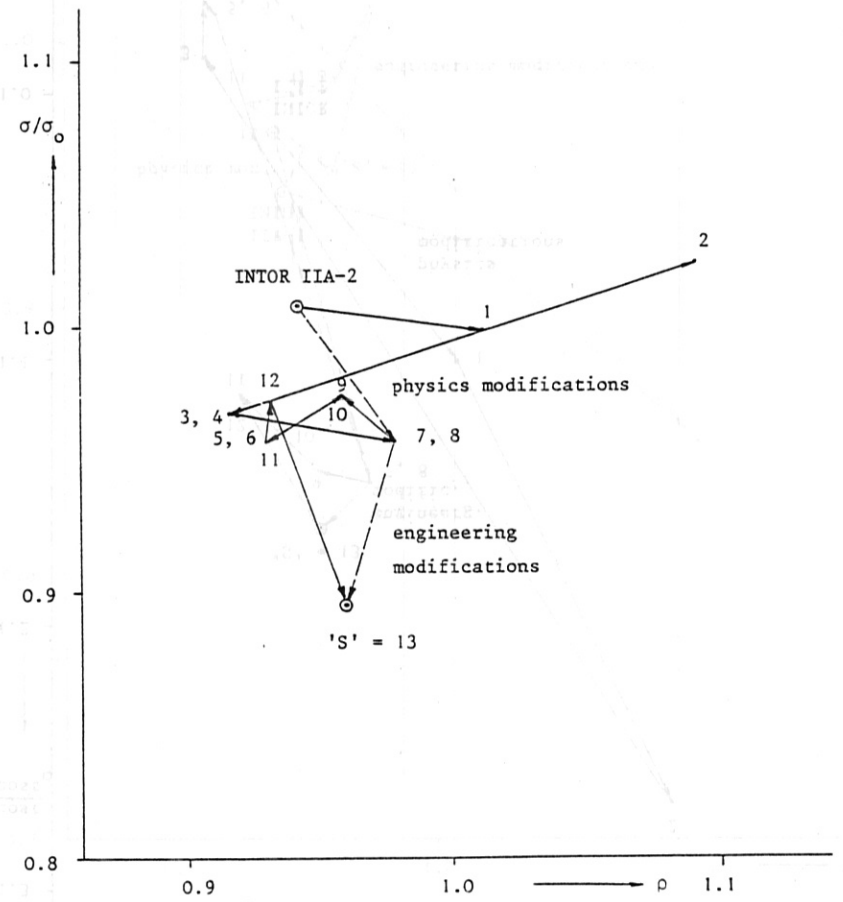

Fig. 5.3.2-32 Stepwise transition from INTOR IIA-2 to 'S'. Average toroidal field coil tensile stress vs. major radius.

the two and to what degree the individual input parameter variations contribute to the overall difference. The procedure is shown for the transitions from INTOR IIA-2 to any of the other design points of Table 2-1. Using the input parameters listed in Tables 5.3.2-1 through 5.3.2-5, Figs. 5.3.2-1 through 5.3.2-30 show the successive introduction of the input parameter changes, with the cumulative impact on fusion power, neutron wall load, plasma current, aspect ratio, beta and cost being seen in each step.

For the transitions from INTOR IIA-2 to NET-DN and to "S" Figs. 5.3.2-31 and 5.3.2-32 show σ/σ_o versus ρ as an indication of how well the simplified rescaling approach keeps the toroidal field coil stress level. For the first case there is a strong change in engineering input and consequently the change in stress is notable, while the physics input changes do not affect the stress level much, as expected. In the second case, where the engineering input changes are not large anyway, there is generally little change in stress.

Below, the various transitions are commented on in an attempt to clarify the major causes of the observed changes in design parameters.

INTOR IIA-2 → NET-DN

In this transition the change of the physics input is almost the only reason for the change of the fusion power, while engineering and physics input changes cooperate in causing the changes in the neutron wall load, plasma current, aspect ratio, beta and cost. The engineering changes lead to an increase in the plasma current and beta and to a decrease in the neutron wall load. The major radius is changed almost entirely by the physics input change.

INTOR IIA-2 → FER

In this transition the change of the physics input is the main reason for the change of the fusion power, neutron wall load and cost, while engineering and physics input changes cooperate in causing the changes in the plasma current, aspect ratio and beta, where their impacts partially compensate. The engineering changes lead to an increase in the plasma

current and beta and to a decrease in the neutron wall load. The major radius is changed by both the engineering and physics input changes.

INTOR IIA-2 → TIBER II

In this transition the change of the physics input mainly causes the change in the fusion power, while the changes in the plasma current, cost and beta are mainly due to changes in the engineering input. The neutron wall load remains nearly the same, because the impacts of engineering and physics input changes cancel. This holds almost equally well for the aspect ratio. Engineering input changes mainly cause the major radius change.

INTOR IIA-2 → OTR

In this transition the change of the physics input is the main reason for the change in the fusion power, neutron wall load, beta and cost, while for the plasma current and the aspect ratio the impacts of engineering and physics input changes nearly cancel. The major radius change is caused by both engineering and physics input changes.

INTOR IIA-2 → "S"

In this transition the change of the physics input is the main reason for the changes in the fusion power, neutron wall load, plasma current and cost, while for the aspect ratio and beta the impacts of physics and engineering input almost cancel. The major radius change is a result of physics and engineering input changes.

It has to be noted that the transitions described above are based on ASDEX H-mode scaling, as mentioned in the parameter list in Table 4-1. The pathway of a transition, however, depends on the confinement scaling assumed. As can be seen from Figs. 5.3.1-1, 5.3.1-4 and 5.3.1-5, the corresponding intermediate data points (for a global exchange of physics and engineering input parameters) are found in rather different positions for the three scalings applied. It can also be seen that the relative importance of the impacts from physics and engineering input changes notably depends on the confinement scaling adopted.

Stepwise transition studies based on a certain confinement scaling can indicate for each design parameter how the impact of individual changes in physics and engineering parameters can add up or cancel. They thus provide a basis for understanding how to tailor, for example, a next-step fusion reactor design for a certain performance.

5.3.3 Sensitivity study of combined input parameter changes

For this study the aforementioned INTOR-like design point "S" was again used (see Table 5.3.1-1). As has been seen in Sections 5.3.1 and 5.3.2, the cumulative impact of input parameter changes is different for each design parameter and could easily lead to undesirable numbers for some of them, e.g. the wall load (see Fig. 5.3.1-2). In order to limit the possible design parameter combinations (still infinite in number) to a certain domain in multiparameter space, the range of input parameter variations is limited to that of Table 5-4 and at the same time desired ranges of the design parameters are given. Changing one of these range definitions or both will shift the resulting domain and vary its size (including cancellation for certain data combinations).

In order to show these effects a number of combined input parameter changes was introduced and selected for fulfilment of two somewhat different design parameter ranges. The listing of alternatives is given in Tables 5.3.3-1 and 5.3.3-2 and the corresponding data points are illustrated in Figs. 5.3.3-1 through 5.3.3-10, showing design parameter points versus the pertaining major radius. These data refer to ASDEX H-mode scaling only. As listed in Table 5.3.3-1, combined parameter changes were introduced first by taking all "best" physics input parameters together with all "best" engineering input parameters which might result in an overall "best" configuration (cases 20, 21). In fact, it can be seen that the dimensions decrease in relation to case "S" and that the performance in terms of fusion power, wall loading and beta notably improves, while cost decreases. The opposite possibility of combining all "worst" physics input parameters with all "worst" engineering parameters leads to a dramatic reduction in performance and increase in dimensions, and hence the corresponding data points are not shown (cases 22, 23). A further "improvement" on cases 20, 21 is possible by increasing the combined radial build of the magnets and

Table 5.3.3-1 List of cases and input parameters as used in the study on the impact of combined input parameter changes (ASDEX H-mode scaling)[++]

Case No.	g/g_o	k/k_o	q/q_o	C	C_f	$\gamma^{\mathcal{S}}$	$\frac{B_{max}}{B_{maxo}}$	F_1	F_2	F_3	F_4
"S"	0.550	1.300	1.000	1.130	0.897	1.627	0.950	0.380	0.240	0.250	0.060
20	0.600	1.375	1.000	1.150	0.950	1.627	1.050	0.330	0.240	0.250	0.040
21	see case 20, but with						0.950				
22[x]	0.500	1.000	1.200	0.850	0.850	1.627	0.900	0.400	0.270	0.270	0.080
23[x]	see case 22, but with						0.950				
24	see case 20, but with										0.080
25	see case 21, but with										0.080
26[x]	see case 22, but with										0.040
27[x]	see case 23, but with										0.040
28	0.600	1.375	1.000	1.150	0.950	1.627	0.900	0.400	0.270	0.270	0.080
29	see case 28, but with						0.950				
30[x]	0.500	1.000	1.200	0.850	0.850	1.627	1.050	0.330	0.240	0.250	0.040
31[x]	see case 30, but with						0.950				
32		1.375	1.096								
33			1.096				1.042				
34				1.150	0.866						
35	0.540			1.150	0.866						
36	0.525	1.375	1.048								
37							1.000	0.361			
38								0.361			0.057
39									0.220		
40								0.361	0.220		0.057
41							1.000	0.361	0.220		0.057

Only the parameters that have been changed are listed. The remaining ones are those of case "S", unless otherwise stated (see also Table 5-4).

Cases with index x lead to design parameters far beyond the range considered here and are not shown in Figs. 5.3.3-1 through 5.3.3-13.

[++]For Mirnov and Kaye-Goldston scaling (Figs. 5.3.3-12 and 5.3.3-13) the $\gamma^{\mathcal{S}}$-value for "S" would be 1.949 and 3.681, respectively.

Table 5.3.3-2 List of cases and input parameters as used in the study on the impact of combined parameter changes (ASDEX H-mode scaling)++

Case No.	g/g_o	k/k_o	q/q_o	C	C_f	$\gamma_{\mathfrak{H}}$	$\frac{B_{max}}{B_{maxo}}$	F_1	F_2	F_3	F_4
"S"	0.550	1.300	1.000	1.130	0.897	1.627	0.950	0.380	0.240	0.250	0.060
1A	0.500					+ 10%					
2A	0.600					- 20%					
2B	0.600					- 10%	0.900				
3A			1.2			+ 10%					
4A	0.600	1.000				+ 10%					
5A		1.375				- 10%					
7A					0.950	- 10%					
15A						- 10%					0.040
24A	see case 24, but with					- 30%	0.950				
25A	see case 24, but with					- 30%	0.950				
28A	see case 28, but with					- 10%					
28B	see case 28, but with					- 20%					
29A	see case 29, but with					- 10%					
29B	see case 29, but with					- 20%					
33A	see case 33, but with						0.950				
37A	see case 37, but with					- 10%					
39A	see case 39, but with					- 10%					
40A	see case 40, but with					- 10%					

Only the parameters that have been changed are listed. The remaining ones are those of case "S", unless otherwise stated (see also Tables 5-4 and 5.3.3-1).

++For Mirnov and Kaye-Goldston scaling (Figs. 5.3.3-12 and 5.3.3-13) the $\gamma_{\mathfrak{H}}$-value for "S" would be 1.949 and 3.681, respectively.

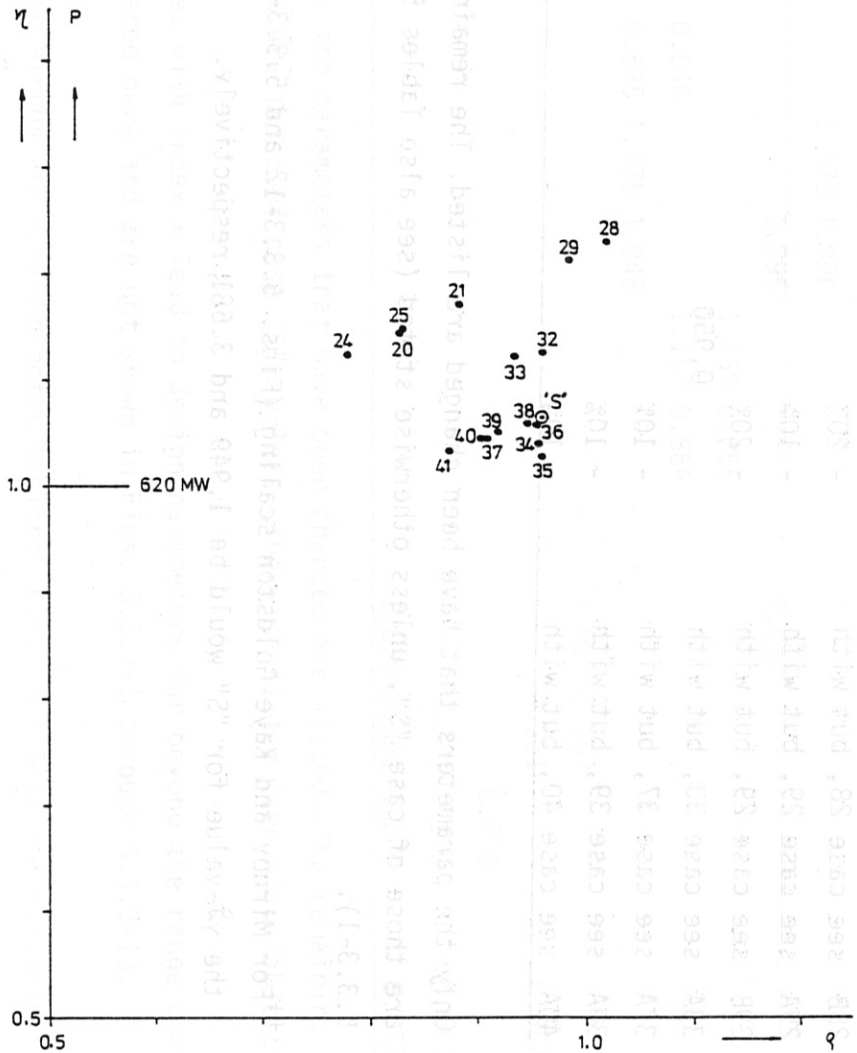

Fig. 5.3.3-1 Fusion power versus major radius.
Sensitivity to combined input parameter changes
(for cases see Table 5.3.3-1, Ref. INTOR IIA-1).

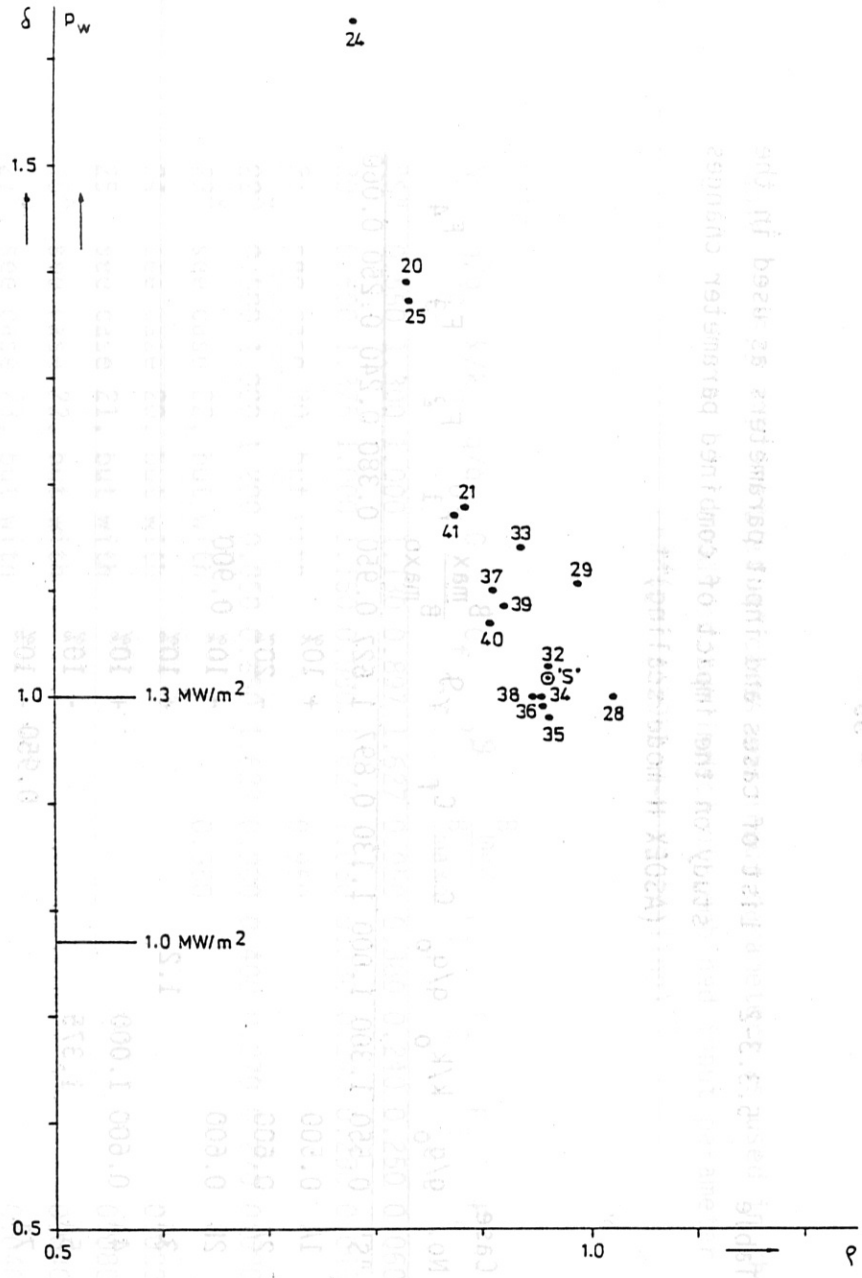

Fig. 5.3.3-2 Neutron wall load vs. major radius.
Sensitivity to combined input parameter changes
(for cases see Table 5.3.3-1, Ref. INTOR IIA-1).

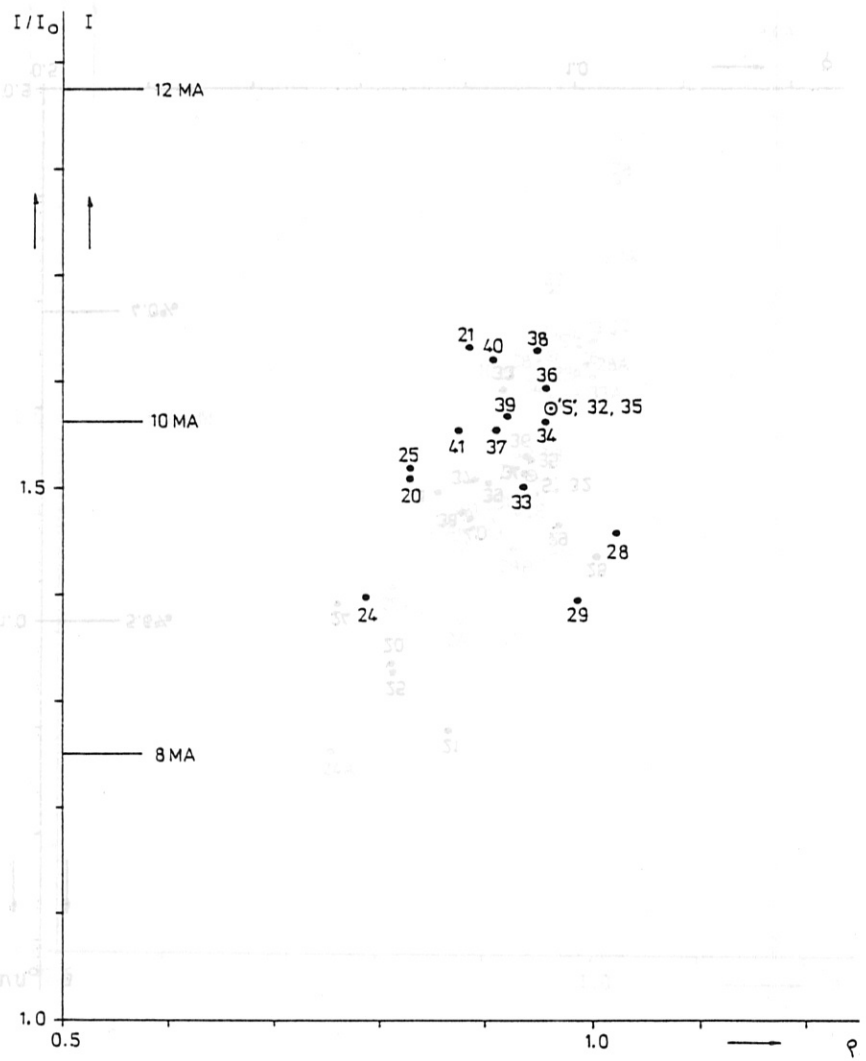

Fig. 5.3.3-3 Plasma current vs. major radius.
Sensitivity to combined input parameter changes
(for cases see Table 5.3.3-1, Ref. INTOR IIA-1).

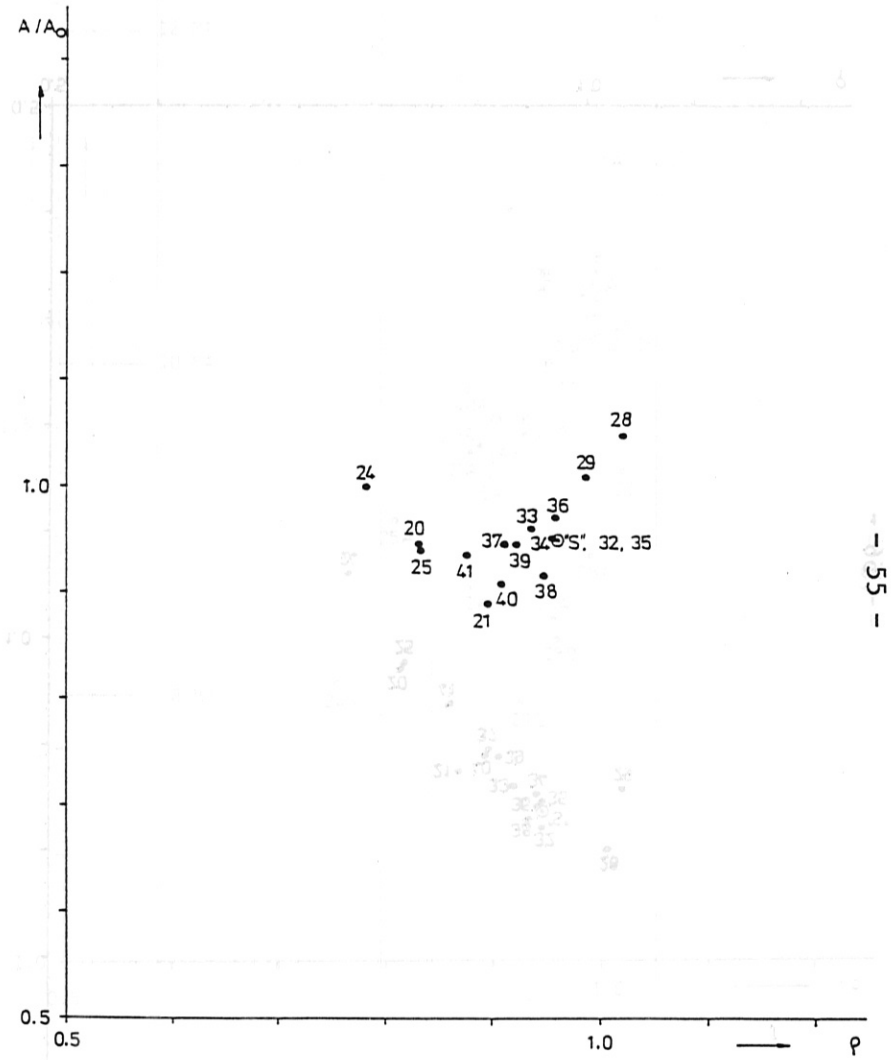

Fig. 5.3.3-4 Aspect ratio vs. major radius.
Sensitivity to combined input parameter changes
(for cases see Table 5.3.3-1, Ref. INTOR IIA-1).

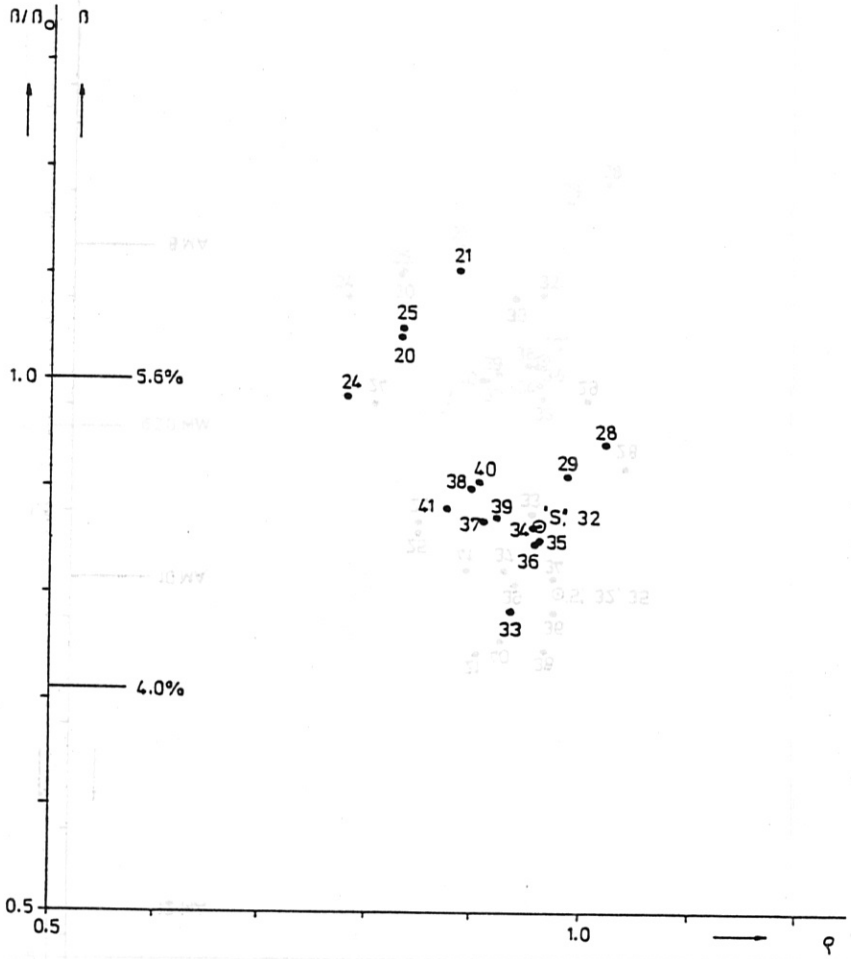

Fig. 5.3.3-5 Total beta vs. major radius.
Sensitivity to combined input parameter changes
(for cases see Table 5.3.3-1, Ref. INTOR IIA-1).

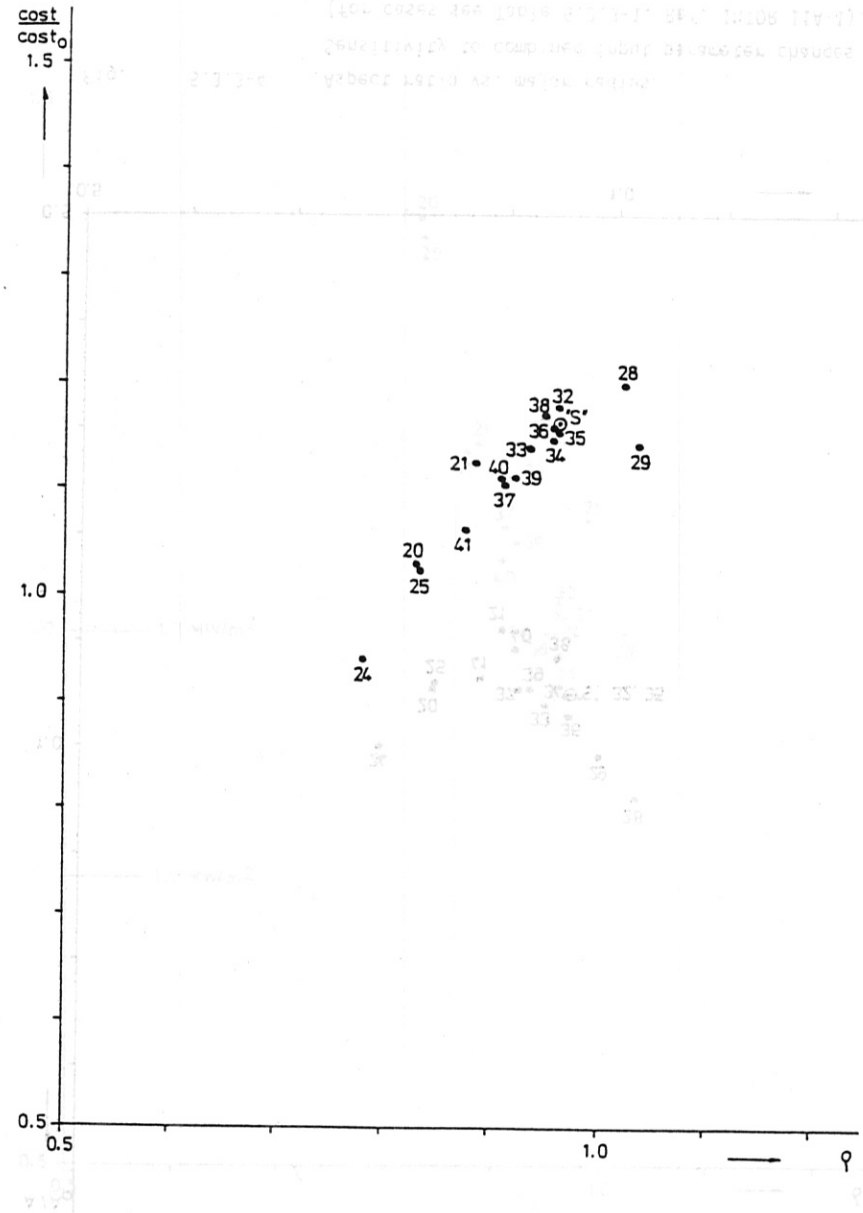

Fig. 5.3.3-6 Cost vs. major radius.
Sensitivity to combined input parameter changes
(for cases see Table 5.3.3-1, Ref. INTOR IIA-1).

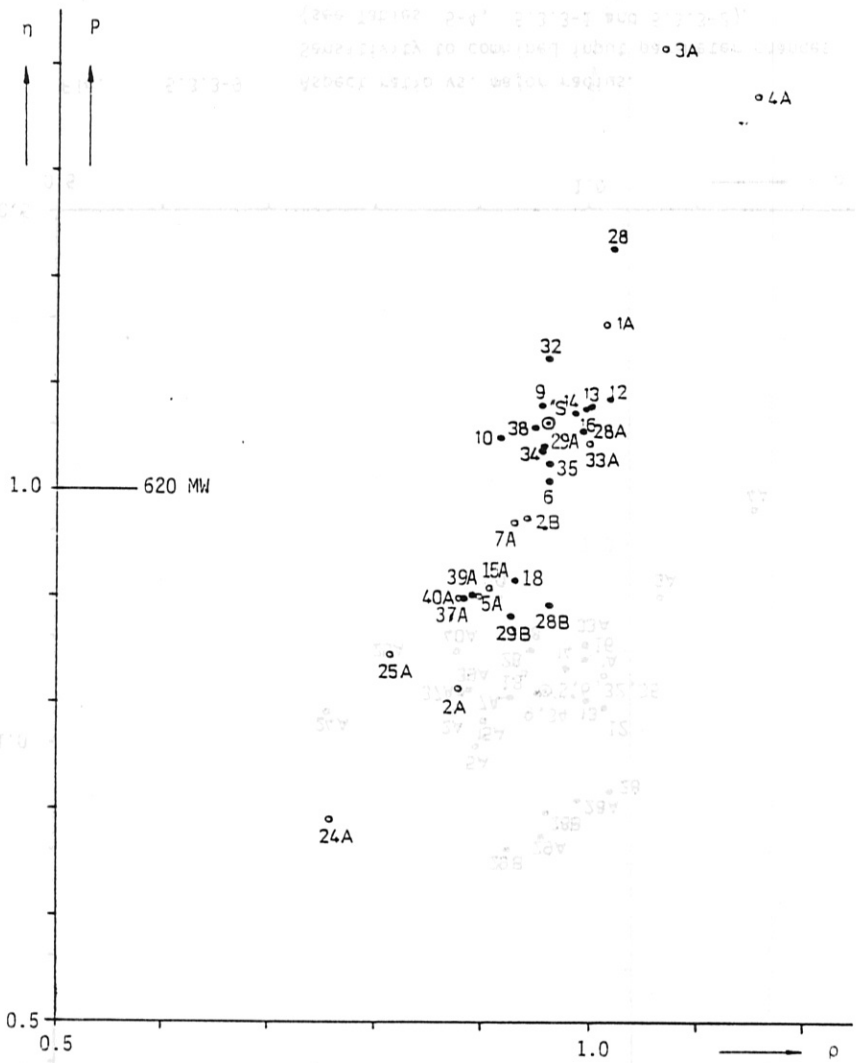

Fig. 5.3.3-7 Fusion power vs. major radius - ASDEX H-mode scaling. Sensitivity to combined input parameter changes (see Tables 5-4, 5.3.3-1 and 5.3.3-2). Accessible design points under constraints I (•) and II (∘) (Reference INTOR IIA-1).

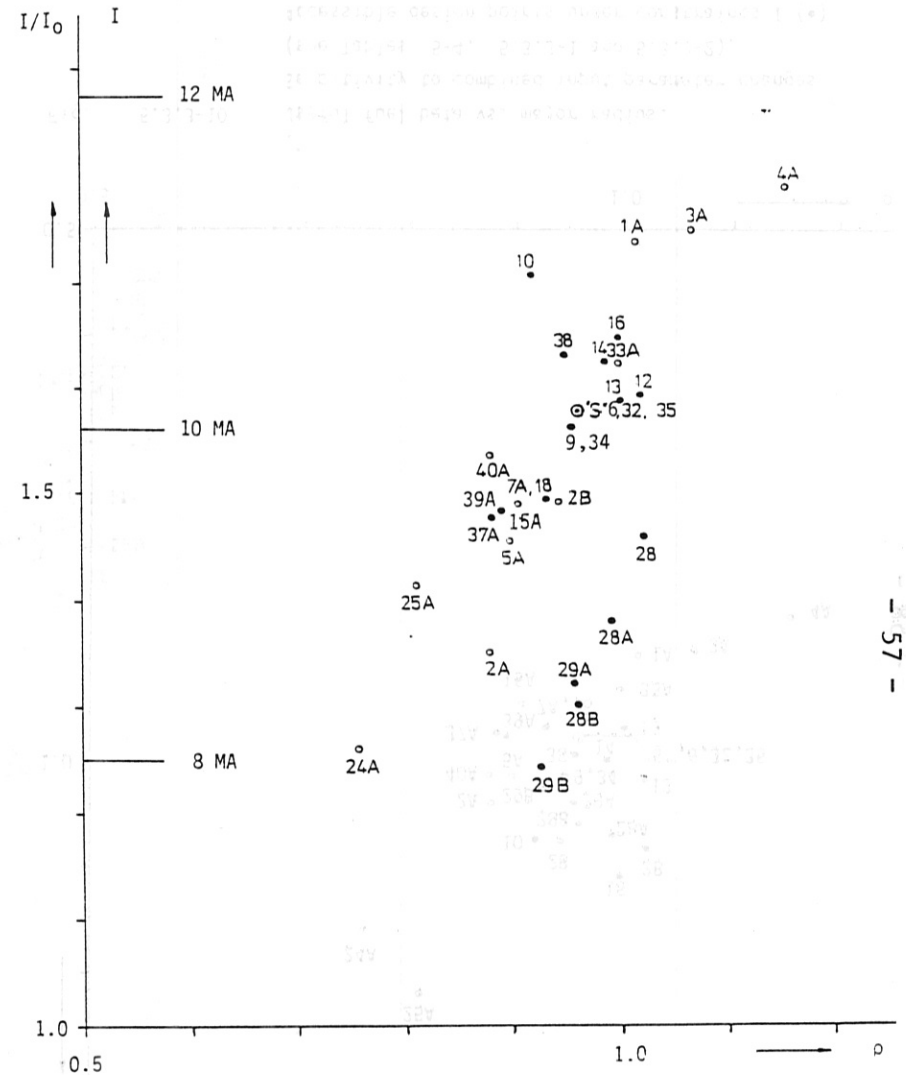

Fig. 5.3.3-8 Plasma current vs. major radius. Sensitivity to combined input parameter changes (see Tables 5-4, 5.3.3-1 and 5.3.3-2). Accessible design points under constraints I (•) and II (∘) (Reference INTOR IIA-1).

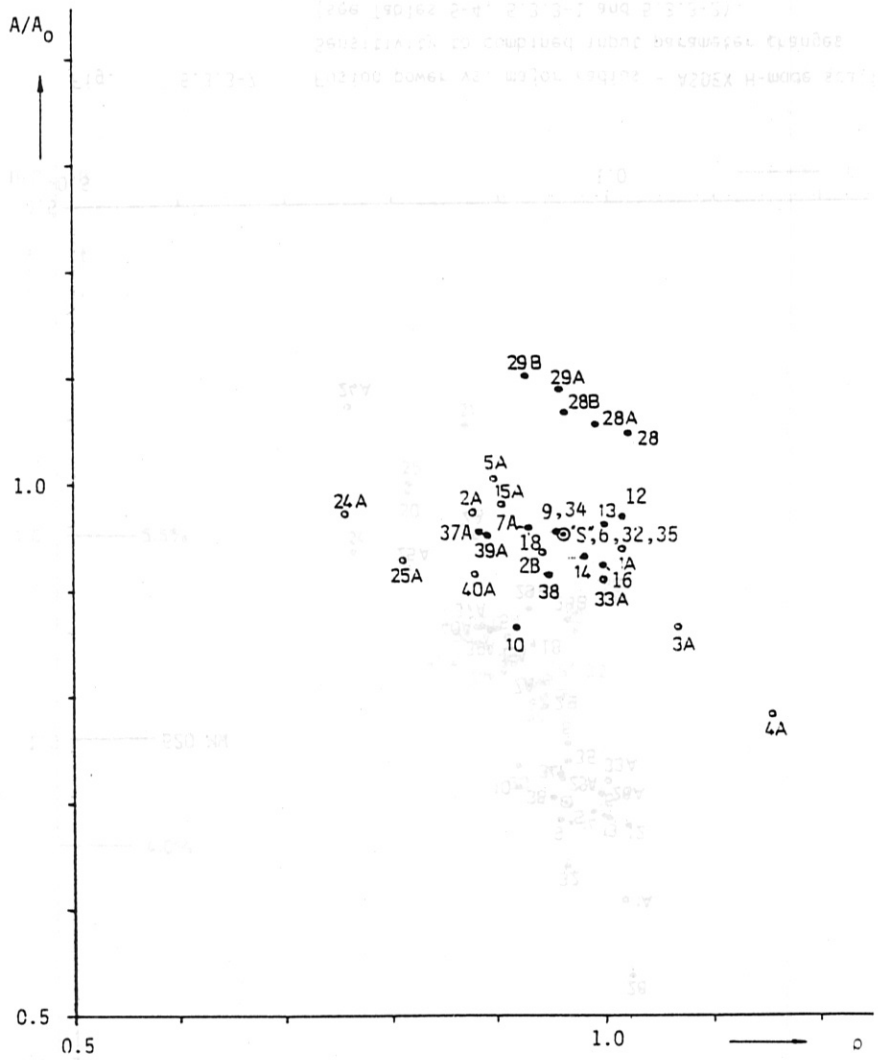

Fig. 5.3.3-9 Aspect ratio vs. major radius.
Sensitivity to combined input parameter changes
(see Tables 5-4, 5.3.3-1 and 5.3.3-2).
Accessible design points under constraints I (•)
and II (∘) (Reference INTOR IIA-1).

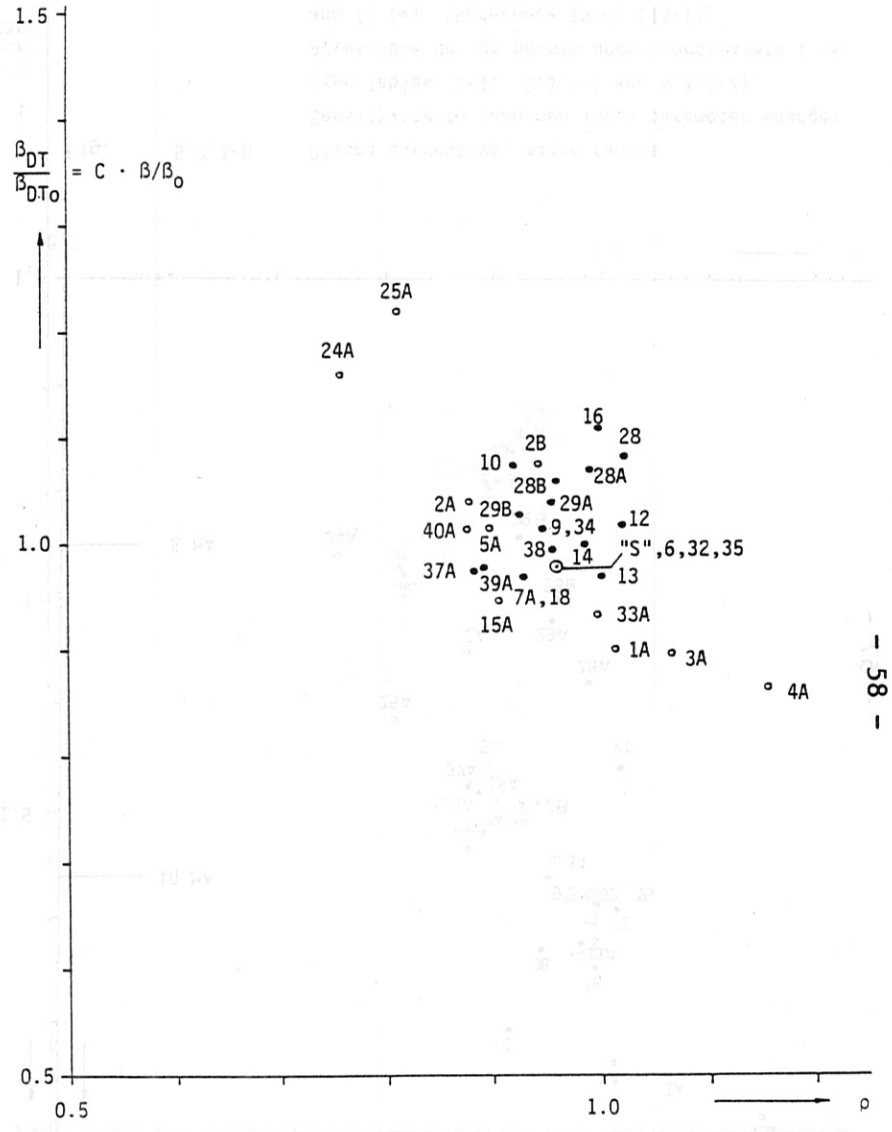

Fig. 5.3.3-10 Useful fuel beta vs. major radius.
Sensitivity to combined input parameter changes
(see Tables 5-4, 5.3.3-1 and 5.3.3-2).
Accessible design points under constraints I (•)
and II (∘) (Reference INTOR IIA-1).

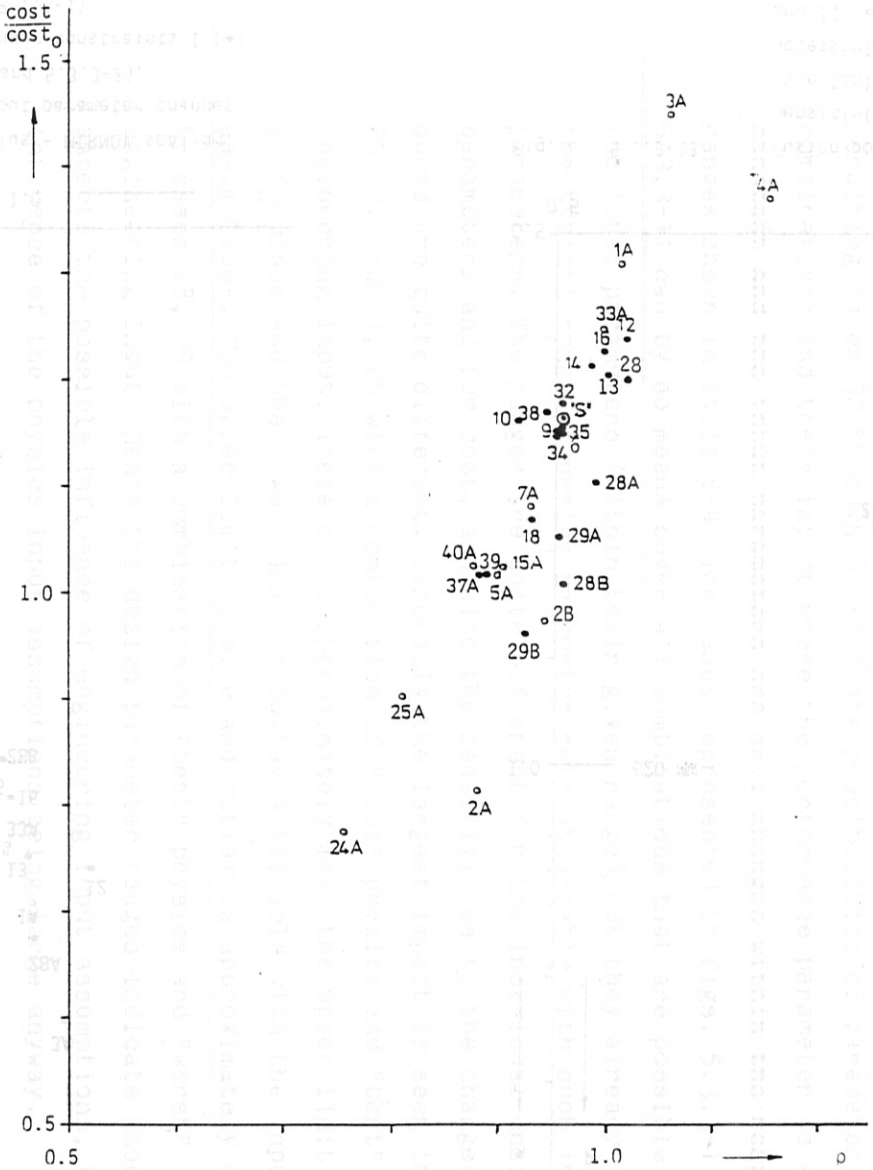

Fig. 5.3.3-11 Cost vs. major radius.
Sensitivity to combined input parameter changes (see Tables 5-4, 5.3.3-1 and 5.3.3-2).
Accessible design points under constraints I (•) and II (∘) (Reference INTOR IIA-1).

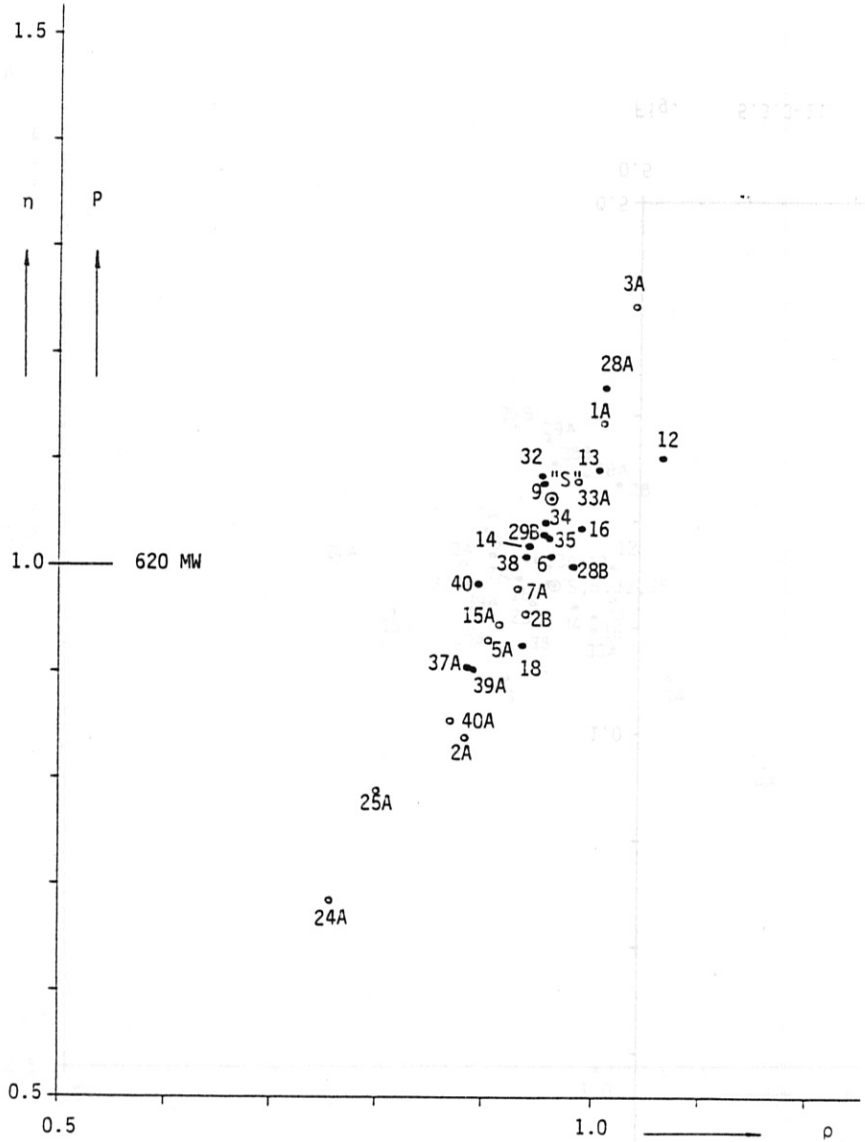

Fig. 5.3.3-12 Fusion power vs. major radius - MIRNOV scaling. Sensitivity to combined input parameter changes (see Tables 5-4, 5.3.3-1 and 5.3.3-2). Accessible design points under constraints I (•) and II (∘) (Reference INTOR IIA-1).

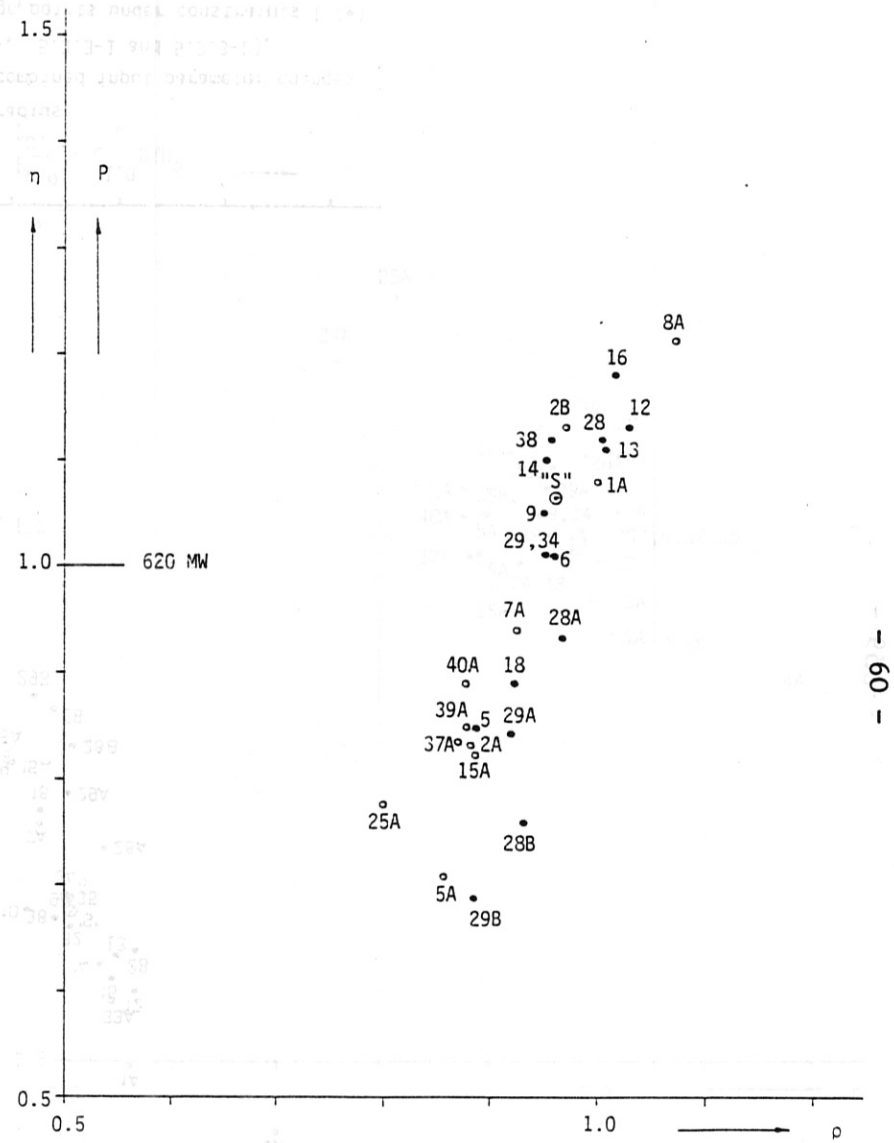

Fig. 5.3.3-13 Fusion power vs. major radius - KAYE-GOLDSTON scaling. Sensitivity to combined input parameter changes (see Tables 5-4, 5.3.3-1 and 5.3.3-2). Accessible design points under constraints I (•) and II (∘) (Reference INTOR IIA-1).

simultaneously decreasing the inner blanket/shield thickness (cases 24, 25). Taking the opposite measure on cases 22, 23 again leads to low performance data points 26 and 27, not shown in Figs. 5.3.3-1 through 5.3.3-11. A combination of the "best" physics input parameters with the "worst" engineering input parameters leads to design parameter sets in the vicinity of case "S", but with larger dimensions (cases 28, 29). The opposite combination ("worst" physics with "best" engineering input parameters) results in low performance data points 30, 31, not shown. The remaining cases 32 through 41 indicate possibilities of parameter combinations and their impact where the performance parameter is kept constant and the input parameters are only changed within the respective ranges shown in Table 5-4. The cases represented in Figs. 5.3.3-1 through 5.3.3-11 can by no means cover all combinations that are possible between the input parameters (within their given range), but they already indicate the typical range of design parameter sets attainable with such input parameters. The ranges are quite different for the individual design parameters and for cost, and also the sensitivities to the changes introduced are quite different. Generally the largest impact is seen in cases 20, 21 and 24, 25 with a combination of "best" physics and "best" engineering input. These cases approximately mark the upper limit in performance and the lower limit in outlay attainable with the input assumptions. The upper limit of size and outlay is approximately determined by cases 28, 29 with a combination of "best" physics and "worst" engineering input. Hence the design parameter ranges indicate among other aspects the possible influence of engineering input assumptions, the influence of the physics input assumptions being large anyway.

So far no reference has been made to any range of desired design parameters. Already from Figs. 5.3.3-1 through 5.3.3-11 it can be seen that for some cases the resulting design parameters are obviously outside the range that may be required for a next-step reactor. For example Fig. 5.3.3-2 indicates values of the neutron wall load that are in some cases much larger than specified for INTOR.

In order to see what parameter combinations would result in what ranges for the design parameters, depending on limitations imposed on some of them, and what impact these limitations would have, the cases listed in Tables 5-4 and 5.3.3-1, containing single and combined parameter changes, were searched

for those which fulfilled either the first or at least the second of the two following INTOR-like sets of constraints:

Constraint I	Constraint II
$0.77 < \delta < 1.05$	$0.77 < \delta < 1.05$
$\beta/\beta_o > 0.85$	$\beta/\beta_o > 0.76$
$M_{iAX} > 2.25$	$M_{iAX} > 2.25$
$M_{iKG} > 0.78$	$M_{iKG} > 0.78$
$M_{iG} > 0.81$	$M_{iG} > 0.64$

(The definitions of M_{iKG} and M_{iG} are those of eqs. 21a and 22a with $f_H = 2.$)
(The cases listed have additionally been checked to ensure that they do not exceed about 1.25 times the averaged current density and/or tensile stress in the inner toroidal field coil legs, in relation to the reference INTOR IIA-1.)

Since the selection according to constraint I from Tables 5-4 and 5.3.3-1 leaves only cases 6, 9, 10, 12 through 14, 16, 18, 28, 32, 34, 35 and 38 (and "S"), an attempt was made to modify the remaining ones so that they would fulfill at least constraint II. This was done mainly by changing the performance parameter $\gamma\vartheta$. The result is listed in Table 5.3.3-2. Figures 5.3.3-7 through 5.3.3-11 show the fusion power, plasma current, aspect ratio, fuel beta and cost versus major radius for all cases that fulfill the above constraints with full dots indicating constraint I and circles indicating constraint II. Although this selection can by no means be complete, it indicates typical ranges of design parameter sets that would be attainable under the above constraints and by variations of input parameters from those of point "S" within given ranges (see Table 5-4). It is seen that for the combination of input parameter ranges and constraints that is used here the modification in constraint II in relation to constraint I has a notable impact on the accessible parameter range. Inspection of the design parameter list shows that cases 1A, 3A and 4A arise mainly because of the relaxation in the β/β_o constraint, while cases 2A, 24A and 25A appear because the boundary on the Goldston ignition margin M_{iG} has been lowered in constraint II. Constraint II would also introduce cases 1, 3, 11, 15 and 17 from Table 5-4. Since the corresponding data points do not alter the overall picture, they have been omitted. Among all

data points that comply with constraint I, case 10 has the largest β/β_o value of 0.95. This is due to the low aspect ratio and the large plasma current (see Figs. 5.3.3-8 and 5.3.3-9) arrived at by decreasing the central solenoid radius (see Table 5-4). Case 10, however, is at the same time, close to the upper limit in neutron wall load imposed by the constraints. Cases 28B and 29B indicate what design parameters could be attained with the "best" physics and the "worst" engineering input parameters and a reduced performance parameter still within constraint I. Figure 5.3.3-11 shows that case 10 would have about the same outlay as case "S", while cases 28B and 29B would be about 15 % lower in cost. Figure 5.3.3-8 shows the strong difference in plasma current between cases 10 and 28B/29B (cases 28B and 29B have β/β_o values of 0.92 and 0.90, respectively). It can be further seen that case 29B comes rather close to INTOR Phase IIA-2 in the design parameters. As seen in Fig. 5.3.3-10, in respect of useful beta all cases fulfilling constraint I are found in a narrow region.

So far all figures refer to ASDEX H-mode scaling. In order to indicate the selection (by constraints I and II) of alternative data points that results when applying Mirnov and Kaye-Goldston scaling for the corresponding variations in input assumptions listed in Tables 5-4, 5.3.3-1 and 5.3.3-2, Figs. 5.3.3-12 and 5.3.3-13 show the data points in terms of η versus ρ and are to be compared with Fig. 5.3.3-7.

Three classes of data points can be identified in such a comparison . The first one refers to changes of input parameters that are not contained - or appear only as a weak function - in the confinement scalings. As one would expect, these data points are found in all three cases in Figs. 5.3.3-7, 5.3.3-12 and 5.3.3-13 at rather similar positions. This is also true of changes in γ_ϑ (which depends on the confinement scaling) because the same relative changes of γ_ϑ have been taken. The following list contains the numbers associated with this class of data points and the input quantity that was changed:

point(s) number	1A	9,34	6,7A	15A,18,37A,39A,40A	2A	12	13	14	25A
input quantity changed	$\frac{g}{g_o}$	C	C_f	γ_ϑ	$\frac{g}{g_o}$, γ_ϑ	F_2	F_3	F_4	$\frac{Bmax}{Bmax_o}$, γ_ϑ

The second class of data points are also found in all three figures, but at rather different positions. They typically refer to combined changes of several input parameters and of changes in $Bmax/Bmax_o$ as listed below:

point(s) number	5A	2B	16	28A,28B,29B	38
input quantity changed	$\frac{k}{k_o}$, $\gamma_{\mathfrak{H}}$	$\frac{g}{g_o}$, $\gamma_{\mathfrak{H}}$, $\frac{Bmax}{Bmax_o}$	$\frac{Bmax}{Bmax_o}$	comb., $\gamma_{\mathfrak{H}}$	F_1, F_4

A third class of points - the remaining ones - only occur in two figures or even only in one. They may refer to single or combined input changes depending on the confinement scaling. Typical cases that only occur for a particular confinement scaling under the constraints imposed are:

point(s) number	10	40	5
input quantity changed	F_1	F_1, F_2, F_4	$\frac{k}{k_o}$
confinement sclg.	ASDEX H-mode	Mirnov	Kaye-Goldston

In summary, it can be stated that within the constraints given a similar range of design parameters in terms of η versus ρ can be covered for different confinement scalings. Any given design point in the η versus ρ plane, however, may require quite different input parameter combinations, depending on the confinement scaling assumed.

5.3.4 Overall comparison of INTOR-like design points and outlook on the impact of changing the input assumptions

Using the relations derived in Section 3 of Annex I, one can gain some insight into the essential properties of the design data sets as of Table 4-1 and get some idea how a next-step parameter set could be arrived at.

Table 5.3.4-1 lists the values of the constituents contained in eqs. 28 and 31 for the design data sets mentioned. It can be seen that the values considerably differ over the range of design data sets taken into account. The extremes are reached in many cases for the TIBER II and/or OTR design(s). For example, C_{phys} - a physics-dominated characteristic figure - is rather low for TIBER II, leading to small size, but at the expense of

Table 5.3.4-1 Numerical values of constituents in eqs. 28 und 31 for design data as of Table 4-1

	$C_f \frac{k}{k_o}$	$m \frac{C_p}{C_n}$	C_{phys}	C_B	F_2-F_4	C_{eng}	C_β	$\rho \frac{B}{B_{max}}$	$\frac{I}{I_o} \frac{A}{A_o}$	F_4	$\eta\rho$	ρ	$\frac{\eta}{\rho}$
INTOR IIA-2	1.000	0.944	1.001	0.500	0.179	1.626	1.179	0.500	1.180	0.062	0.893	0.943	1.000
NET-DN	1.182	0.910	1.024	0.457	0.219	2.272	1.432	0.468	1.466	0.036	1.026	0.977	1.068
FER	1.328	0.735	0.874	0.462	0.157	2.835	1.251	0.404	1.093	0.079	0.548	0.834	0.788
TIBER II	1.992	0.544	0.698	0.423	0.098	3.393	1.831	0.295	1.278	0.039	0.287	0.566	0.893
OTR	0.806	0.827	1.318	0.508	0.179	1.200	0.901	0.670	1.188	0.090	0.958	1.189	0.677
"S"	1.166	0.933	1.004	0.526	0.180	1.731	1.496	0.528	1.502	0.060	1.022	0.960	1.110

C_{eng} getting large, which means a very compact central region and fits with noninductive current drive. On the other hand, C_{phys} for OTR is the largest of all designs listed, and so the major radius is also large, but now C_{eng} is modest and hence there is ample space for inductive current drive. The rather large difference between the C_β values indicates the different β/β_o levels resulting when C_β is multiplied by $g/g_o * A_o/A$. A comparison between ρ*B/Bmax and ρ shows how well the toroidal field is being exploited in the various designs. The inner blanket/shield thickness (F_2 - F_4) varies by a factor of more than two. A strong dependence of the outlay, as measured by $\eta\rho$, on C_{phys} can be seen.

C_{phys} (as shown in Annex I, Section 3) appears in many relations when rewritten accordingly. It combines all essential physics input quantities that occur in the Murakami and Troyon relations and it determines the outlay, dimensions and plasma current to a large extent. C_{eng} describes the degree of advanced engineering and/or of noninductive current drive implied

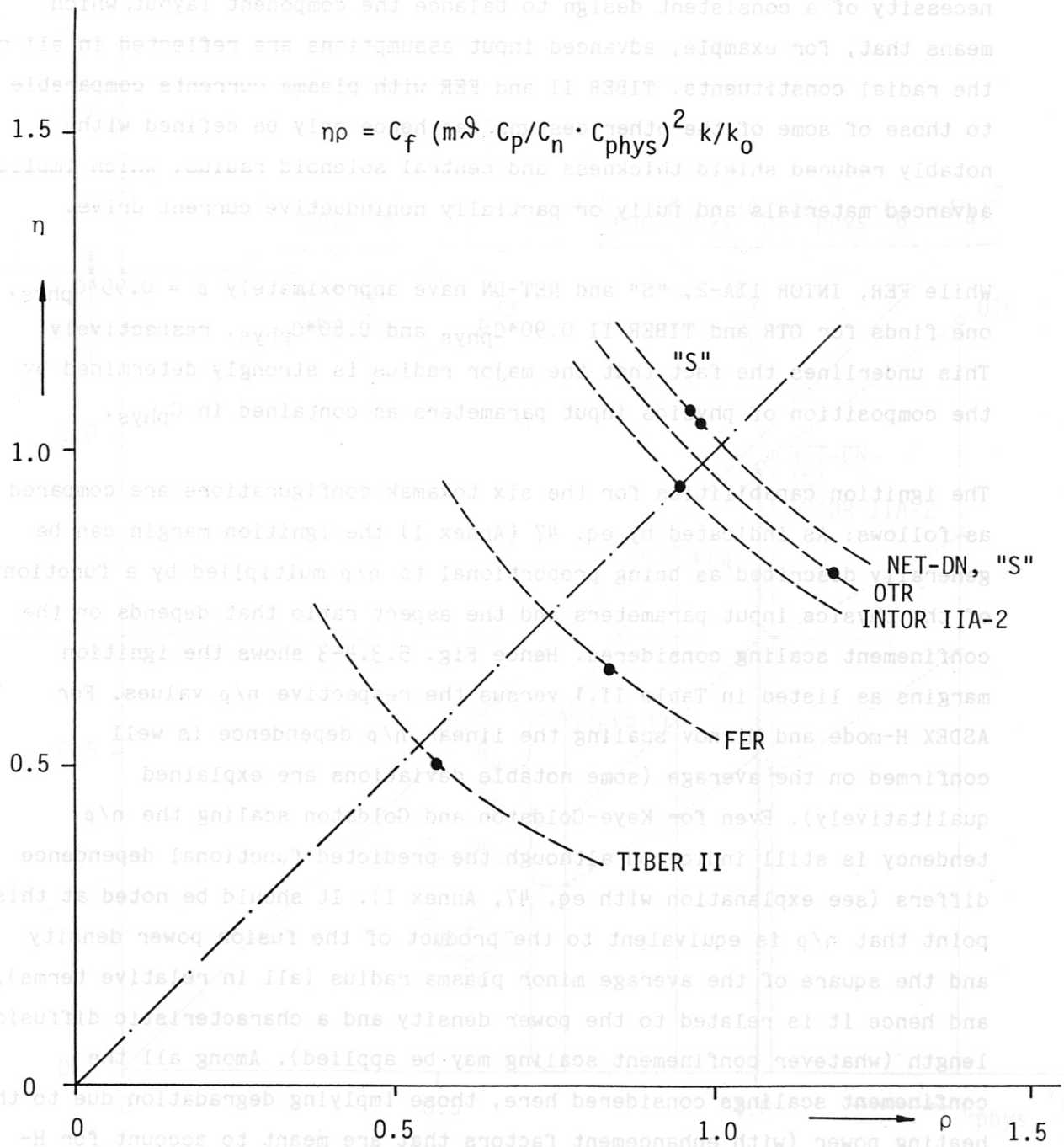

Fig. 5.3.4-1 Fusion power vs. major radius for respective constant $\eta\rho$ as given for the designs of Table 2-1.

Figure 5.3.4-2 shows for the above design data sets the major radius versus the pertinent C_{phys} value. The nearly linear dependence indicated by eq. 31 is seen. Even the three constituents that make up the major radius show an approximately linear dependence on C_{phys}. This demonstrates the necessity of a consistent design to balance the component layout, which means that, for example, advanced input assumptions are reflected in all of the radial constituents. TIBER II and FER with plasma currents comparable to those of some of the other designs can hence only be defined with notably reduced shield thickness and central solenoid radius, which implies advanced materials and fully or partially noninductive current drive.

While FER, INTOR IIA-2, "S" and NET-DN have approximately $\rho = 0.95 * C_{phys}$, one finds for OTR and TIBER II $0.90 * C_{phys}$ and $0.80 * C_{phys}$, respectively. This underlines the fact that the major radius is strongly determined by the composition of physics input parameters as contained in C_{phys}.

The ignition capabilities for the six tokamak configurations are compared as follows: As indicated by eq. 47 (Annex I) the ignition margin can be generally described as being proportional to η/ρ multiplied by a function of the physics input parameters and the aspect ratio that depends on the confinement scaling considered. Hence Fig. 5.3.4-3 shows the ignition margins as listed in Table II.1 versus the respective η/ρ values. For ASDEX H-mode and Mirnov scaling the linear η/ρ dependence is well confirmed on the average (some notable deviations are explained qualitatively). Even for Kaye-Goldston and Goldston scaling the η/ρ tendency is still indicated although the predicted functional dependence differs (see explanation with eq. 47, Annex I). It should be noted at this point that η/ρ is equivalent to the product of the fusion power density and the square of the average minor plasma radius (all in relative terms), and hence it is related to the power density and a characteristic diffusion length (whatever confinement scaling may be applied). Among all the confinement scalings considered here, those implying degradation due to the heating power (with enhancement factors that are meant to account for H-mode operation) are most pessimistic and just allow $M_i \approx 1$ to be attained for NET-DN or "S"-like size and physics input assumptions.

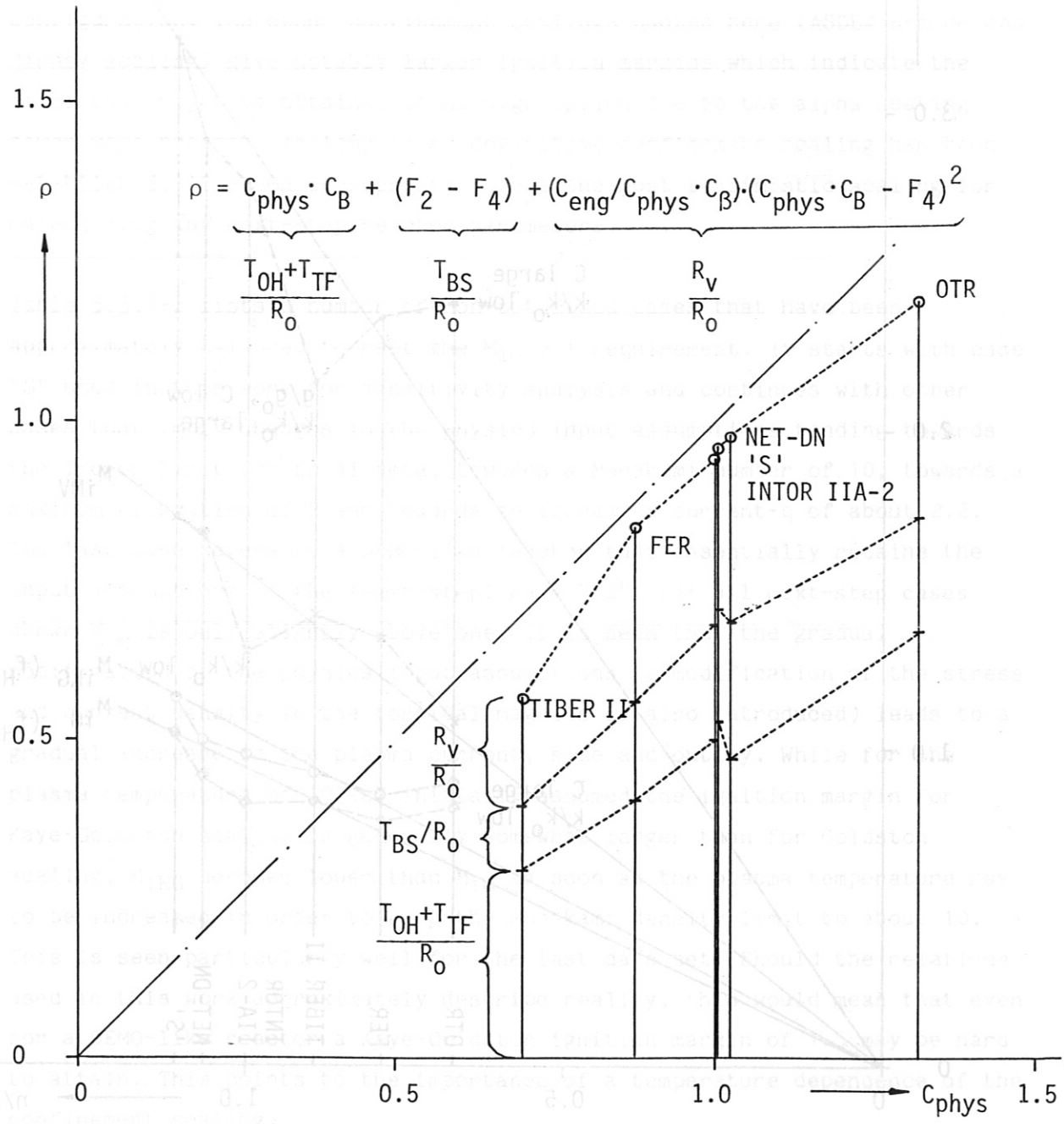

Fig. 5.3.4-2 Major radius vs. C_{phys} as given for the designs of Table 2-1.

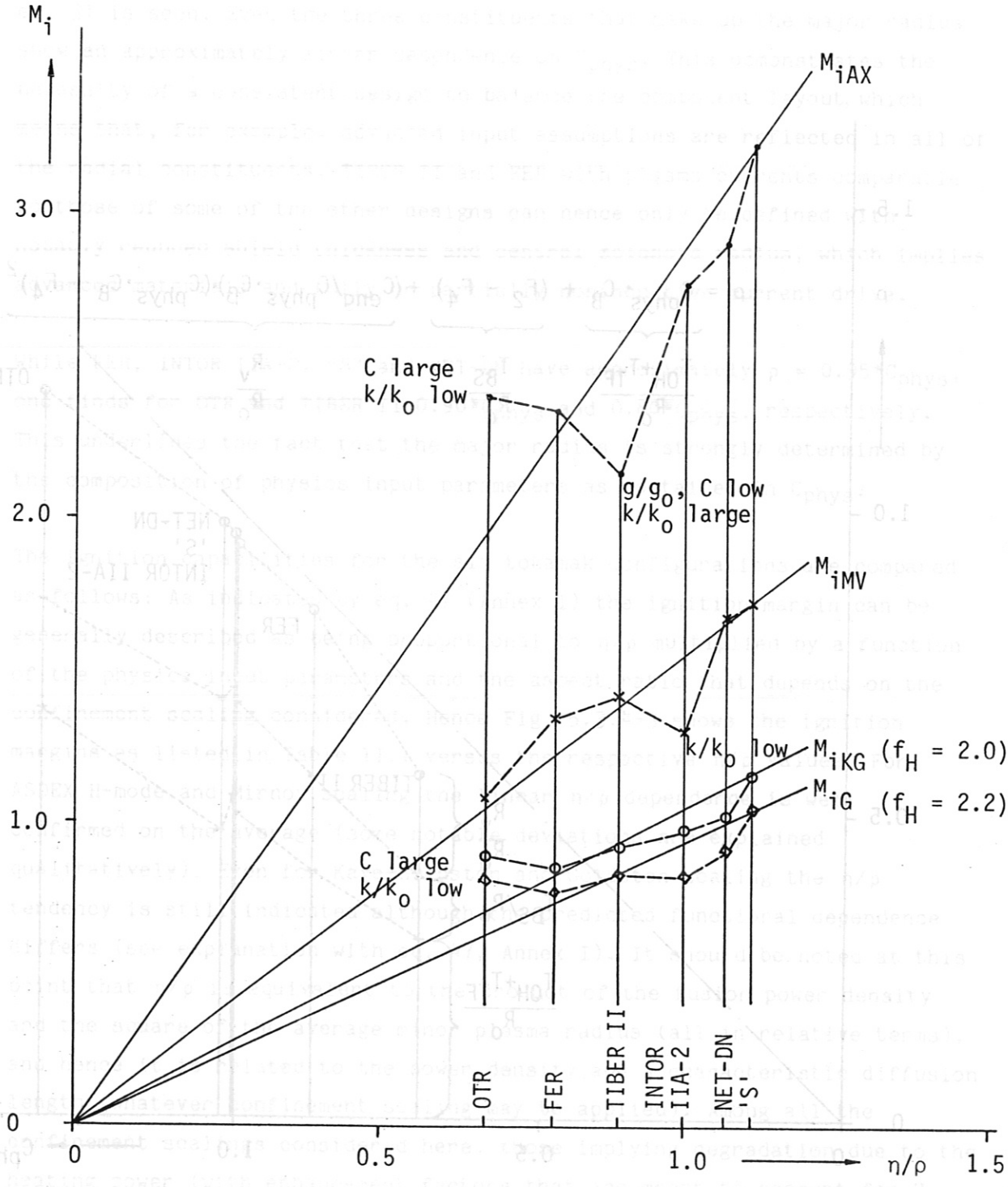

Fig. 5.3.4-3 Ignition margins as of Table II-1 vs. η/ρ.

On the basis of one of the confinement scalings shown in Sec. 1 Annex 1 and of physics input parameters thought to be attainable in a reacting plasma it is possible to produce sets of design parameters for next-step reactors by tailoring them for a certain minimum ignition margin. In general Goldston scaling with an enhancement factor of 2.2 (for H-mode operation, quoted by JET) leads to a somewhat lower calculated ignition margin than Kaye-Goldston scaling with an enhancement factor of 2 for the same configuration. The other confinement scalings quoted here (ASDEX H-mode and Mirnov scaling) give notably larger ignition margins which indicate the level that might be attained if no degradation due to the alpha heating power were present. As long as no definitive confinement scaling has been established, it seems appropriate to use the most pessimistic scaling for determining any next-step reactor parameters.

Table 5.3.4-2 lists a number of non-optimized cases that have been approximately tailored to meet the $M_{iG} > 1$ requirement. It starts with case "S" used in this work for sensitivity analysis and continues with other cases that imply changes in the physics input assumptions tending towards the Troyon limit for total beta, towards a Murakami number of 10, towards a maximum elongation of 2 and towards an increased current-q of about 2.2. The last case refers to a DEMO-like reactor that essentially retains the input assumptions of the (next-step) case "S2". For all next-step cases shown M_{iG} is only slightly above one. It is seen that the gradual modification of the physics input assumptions (a modification of the stress and current density in the toroidal magnets is also introduced) leads to a gradual increase in the plasma current, size and outlay. While for the plasma temperature of 10 keV initially assumed the ignition margin for Kaye-Goldston scaling is generally somewhat larger than for Goldston scaling, M_{iKG} becomes lower than M_{iG} as soon as the plasma temperature has to be increased in order to keep the Murakami density limit to about 10. This is seen particularly well for the last data set. Should the relations used in this work approximately describe reality, this would mean that even for a DEMO-like reactor a Kaye-Goldston ignition margin of 1.5 may be hard to attain. This points to the importance of a temperature dependence of the confinement scaling.

Table 5.3.4-2 Some next-step design data sets

Name	"S"	"S1"	"S2"	"DEMO"
R (m)	5.o86	5.284	5.687	7.819
a (m)	1.21o	1.315	1.477	2.131
A	4.2o3	4.o18	3.85o	3.67o
I (MA)	1o.1o	11.43	12.48	19.98
B (T)	5.47	5.78	5.79	6.12
p_w (MW/m^2)	1.32	1.12	o.96	1.89
P_f (MW)	631	621	636	25o5
ß (%)	4.48	4.o7	3.79	3.98
$ß_{DT}$ (%)	4.o1	3.13	2.78	2.92
M (Murakami)	16.8	11.4	1o.9	1o.4
T (keV)	1o	12.5	12.5	2o
M_{iAX}	3.23	3.2o	3.1o	8.o1
M_{iMV}	1.72	1.76	1.77	4.79
M_{iKG} (f_H = 2)	1.18	1.1o	1.o3	1.26
M_{iG} (f_H = 2.2)	1.o4	1.o5	1.o1	1.46
T_{OH} (m)	1.81o	2.o79	2.254	3.344
T_{TF} (m)	o.986	o.799	o.85o	1.169
T_{BS} (m)	o.954	o.954	o.954	o.954
R_V (m)	1.336	1.452	1.63o	2.35o
σ/σ_o	o.9o	1.21	1.21	1.14
j/j_o	1.o6	1.34	1.25	o.9o
F_{OH}	1.24	1.11	1.11	1.11
k	2.o8	2.o5	2.oo	2.oo
q	2.o8	2.15	2.22	2.22
g	3.18	2.7o	2.6o	2.6o
C_f	o.897	o.923	o.897	o.897
C_n	o.923	o.923	o.923	o.923
C_p	o.9oo	o.91o	o.91o	o.91o
	1.13	1.o5	1.oo	1.oo
F_1	0.38o	o.38o	o.38o	o.38o
F_2	o.24o	o.216	o.216	o.216
F_3	o.25o	o.25o	o.25o	o.25o
F_4	o.o6o	o.o36	o.o36	o.o36
$Bmax/Bmax_o$	o.95o	1.o12	1.o12	1.o12
$cost/cost_o$	1.16	1.28	1.46	3.58

An overall preliminary conclusion from Table 5.3.4-2 is that for a next step in tokamak reactor development somewhat larger dimensions than used for INTOR and plasma currents between 12 and 19 MA are obtained, the largest value for the plasma current referring to a DEMO-like step. Obviously, the outlay strongly depends on the confinement scaling and desired ignition margin. It appears hard to restrict the outlay required to the INTOR cost estimates. The last data set but one can be considered as a marginal example of a next-step design. All cases shown can operate with inductive current drive; all have the same inner blanket/shield thickness. The DEMO set shown may thus require advanced blanket/shield solutions. A reduction of the inner solenoid radius generally leads to a further increase in the plasma current and to a reduction of M_{iG} and M_{iKG}.

6. Direct capital cost comparison

Table 6-1 shows a comparison between relative direct capital cost estimates (with INTOR IIA-2 as the reference case, for which the relative cost would be 1.00) calculated by the simple cost model mentioned in Section 3 and the corresponding national estimates.

Table 6-1 Cost comparison

	calculated estimate	respective national estimate
NET-DN	1.21	1.04
FER	0.86	0.86
TIBER II	0.62	0.61
OTR	1.23	1.10

The comparison shows agreement within a deviation range of + 16 % to - 10 %.

7. Summary and Conclusions

1. The simplified non-optimizing rescaling approach (using relative quantities with INTOR II A-1 as the reference case) allows a rather good representation of the essential design parameters of INTOR II A-2 and the four national designs with some minor adjustments. This inspires confidence to apply the method in sensitivity analyses.

2. Single sensitivity studies show that the group of single parameters whose individual change shows the strongest impact on non-optimized design parameters consists of the physics input parameters, the maximum toroidal field and the central solenoid radius. The sensitivities depend notably on the confinement scaling assumed. Strong impact can be expected from simultaneous changes of input parameters for the combination of design parameters.

3. Global substitution analysis allows a wide range of design parameter space to be covered by mutual substitution of the entire physics or engineering input parameter sets among INTOR II A-2 and the four national designs. This kind of analysis reveals that the accessible domain of design parameters is rather limited when certain limits on the desired output parameters neutron wall load, total beta and ignition margins are imposed. The domains found for accessible design parameters versus major radius depend on the confinement scaling assumed for the substitution procedure (retaining the ignition margin in terms of that scaling constant for each physics input parameter set). A parameter range around INTOR II A-2 and NET-DN data is found to comply for all confinement scalings considered, with the constraints imposed.

4. A stepwise transition in input parameters from one design point to another can help to clarify the essential differences between the two. It has to be noted, however, that the pathway of the transition and the conclusions about the relative importance of physics and engineering input changes depend notably on the confinement scaling adopted.

5. Sensitivity studies on combined input parameter changes were made around a suggested INTOR-like design point "S" that appears somewhat more adjusted to physics guidelines as developed at the INTOR workshop. The following can be concluded (study for ASDEX H-mode scaling mainly). As in the global substitution analysis, a rather limited accessible domain of design parameters is found. Further improvements in physics input parameters would allow a reduction in outlay. Making the design more compact by advanced engineering may encounter limits due to rising neutron wall load, magnet stress and current density. The typical accessible design parameter range found would greatly change if the combination of input assumptions and constraints on the resulting design parameters were altered.

6. A simplified direct capital cost evaluation shows agreement with the respective national cost estimate (relative to INTOR II A-2) within a deviation range of + 16 % to - 10 %.

7. An overall comparison of INTOR-like design points shows that a certain combination of the physics input parameters called C_{phys} enters strongly into most of the main design parameters.

8. An outlook on next-step design parameters arrived at with modified input assumptions according to existing physics results leads to the preliminary conclusion that somewhat larger dimensions than used for INTOR and a plasma current >12 MA may be required for reaching ignition. It may then be hard to restrict the outlay to the previous INTOR estimates unless sub-ignited operation were accepted.

8. Acknowledgements

Thanks are extended to INTOR workshop participants for discussions of the material presented here (except for some extensions and Sec. 5.3.4) and to Claudia Alberter, who performed much of the numerical evaluation and took care of the layout of the report with tables and figures.

References

/1/ A. F. Knobloch, Sensitivity study on the impact of input parameter changes on INTOR-like parameter sets, EC contribution to INTOR workshop Phase Two A Part 3 Session 16, IAEA, Vienna, Nov. 1987; see also /4/

/2/ INTOR Phase Two A Report, STI/PUB/714, IAEA, Vienna 1986

/3/ Report of an INTOR-related specialists' meeting on engineering test reactor national design concepts, IAEA, Vienna, March 1987; see also EURATOM reports EURFUBRU/XII-226/87/EDV10-13, Brussels, March 1987

/4/ A. F. Knobloch, EC INTOR Phase Two A Part III report, Chapter XVI (method B), EURFUBRU/XII-139/88/EDV3, Brussels, March 1988

/5/ A. F. Knobloch, Parameter studies on the impact of plasma physics/ engineering assumptions on the data of possible next-step tokamak reactors; Paper 18C-11-6, Energy Independence Conference, Rio de Janeiro, August 1987, to be published

/6/ A. F. Knobloch, IPP Report 4/220, March 1985

/7/ A. F. Knobloch, IPP Report 4/224, November 1986

Annex I

Simplified rescaling procedure for establishing possible next-step tokamak reactor design parameters

This is a condensed version of rescaling as used in the course of the INTOR studies in Phase IIA Part 3 when an attempt was made to compare INTOR with the four national next-step designs and derive recommendations for a later parameter selection.

The rescaling approach uses a certain "consistent" design point and studies the variations that are possible around that point by changes of the input assumptions. INTOR as of Phase IIA Part 1 is used here as the reference design point. A relative representation of all quantities considered is applied which makes all variations directly visible in the form of deviations from unity to facilitate comparison.Another benefit is that changes in numerical factors can sometimes be accommodated without changing most of the calculations.

The purpose of the simplified approach is to identify the essential quantities and parameter combinations that lead to certain design parameter sets. Such identification may be less straightforward when some existing detailed design codes are used. The important issue is to try and find the best compromise between "realistic" input assumptions and "suitable" performance requirements of a next-step tokamak.

Earlier versions of the rescaling approach are found in /6/, /7/. /5/ gives results of the above-mentioned comparison study. Below the present status of the rescaling approach is given in relation to /1/ through /5/. For a list of symbols see Appendix III.

1. Physics part of simplified rescaling

The essential relations refer to the limiting safety factor written as the so-called current-q, to Troyon scaling for the total beta, to the Murakami density limit (in the absence of an agreed more suitable relation), and to a number of energy confinement scalings considered for comparison. Profile effects are taken into account by defining certain profile-dependent factors:

q-condition: $$\frac{I\,A}{I_o A_o} = \frac{B}{B_o}\,\rho\,\frac{A_o}{A}\,\frac{g}{g_o}\,M \quad \text{with } M = \frac{g_o q_o}{g\,q}\,\frac{1+k^2}{1+k_o^2}\,, \qquad (1)$$

Troyon scaling: $$\frac{\beta}{\beta_o} = \frac{g}{g_o}\,\frac{\frac{I\,A}{I_o A_o}}{\rho\,\frac{B}{B_o}} = \left(\frac{g}{g_o}\right)^2 M\,\frac{A_o}{A}\,, \qquad (2)$$

Murakami limit: $$\frac{n_e}{n_{eo}} = C_n\,\frac{n_{DT}}{n_{DTo}} = m\,\frac{B}{B_o}\,\frac{1}{\rho}\,, \qquad (3)$$

Profile-dependent factors are used as follows:

fusion fuel pressure: $$\frac{\beta_{DT}}{\beta_{DTo}} \cdot \left(\frac{B}{B_o}\right)^2 = C_p\,\frac{n_{DT}}{n_{DTo}}\,\vartheta\,, \qquad (4)$$

fusion power density: $$n\,\frac{V_o}{V} = C_f\left(\frac{\beta_{DT}}{\beta_{DTo}}\right)^2\left(\frac{B}{B_o}\right)^4, \qquad (5)$$

with $$\frac{V}{V_o} = \rho^3\left(\frac{A_o}{A}\right)^2\frac{k}{k_o}\,,$$

fusion fuel beta: $$\frac{\beta_{DT}}{\beta_{DTo}} = C\,\frac{\beta}{\beta_o}\,. \qquad (6)$$

From eqs. 1 through 4 and 6 one obtains a relation between the Murakami parameter and the plasma current,

$$m\vartheta = \frac{C_n C}{C_p}\,\frac{g}{g_o}\,\frac{I\,A}{I_o A_o}\,, \qquad (7)$$

which can be interpreted as follows: The product of the plasma current and aspect ratio is determined by the Murakami number, temperature, Troyon factor and three profile-related factors.
Using eq. 5, one obtains a relation that to some extent characterizes the outlay:

$$n\rho = C_f \left(\frac{I\,A}{I_o A_o} \right)^4 \left(\frac{C}{M} \right)^2 \frac{k}{k_o} , \qquad (8)$$

which can be interpreted as follows: The product of the fusion power and major radius is entirely given by plasma physics input parameters if eq. 7 is used to replace the plasma current and aspect ratio.

The performance parameter

$$\gamma\vartheta = \frac{n_{DT}}{n_{DTo}} \frac{\tau_E}{\tau_{Eo}} \vartheta \qquad (9)$$

allows any design parameter set to be defined with respect to ignition. The ignition margin, however, needs to be separately defined. A very simple version, used here, is

$$m_i = \frac{P_\alpha}{P_{\alpha o}} \frac{\tau_E}{\tau_{Eo}} C_p' \frac{\beta_o}{\beta} \left(\frac{B_o}{B} \right)^2 \frac{V_o}{V} , \qquad (10)$$

which neglects radiation losses. With the alpha power proportional to the fusion power and with eqs. 5 and 6, one gets

$$m_i = C_f\, C\, C_p\, C_p'\, \gamma\vartheta . \qquad (11)$$

The energy confinement time scaling is often expressed as a product of exponential functions of design parameters such as dimensions, plasma elongation, electron density, toroidal field, beta etc. Provided such a representation is relevant and known, it can be transformed by applying the above equations, into the form

$$\frac{\tau_E}{\tau_{Eo}} = F_\tau \left(\frac{I}{I_o} \right)^\lambda \cdot \rho^\mu \cdot \left(\frac{A}{A_o} \right)^\nu , \qquad (12)$$

where F_τ can comprise functions of all physics input parameters. In the case of ASDEX H-mode and Mirnov scalings (which do not imply any confinement degradation due to heating, i.e. heating by the alpha particles) and of Goldston scaling (which implies confinement degradation) the characteristic confinement parameter F_τ is particularly simple, while

for Kaye-Goldston scaling, also implying degradation, it turns out to contain several of the physics input parameters (see Appendix I, $C_p' = 1$).

	F_τ	λ	μ	ν
ASDEX H-mode scaling:	1.000	1.000	1.000	0.000
Mirnov scaling:	$(k/k_o)^{0.5}$	1.000	1.000	-1.000
Goldston scaling: (eqs. I.8 through I.11)	M	0	1.760	-0.260
Kaye-Goldston scaling: (eqs. I.8 through I.11)	$\dfrac{(g/g_o)^{0.214}\, M^{0.976}}{(\frac{C_p}{CC_n})^{0.619}\,(\frac{k}{k_o})^{0.714}}$	1.214	0.357	1.214

With the energy confinement time according to eq. 12 one can find an equation for the major radius that contains physics input parameters only and the aspect ratio. First one gets from eqs. 4 and 9 together with eq. 1

$$\rho = \frac{I}{I_o}\frac{A}{A_o}\left(\frac{1}{C_p \cdot \gamma \vartheta}\frac{C}{M}\frac{A}{A_o}\frac{\tau_E}{\tau_{Eo}}\right)^{1/2} \qquad (13)$$

and after insertion of eqs. 11 and 12 one obtains with eq. 1

$$\rho = \left(\frac{C_p' F_\tau}{m_i}\frac{C^2 C_f}{M}\right)^{\frac{1}{2-\mu}} \left(m\vartheta \frac{C_p}{C_n C}\frac{g_o}{g}\right)^{\frac{2+\lambda}{2-\mu}} \left(\frac{A}{A_o}\right)^{\frac{1+\nu-\lambda}{2-\mu}} . \qquad (14)$$

Accordingly, one gets from eq. 8 an expression for the fusion power

$$\eta = \left(\frac{m_i}{C_p' F_\tau}\frac{(C^2 C_f)^{1-\mu}}{M^{3-2\mu}}\right)^{\frac{1}{2-\mu}} \frac{k}{k_o}\left(m\vartheta \frac{C_p}{C_n C}\frac{g_o}{g}\right)^{\frac{6-\lambda-4\mu}{2-\mu}} \left(\frac{A_o}{A}\right)^{\frac{1+\nu-\lambda}{2-\mu}} . \qquad (15)$$

An important measure of the nuclear and heat load on the first wall is the average neutron wall load defined as

$$\delta = \frac{\eta}{\rho^2}\frac{A}{A_o}\left(\frac{1+k_o^2}{1+k^2}\right)^{1/2}\frac{F_{3o}}{F_3} . \qquad (16)$$

Written in terms of the same quantities as ρ and η, it becomes

$$\delta = \left\{\left(\frac{m_i}{C_p' F_\tau}\right)^3 \frac{M^{2\mu-1}}{(C^2 C_f)^{1+\mu}}\right\}^{\frac{1}{2-\mu}} \frac{k}{k_o}\left(\frac{1+k_o^2}{1+k^2}\right)^{1/2} \left(m\vartheta \frac{C_p}{C_n C}\frac{g_o}{g}\right)^{\frac{2-3\lambda-4\mu}{2-\mu}} \left(\frac{A_o}{A}\right)^{\frac{1+3\nu-3\lambda+\mu}{2-\mu}} \frac{F_{3o}}{F_3} . \qquad (17)$$

Equations 14, 15 and 17 all show essentially three groups of parameters that determine the reactor characteristics. The first group comprises the ignition margin and M together with three profile-dependent factors, the second contains all quantities that determine the product of the plasma current and aspect ratio, and the third the aspect ratio and, in the case of the neutron wall load, geometry factors that determine the plasma-wall distance. All three groups of parameters show exponents that depend on the confinement scaling, which clearly demonstrates the importance of this aspect. In the first group the plasma elongation - in addition to being contained in M - appears in the equations for η and δ.

It does not appear practical and useful to sort out isolated functions of parameters that are contained in more than one parameter group, since the groups are so clearly related to the ignition margin and beta, to the Murakami limit and the Troyon factor, and to the aspect ratio and geometry factors. The principal impact of each group of parameters can be seen from eqs. 14, 15 and 17. Consistent parameter sets, however, can only be derived by iteration which essentially has to ensure that eq. 14 is in accordance with the radial build-up consisting of the engineering components, and that the toroidal field on axis agrees with that defined by eq. 1.

The absolute ignition margins can be derived from the relative ones defined in eq. 11 by relating the latter to the ratio of the confinement time quoted for the reference case to the confinement time calculated by using the respective scaling with the reference parameters. This ratio m_{io} contains only the confinement times mentioned since obviously the other quantities involved cancel. Using eqs. 1, 2, 6, 9 and 11, one obtains

$$M_i = \frac{m_i}{m_{io}} = \frac{C_f C^2 C_p' \left(\frac{I}{I_o} \frac{A}{A_o}\right)^2 \frac{A}{A_o}}{m_{io}\, \rho^2\, M} \; \frac{\tau_E}{\tau_{Eo}} \; . \qquad (18)$$

Appendix I describes the general form taken by τ_E/τ_{Eo}. The M_i formulae are given below for the confinement scalings used in this work: ASDEX H-mode, Mirnov, Kaye-Goldston and Goldston scaling. For the latter two both alternative equations are given, the first one assuming $P = P_\alpha$, the second assuming $P = W_{th}/\tau_E$.

ASDEX H-mode scaling: with $m_{io} = 0.413$ (reference case INTOR IIA-1)

$$M_{iAX} = \frac{C_f C^2 C_p' \left(\frac{I}{I_o}\frac{A}{A_o}\right)^3}{m_{io} M \rho}, \tag{19}$$

Mirnov scaling: with $m_{io} = 0.930$ (reference case INTOR IIA-1)

$$M_{iMV} = \frac{C_f C^2 C_p' \left(\frac{k}{k_o}\right)^{0.5} \left(\frac{I}{I_o}\right)^3 \left(\frac{A}{A_o}\right)^2}{m_{io} M \rho}, \tag{20}$$

Kaye-Goldston scaling ($P = P_\alpha$): with $m_{io} = 1.273$ (ref. case INTOR IIA-1)

$$M_{iKG} = \frac{C_f^{0.42} \left(\frac{C_n}{C_p}\right)^{0.26} C^{1.10} C_p' \left(\frac{g}{g_o}\right)^{0.09} \left(\frac{I}{I_o}\right)^{1.35} \left(\frac{A}{A_o}\right)^{1.77}}{m_{io} \mathfrak{R}^{0.26} \left(\frac{k}{k_o}\right)^{0.30} M^{0.01} \rho^{0.69}} \frac{f_H}{2} \tag{21}$$

Kaye-Goldston scaling ($P = W_{th}/\tau_E$): (see eq. 21)

$$M_{iKG}(P = W_{th}/\tau_E) = \{M_{iKG}(P = P_\alpha)\}^{2.381}, \tag{21a}$$

Goldston scaling ($P = P_\alpha$): with $m_{io} = 1.504$ (ref. case INTOR IIA-1)

$$M_{iG} = \frac{C_f^{0.50} C C_p' \frac{I}{I_o} \left(\frac{A}{A_o}\right)^{1.37}}{m_{io} \rho^{0.12}} \frac{f_H}{2}, \tag{22}$$

Goldston scaling ($P = W_{th}/\tau_E$): (see eq. 22)

$$M_{iKG}(P = W_{th}/\tau_E) = \{M_{iG}(P = P_\alpha)\}^2. \tag{22a}$$

It can be shown that there is a general relation

$$M_i(P = W_{th}/\tau_E) = \{M_i(P = P_\alpha)\}^{\frac{1}{1+\alpha_7}} \tag{22b}$$

for scalings that imply degradation due to the heating power. For α_7 see Appendix I.

f_H is the assumed enhancement factor to account for H-mode operation while using confinement scaling relations derived from L-mode results. In this work $f_H = 2$ is used unless stated otherwise.

2. Engineering part of simplified rescaling

Taking the central solenoid flux swing as proportional to the required plasma flux and assuming the latter to be proportional to the product of the plasma current and major radius, one can write the composition of the major radius in terms of engineering components and the plasma current as follows:

$$\rho = \frac{T_{OH}}{R_o}\left(\frac{I}{I_o}\rho\right)^{1/2} + \frac{T_{TF}}{R_o}\,\frac{T_{OH}\left(\frac{I}{I_o}\rho\right)^{1/2}+T_{TF}}{T_{OH}+T_{TF}} + \frac{T_{BS}}{R_o} + \frac{R_v}{R_o}\frac{a}{a_o} \quad . \qquad (23)$$

The radial build of the toroidal field coils is assumed to increase as the ampere-turns required, the blanket/shield thickness is taken to be constant (which means that it has to be adjusted according to the neutron flux envisaged) and the horizontal minor vessel radius is assumed to be proportional to the horizontal minor plasma radius. Equation 23 can be rewritten by using dimensionless geometry factors that are characteristic of the degree of advancement in engineering of a particular design:

$$\rho = F_{1A}\left(\frac{I}{I_o}\rho\right)^{1/2} + \left\{F_{1B}\left(\frac{I}{I_o}\rho\right)^{1/2} + F_4\right\} + (F_2 - F_4) + F_3\,\frac{A_o}{A}\,\rho \qquad (24)$$

Here the four components represent the central solenoid radius, the toroidal magnet build, the blanket/shield thickness and the horizontal minor vessel radius. For practical reasons the relation is used in the following form:

$$\rho = F_1\left(\frac{I}{I_o}\rho\right)^{1/2} + F_2 + F_3\,\frac{A_o}{A}\,\rho \quad \text{with } F_4 = \frac{F_{1B}^2}{F_{1A}-F_{1B}} \quad . \qquad (25)$$

For any design a comparison between eqs. 23 und 24 provides the relation between dimensions and geometry factors, as shown in Table I.1.

Table I.1 Relationships between geometry factors and radial dimensions

$$T_{OH} = F_{1A}\left(\frac{I}{I_o}\rho\right)^{1/2} R_o$$ Central solenoid outer radius

$$T_{TF} = \{F_{1B}\left(\frac{I}{I_o}\rho\right)^{1/2} + F_4\} R_o$$ Radial thickness of toroidal field inner leg

$$T_{BS} = (F_2 - F_4) R_o$$ blanket shield thickness

$$R_v = F_3 \frac{a}{a_o} R_o$$ inner horizontal vessel radius

$$F_{1A} = \frac{T_{OH}}{\left(\frac{I}{I_o}\rho\right)^{1/2} R_o}$$

$$F_{1A} = F_1 + F_4 - F_4\left(1 + \frac{F_1}{F_4}\right)^{1/2}$$

$$F_{1B} = \frac{\frac{T_{TF}}{R_o} + F_{1A}\left(\frac{I}{I_o}\rho\right)^{1/2} - \left\{\left(\frac{T_{TF}}{R_o} + F_{1A}\left(\frac{I}{I_o}\rho\right)^{1/2}\right)^2 - 4\frac{T_{TF}}{R_o} F_{1A}\left(\left(\frac{I}{I_o}\rho\right)^{1/2} - 1\right)\right\}^{1/2}}{2\left\{\left(\frac{I}{I_o}\rho\right)^{1/2} - 1\right\}}$$

$$F_{1B} = F_4\left\{\left(1 + \frac{F_1}{F_4}\right)^{1/2} - 1\right\}$$

$$F_2 = \frac{T_{BS}}{R_o} + F_4$$

$$F_3 = \frac{R_v}{a/a_o\, R_o}$$

$$F_4 = \frac{F_{1B}^2}{F_{1A} - F_{1B}}$$

As already mentioned, one condition for consistency is that eqs. 25 and 14 be equal. The second consistency requirement derives from

$$\frac{B}{B_o} = \frac{F_1(\frac{I}{I_o}\rho)^{1/2} + F_4}{(F_{1o} + F_{4o})\,\rho} \frac{B_{max}}{B_{maxo}}, \qquad (26)$$

which should be equal to B/B_o from eq. 1.

The iteration procedure which yields consistent values of ρ, A/A_o and B/B_o on the basis of the physics and engineering input is described below. Equation 24 can be written in such a form as to show better the impact of engineering and physics input parameter groups when eqs. 7 and 26 are inserted. Equation 27 is used further in Section 3:

$$\rho = \{F_1 - F_4\{(1+\frac{F_1}{F_4})^{1/2} - 1\}\}\{F(\text{param.})\}$$

$$+ F_4\{1+\{(1+\frac{F_1}{F_4})^{1/2} - 1\}\{F(\text{param.})\}\} + (F_2 - F_4)$$

$$+ F_3 \frac{C_n C}{m\vartheta C_p} \frac{g}{g_o}\{F(\text{param.})\}^2$$

$$\text{with } F(\text{param.}) = \frac{1}{F_1}\{\frac{m\vartheta C_p (F_{1o}+F_{4o})}{C_n C \quad M} \frac{B_{maxo}}{B_{max}} (\frac{g_o}{g})^2 \frac{A}{A_o} - F_4\}. \qquad (27)$$

The iteration procedure for obtaining a consistent design parameter set is as follows:

- Select the input data as listed in Table 4-1
- Calculate ρ from eqs. 14, 7, and 1 with $B/B_o = 1$ as an initial assumption. Iterate by varying $m\vartheta$ until the results of eqs. 1 and 26 (rewritten for B/B_o) conincide. The iteration may be carried out for fixed $\gamma\vartheta$, or both $\gamma\vartheta$ and $m\vartheta$ may be varied by iterating for a third quantity, e.g. the neutron wall load. The results are $m\vartheta$, $\gamma\vartheta$, A/A_o, B/B_o, m_i and ρ.
- Calculate I/I_o from eq. 7, η and δ from eqs. 8 and 16, β/β_o from eq. 2, the ignition margins from eqs. 19 through 22a, etc.

From the above it is clear that all equations shown are meant for iterated design parameter sets. Any changes to one or more of the input assumptions will produce a general change in the entire configuration. Attempts at showing typical dependences have been made in /1/ through /5/.
The simplified rescaling approach can help towards an understanding of the cumulative impact of alternative choices of input parameters on the performance data of a design point.

3. Some relations for comparing existing design parameter sets and for determining essential next-step design parameters from given input.

According to eqs. 1, 7 and 8 the product of the fusion power and major radius can be written as

$$\eta\rho = C_f \, (m\vartheta \frac{C_p}{C_n} C_{phys})^2 \frac{k}{k_o} \tag{28}$$

$$\text{with } C_{phys} = m\vartheta \frac{C_p}{C_n} \frac{1}{C} \frac{g_o}{g} \frac{q}{q_o} \frac{1+k_o^2}{1+k^2} = m\vartheta \frac{C_p}{C_n} \frac{\beta_{DTo}}{\beta_{DT}} \frac{A_o}{A} . \tag{29}$$

Like all constituents of eq. 28, C_{phys} consists of physics input parameters only. On the other hand, it can also be shown that

$$C_{phys} = \frac{a}{a_o} \frac{B}{B_o} . \tag{30}$$

Hence the physics input parameters as combined in C_{phys} determine the product of the minor plasma radius and the toroidal field on axis. One can also use C_{phys} to rewrite eq. 27 in the following form:

$$\rho = C_{phys} C_B + (F_2 - F_4) + \frac{C_{eng}}{C_{phys} C_\beta} (C_{phys} C_B - F_4)^2 , \tag{31}$$

$$\text{with } C_B = \frac{A}{A_o} \frac{B_{maxo}}{B_{max}} (F_{1o} + F_{4o}) , \tag{32}$$

$$C_{eng} = \frac{F_3}{F_1^2} \quad , \tag{33}$$

$$C_\beta = \frac{q_o}{q} \frac{1+k^2}{1+k_o^2} = \frac{g}{g_o} M \quad . \tag{34}$$

The three constituents of ρ are the radial build-up of the magnets up to the radius with the maximum toroidal field, the blanket/shield thickness and the horizontal minor vessel radius (see also eqs. 23 through 27). $C_{phys}{}^{*}C_B$ determines the first constituent, and hence the physics input and the configuration as characterized by the aspect ratio and the maximum toroidal field are essential here. The second constituent is essentially determined by nuclear engineering considerations. The minor vessel radius involves all physics (except C_f) and all engineering (except F_2) input parameters. The following further relations can be shown to hold:

$$C_{phys} C_B = \rho \frac{B}{B_{max}} \quad , \tag{35}$$

$$C_B = \frac{A}{A_o} \frac{B_o}{B_{max}} \quad , \tag{36}$$

$$C_{phys} C_\beta = \frac{I\ A}{I_o A_o} \quad . \tag{37}$$

Equations 35 and 36 are related to the toroidal field utilization, and $C_{phys}{}^{*}C_\beta$ turns out to represent the product of the plasma current and aspect ratio, which occurs as an important quantity in the equations for the q-condition, the Troyon β-scaling, the density limit, the overall outlay, the major radius, the fusion power, the neutron wall load and the ignition margin for all confinement scalings considered (see eqs. 1, 2, 7, 8, 13 through 16, 18 through 22a).

All of the above equations require iterative determination of a consistent value of the aspect ratio, except eq. 8, which determines $n\rho$.
In order to predict also the major radius and the ignition margin for a next-step reactor that has to demonstrate operation of a burning plasma with reactor-relevant specific data, one can specify the fuel beta as an important design value which impacts on the compactness of the reactor plasma.
If β_{DT}/β_{DTo} is prescribed, for a given set of physics input parameters the plasma aspect ratio is fixed, as can be seen by rewriting eqs. 2 and 6:

$$\frac{A}{A_o} = C \left(\frac{g}{g_o}\right)^2 M \frac{\beta_{DTo}}{\beta_{DT}} = C \frac{g}{g_o} C_\beta \frac{\beta_{DTo}}{\beta_{DT}} \quad . \tag{38}$$

Together with eqs. 7 and 8 one can now determine the plasma current:

$$\frac{I}{I_o} = \left(\frac{n\rho}{C_f}\frac{k_o}{k}\right)^{1/4} \frac{1}{C^{3/2}.M^{1/2}} \left(\frac{g_o}{g}\right)^2 \frac{\beta_{DT}}{\beta_{DTo}} \quad . \tag{39}$$

The pertaining version of eq. 7 is

$$\frac{m\dot{\vartheta} C_p}{C_n C} = \left(\frac{n\rho}{C_f}\frac{k_o}{k}\right)^{1/4} \left(\frac{M}{C}\right)^{1/2} \frac{g}{g_o} \quad . \tag{40}$$

Using eqs. 27, 38 and 40, one can establish a condition for the geometry factor F_1 with the other engineering and the physics input parameters except $m\dot{\vartheta}$ given, which directly defines a consistent configuration for a prescribed fuel beta and a given product $n\rho$:

$$F_1 = \frac{\left(\frac{A}{A_o} - F_3\right)^{1/2} \left(C_{phys} C_B - F_4\right)}{\left(\frac{I}{I_o}\frac{A}{A_o}\right)^{1/2} \left(C_{phys} C_B + F_2 - F_4\right)^{1/2}} = \frac{\left(C \frac{g}{g_o} C_\beta \frac{\beta_{DTo}}{\beta_{DT}} - F_3\right)^{1/2} \left(F_5 - F_4\right)}{\left(\frac{n\rho}{C_f}\frac{k_o}{k}\right)^{1/8} \left(\frac{M}{C}\right)^{1/4} \left(F_5 + F_2 - F_4\right)^{1/2}} \tag{41}$$

$$\text{with } F_5 = C_{phys} C_B = \left(\frac{n\rho}{C_f}\frac{k_o}{k}\right)^{1/4} \left(C \frac{g}{g_o} C_\beta\right)^{1/2} \frac{\beta_{DTo}}{\beta_{DT}} \frac{B_{maxo}}{B_{max}} \left(F_{1o} + F_{4o}\right) . \tag{42}$$

In general, a set of arbitrary input assumptions may not immediately lead to a satisfactory consistent value of F_1 according to eq. 41 (e.g. $F_1 = 0.35$ would be close to a lower limit for inductive current drive). In that case iterative adjustment can take place, where variations in β_{DT}/β_{DTo}, g/g_o, C, k/k_o, $Bmax/Bmax_o$, q/q_o have the strongest impact. Additional adjustment may be obtained by changes in F_2 and F_4 (F_3 being almost fixed at 0.24 - 0.25). The sensitivity to changes of $\eta\rho$ and C_f is rather low.

Since one also has

$$F_5 = C_{phys} C_B \quad , \tag{43}$$

eq. 41 can be written accordingly. With eqs. 31 through 34 one obtains

$$\rho = (C_{phys} C_B + F_2 - F_4) \cdot F_6 \tag{44}$$

with $$F_6 = \frac{A/A_o}{A/A_o - F_3} \quad (A/A_o \text{ from eq. 38}). \tag{45}$$

Assuming $0.8 \leq A/A_o \leq 1$ and $0.24 \leq F_3 \leq 0.25$, one has $1.23 \leq F_6 \leq 1.46$, which is 1.39 ±5%.

Hence, $C_{phys} C_B$ constitutes the important quantity for determining the major radius, with the inner blanket/shield thickness ($F_2 - F_4$) also having a notable impact. In existing design parameter sets one observes a clear tendency to adjust ($F_2 - F_4$) to the respective value of $C_{phys} C_B$ in order to preserve reasonable toroidal field utilization and reduce size/outlay. This means that the major radius can be approximately written as

$$\rho = F_7 \cdot C_{phys} \quad , \tag{46}$$

where F_7 involves F_6 and the (approximately constant) ratio between the relative shield thickness and $C_{phys} C_\beta$. Taking the design points as of Table 2-1, one obtains on the average $F_7 \approx 0.9$. Taking, however, only

INTOR IIA-2, NET-DN, FER and "S", which comply with INTOR-like design parameters, one gets almost exactly $F_7 = 0.95$ for all of them.
This practical observation provides a possibility to tackle also the ignition margin as of eqs. 19 through 22a in the same manner as $\eta\rho$ and ρ so as to show the principal and essential dependences.

Using eqs. 1, 3, 11, 28, 37 and 46, one can get the following form for the ignition margin:

$$M_i \simeq \frac{\eta}{\rho^{3-\lambda-\mu}} \frac{F_7^{2-\lambda} F_\tau C_p^{-} C_\beta^{\lambda-1}}{m_{io} \frac{g}{g_o} \frac{k}{k_o}} \left(\frac{A}{A_o}\right)^{1+\nu-\lambda} . \qquad (47)$$

Hence, generally the ignition margin tends to increase with the fusion power divided by some function of the major radius for any given set of physics input parameters and confinement scaling with a tendency to decrease with decreasing aspect ratio (which occurs for increased device size) and with decreasing F_7 (see eq. 46). Depending on F_τ, there may be an increase in ignition margin even for decreasing Troyon factor and elongation. While for ASDEX H-mode and Mirnov scaling M_i depends on η/ρ (both have $\eta = \mu = 1$), and hence an increase in device size would notably increase the ignition margin, for Goldston and Kaye-Goldston scaling (scalings that imply confinement degradation due to the heating power) the ignition margin increases only slightly for larger device size. For Goldston scaling M_i depends on $\eta/\rho^{2.12}$ (with $\lambda = -1.0$ and $\mu = 1.88$ for $P = P_\alpha$), while for Kaye-Goldston scaling M_i depends on $\eta/\rho^{2.34}$ (with $\lambda = -0.65$ and $\mu = 1.31$ for $P = P_\alpha$). Therefore, if one of the confinement scalings with degradation due to the heating power is confirmed, the attainment of ignited tokamak operation may remain marginal over quite some range in a device size between an INTOR-like "minimum size" step and a DEMO-like reactor for which the ignition margin may still be about 1.5 only.

Appendix I

Reduction of the confinement scaling equation to the form $\frac{\tau_E}{\tau_{Eo}} = F_\tau \left(\frac{I}{I_o}\right)^\lambda \rho^\mu \left(\frac{A}{A_o}\right)^\nu$

In a relative form the confinement scalings usually represented in a power product form involving the essential quantities characterizing a tokamak configuration can be written as

$$\frac{\tau_E}{\tau_{Eo}} = \left(\frac{n_e}{n_{eo}}\right)^{\alpha_1} \left(\frac{a}{a_o}\right)^{\alpha_2} \left(\frac{k}{k_o}\right)^{\alpha_3} \rho^{\alpha_4} \left(\frac{q}{q_o}\right)^{\alpha_5} \left(\frac{B}{B_o}\right)^{\alpha_6} \left(\frac{P}{P_o}\right)^{\alpha_7} \left(\frac{I}{I_o}\right)^{\alpha_8} \vartheta^{\alpha_9} \left(\frac{A_i}{A_{io}}\right)^{\alpha_{10}} \left(\frac{Z_{eff}}{Z_{effo}}\right)^{\alpha_{11}} . \quad (I.1)$$

As regards the heating power, which can imply confinement degradation (as sometimes observed experimentally), two alternatives are considered. The first takes the alpha power as the heating power. In that case, the excess alpha power would be diverted for ignition margins larger than 1, but its magnitude would still affect the confinement time. The second alternative takes the loss power (= W_{th}/τ_E, if radiation losses are neglected) as a measure of the degrading heating power, and the excess alpha power would again be diverted for ignition margins larger than 1. Obviously, both definitions have the same result for $M_i = 1$. The second definition yields larger values for $M_i > 1$ and lower values for $M_i < 1$.
The relations for both definitions are given below.
Taking $P = P_\alpha$, one gets with eq. 8 of Annex I

$$\frac{P}{P_o} = C_f \left(\frac{C}{M}\right)^2 \left(\frac{I}{I_o}\right)^4 \left(\frac{A}{A_o}\right)^1 \frac{k}{\rho} \frac{}{k_o} . \quad (I.2)$$

Taking $P = W_{th}/\tau_E$, one gets with eqs. 1 and 2 of Annex I

$$\frac{P}{P_o} = \frac{n}{n_o} \vartheta \frac{\tau_{Eo}}{\tau_E} \rho^3 \left(\frac{A_o}{A}\right)^2 \frac{k}{k_o} = \frac{1}{c_p} \left(\frac{I}{I_o}\right)^2 \frac{A}{A_o} \rho \frac{k}{k_o} \frac{1}{M} \frac{\tau_{Eo}}{\tau_E} . \quad (I.3)$$

After insertion of these definitions into eq. I.1 one gets the respective relations for F_τ, λ, μ and ν:

$$F_\tau = C_f \left(\frac{n}{C_p}\right)^{\alpha_7} C^{\alpha_1(\alpha_1+2\alpha_7)} \mathfrak{F}^{(\alpha_9-\alpha_1)} \left(\frac{k}{k_o}\right)^{(\alpha_3+\alpha_7)} \left(\frac{q}{q_o}\right)^{\alpha_5} \left(\frac{g_o}{g}\right)^{\alpha_6} M^{-(\alpha_1+\alpha_6+2\alpha_7)} \left(\frac{A_i}{A_{io}}\right)^{\alpha_{10}} \left(\frac{Z_{eff}}{Z_{effo}}\right)^{\alpha_{11}}, \quad \text{(I.4)}$$

$$\lambda = 2\alpha_1 + \alpha_6 + 4\alpha_7 + \alpha_8 \quad \text{(I.5)}$$

$$\mu = -2\alpha_1 + \alpha_2 + \alpha_4 - \alpha_6 - \alpha_7 \quad \text{(I.6)}$$

$$\nu = 3\alpha_1 - \alpha_2 + 2\alpha_6 + 4\alpha_7 \quad \text{(I.7)}$$

$$F_\tau = \left\{\left(\frac{n}{C_p}\right)^{\alpha_7} C^{\alpha_1(\alpha_9-\alpha_1)} \mathfrak{F}^{(\alpha_3+\alpha_7)} \left(\frac{k}{k_o}\right)^{\alpha_5} \left(\frac{q}{q_o}\right)^{\alpha_6} \left(\frac{g_o}{g}\right)^{-(\alpha_1+\alpha_6+\alpha_7)} M^{-\alpha_7} C_p^{\alpha_{10}} \left(\frac{A_i}{A_{io}}\right)^{\alpha_{11}} \left(\frac{Z_{eff}}{Z_{effo}}\right)\right\}^{\left(\frac{1}{1+\alpha_7}\right)}, \quad \text{(I.8)}$$

$$\lambda = (2\alpha_1 + \alpha_6 + 2\alpha_7 + \alpha_8)/(1 + \alpha_7) \quad \text{(I.9)}$$

$$\mu = (-2\alpha_1 + \alpha_2 + \alpha_4 - \alpha_6 + \alpha_7)/(1 + \alpha_7) \quad \text{(I.10)}$$

$$\nu = (3\alpha_1 - \alpha_2 + 2\alpha_6 + \alpha_7)/(1 + \alpha_7) \quad \text{(I.11)}$$

Equations I.4 through I.7 refer to relation I.2 whereas according to relation I.3 one obtains eqs. I.8 through I.11.

The exponents used for the different confinement scalings are given below (exponents not mentioned are zero).

ASDEX H-mode scaling: $\alpha_4 = 1$, $\alpha_8 = 1$

Mirnov scaling: $\alpha_2 = 1$, $\alpha_3 = 0.5$, $\alpha_8 = 1$

Kaye-Goldston scaling: $\alpha_1 = 0.26$, $\alpha_2 = -0.49$, $\alpha_3 = 0.28$, $\alpha_4 = 1.65$, $\alpha_6 = -0.09$, $\alpha_7 = -0.58$, $\alpha_8 = 1.24$

Goldston scaling: $\alpha_2 = -0.37$, $\alpha_3 = 0.50$, $\alpha_4 = 1.75$, $\alpha_7 = -0.50$, $\alpha_8 = 1$.

Appendix II

Ignition margins calculated according to different scalings

Recalculating the ignition margins for the design parameter sets as of Table 2-1 using eqs. 19, 20 and 21a, one finds that the resulting values come rather close to the results of code calculations presented in /3/.

Table II.1 lists the calculated ignition margins for the above design parameter sets for all definitions of the ignition margin as described by eqs. 19 through 22a with the enhancement factors indicated. $f_H = 2.2$ refers to JET results using Goldston scaling. It can be seen that none of the INTOR-like designs as of Table 2-1 would ignite with Kaye-Goldston scaling and an enhancement factor lower than 2, and that only "S" would ignite with Goldston scaling and an enhancement factor of 2.2.

Table II.1 Calculated ignition margins based on eqs. 19 through 22a for existing design parameter sets

	M_{iAX}	M_{iMV}	M_{iKG} $(P=P_\alpha)$ $f_H = 2$	M_{iKG} $(P=W_{th}/\tau_E)$ $f_H = 2$	M_{iG} $(P=P_\alpha)$ $f_H = 2$	M_{iG} $(P=W_{th}/\tau_E)$ $f_H = 2$	M_{iG} $(P=P_\alpha)$ $f_H = 2.2$	M_{iG} $(P=W_{th}/\tau_E)$ $f_H = 2.2$
INTOR IIA-2	2.768	1.304	0.984	0.962	0.748	0.560	0.823	0.677
NET-DN	2.904	1.678	1.027	1.056	0.831	0.691	0.914	0.835
FER	2.354	1.348	0.853	0.685	0.705	0.497	0.776	0.602
TIBER II	2.142	1.422	0.925	0.831	0.758	0.575	0.834	0.696
OTR	2.395	1.083	0.893	0.764	0.745	0.555	0.819	0.671
"S"	3.234	1.721	1.176	1.471	0.948	0.899	1.043	1.089

Appendix III

List of symbols
(relative quantities with INTOR IIA-1 as the reference case)

η	fusion power
δ	neutron wall load (average)
ρ	major radius
a/a_o	minor radius
A/A_o	aspect ratio
I/I_o	plasma current
B/B_o	toroidal field on axis
B_{max}/B_{maxo}	max. tor. field at coil inner bore
β_{DT}/β_{DTo}	useful fuel beta
β/β_o	total beta
β_{pol}/β_{polo}	poloidal beta
m	Murakami parameter
n_e/n_{eo}	electron density
n/n_o	plasma density
n_{DT}/n_{DTo}	fuel ion density
τ_E/τ_{Eo}	energy confinement time
V/V_o	plasma volume
g/g_o	Troyon factor
q/q_o	current-q (safety factor)
k/k_o	elongation
ϑ	plasma temperature ($<T_i>=<T_e>$)

$$C_f = \frac{\eta}{V/V_o} \cdot \left(\frac{\beta_{DTo}}{\beta_{DT}}\right)^2 \cdot \left(\frac{B_o}{B}\right)^4$$ fusion power density

$$C_n = n_e \cdot n_{DTo} / n_{eo} \cdot n_{DT}$$ electron density/ion density

$$C = \beta_{DT} \cdot \beta_o / \beta_{DTo} \cdot \beta$$ useful beta/total beta

$$C_p = \frac{\beta_{DT}}{\beta_{DTo}} \cdot \left(\frac{B}{B_o}\right)^2 \cdot \frac{n_{DTo}}{n_{DT}} \cdot \frac{1}{\vartheta}$$ profile factor

$$C_p' = \frac{\beta}{\beta_o} \cdot \left(\frac{B}{B_o}\right)^2 \cdot \frac{n_o}{n} \cdot \frac{1}{\vartheta}$$ profile factor

$$\gamma\vartheta = n_{DT}\tau_E / n_{DTo}\tau_{Eo} \cdot \vartheta$$ performance parameter

M_{iAX}, M_{iMV}, M_{iKG}, M_{iG} — ignition margins (assuming ignition margin of INTOR IIA-1 to be unity) for ASDEX H-mode, Mirnov, Kaye-Goldston and Goldston scalings

F_1, F_2, F_3, F_4 — geometry factors, see Sec. 2 of Annex I.

Appendix IV

Evaluation of some engineering design constraints

1. Central solenoid

   Within the accuracy to be expected from simplified rescaling procedures the quantity

$$F_{OH} = \frac{I/I_o \; \rho}{\left(\frac{T_{OH}}{T_{OHo}}\right)^2} = \left(\frac{T_{OHo}}{F_{1A} R_o}\right)^2 = \frac{0.0957}{(F_{1A})^2}$$

   gives a clear indication whether the given central solenoid dimensions will imply a large maximum poloidal field and/or noninductive current drive for a certain burn pulse length.

2. TF coils

   On the basis of the reference values for INTOR IIA-1 the relations for the average tensile stress and the average current density over the entire inner leg coil cross section can be written as

$$\frac{\sigma}{\sigma_o} = \left(\frac{B_{max}}{B_{maxo}}\right)^2 \frac{\frac{2}{1-(T_{OH}/R_1)^2}\left\{\frac{R_2+T_{TF}/2}{R_2-T_{OH}} \ln\frac{R_2}{R_1} - \frac{R_2-R_1}{R_2-T_{OH}} + \left(\frac{T_{TF}}{R_1}\right)^2 \left(\frac{1}{4} + \frac{1}{3}\frac{T_{OH}}{T_{TF}}\right)\right\}}{2.552},$$

$$\frac{j}{j_o} = \frac{B_{max}}{B_{maxo}} \cdot 0.908 \, \frac{R_1}{T_{TF}\,(T_{OH}+T_{TF}/2)} \qquad \text{(dimensions in m)},$$

   with $R_1 = T_{OH} + T_{TF}$ = inner TF coil leg radius

   $R_2 = R + R_V + 2*T_{BS}$ = approximate outer TF coil leg radius

APPENDIX V List of the values calculated (examples)

MIRNOV SKALIERUNG - ACCESSIBILITY CHARTS INTOR IIA-2
EINGABEDATEN
GT = 1.4785 THETA= 1.0000 C = 1.1430 BMBMO= 0.9910 EE0 = 1.0000 QQ0 = 0.8480 GG0 = 0.7000
CN = 1.0000 CP = 0.8470 CF = 1.0000 F1 = 0.4030 F2 = 0.2410 F3 = 0.2640 F4 = 0.0620
AUSGABEDATEN RELATIV
EM = 1.6846 TM = 0.8255 TMX = 1.1140 DEL = 1.0753 RHO = 0.9424 AA0 = 0.9429
BB0 = 1.0006 X = 1.0000 SS0 = 1.2507 ETA = 0.9447 BETA = 0.8755 DBET = 0.7999
BPBPO= 0.5597 AKAKO= 0.9994 BKBKO= 0.9994 COST = 1.0154 MK = 1.1140 MI = 1.4314
MIKG = 1.4303 MIJG = 0.7804 MIGH = 3.9244 MIAX = 3.2703 MIMV = 1.5391 TETEO= 1.2500
SIGMA= 1.0080 JJO = 1.1554 NNDTO= 1.1828 NENEO= 1.1828 ETARO= 0.8903 BBDTO= 1.0007
AUSGABEDATEN ABSOLUT
R = 4.995 A = 4.164 B = 5.503 S = 8.004 P = 585.7 PW = 1.398 BET = 4.903 E = 1.600
G = 4.042 Q = 1.762 TS = 0.949 TOH = 1.699 TTF = 0.949 AKW = 1.398 PR = 0.000 FOH = 1.099
R1 = 2.647 R2 = 8.290 AK = 1.199 QS = 2.377 BTUDA= 5.729 BBERN= 6.970 BKINK= 3.827 BYAMA= 5.135
GIN = 1.213 TE = 1.162 SOL = 0.199 NE = 0.215E+21 NDT= 0.166E+21

MIRNOV SKALIERUNG - ACCESSIBILITY CHARTS NET-DN
EINGABEDATEN
GT = 1.9944 THETA= 1.0000 C = 1.0240 BMBMO= 0.9970 EE0 = 1.2810 QQ0 = 1.0200 GG0 = 0.6060
CN = 1.0000 CP = 0.9100 CF = 0.9230 F1 = 0.3370 F2 = 0.2550 F3 = 0.2580 F4 = 0.0360
AUSGABEDATEN RELATIV
EM = 2.3635 TM = 0.8880 TMX = 0.9992 DEL = 0.8646 RHO = 0.9775 AA0 = 0.8697
BB0 = 0.9102 X = 1.0000 SS0 = 1.6849 ETA = 1.0467 BETA = 0.9980 DBET = 1.3989
BPBPO= 0.5376 AKAKO= 1.1240 BKBKO= 1.4398 COST = 1.2305 MK = 0.9992 MI = 1.7154
MIKG = 1.3320 MIJG = 0.8334 MIGH = 3.8325 MIAX = 3.1937 MIMV = 1.8444 TETEO= 2.1434
SIGMA= 1.3281 JJO = 1.4471 NNDTO= 0.9304 NENEO= 0.9304 ETARO= 1.0231 BBDTO= 1.0220
AUSGABEDATEN ABSOLUT
R = 5.181 A = 3.841 B = 5.006 S = 10.783 P = 649.0 PW = 1.124 BET = 5.589 E = 2.050
G = 3.500 Q = 2.120 TS = 1.161 TOH = 1.749 TTF = 0.734 AKW = 1.537 PR = 0.000 FOH = 1.448
R1 = 2.483 R2 = 9.039 AK = 1.349 QS = 3.318 BTUDA= 7.971 BBERN= 8.506 BKINK= 5.131 BYAMA= 6.473
GIN = 1.597 TE = 1.993 SOL = 0.188 NE = 0.169E+21 NDT= 0.130E+21

MIRNOV SKALIERUNG - ACCESSIBILITY CHARTS FER
EINGABEDATEN
GT = 1.3062 THETA= 1.2000 C = 1.1100 BMBMO= 0.9090 EE0 = 1.0630 QQ0 = 0.8740 GG0 = 0.6060
CN = 0.9150 CP = 0.8320 CF = 1.2490 F1 = 0.3040 F2 = 0.2360 F3 = 0.2620 F4 = 0.0790
AUSGABEDATEN RELATIV
EM = 2.0645 TM = 0.6626 TMX = 0.8088 DEL = 0.7816 RHO = 0.8338 AA0 = 0.7996
BB0 = 0.8381 X = 1.0000 SS0 = 1.3674 ETA = 0.6578 BETA = 0.9482 DBET = 0.9946
BPBPO= 0.4235 AKAKO= 1.0427 BKBKO= 1.1084 COST = 0.8717 MK = 0.6740 MI = 1.5067
MIKG = 1.0625 MIJG = 0.7203 MIGH = 3.3978 MIAX = 2.8315 MIMV = 1.6201 TETEO= 1.4700
SIGMA= 0.8125 JJO = 1.1118 NNDTO= 0.7404 NENEO= 0.6775 ETARO= 0.5485 BBDTO= 1.0525
AUSGABEDATEN ABSOLUT
R = 4.419 A = 3.532 B = 4.610 S = 8.751 P = 407.9 PW = 1.016 BET = 5.310 E = 1.701
G = 3.500 Q = 1.816 TS = 0.832 TOH = 1.183 TTF = 0.956 AKW = 1.448 PR = 0.000 FOH = 2.191
R1 = 2.139 R2 = 7.531 AK = 1.251 QS = 2.548 BTUDA= 7.224 BBERN= 8.989 BKINK= 4.810 BYAMA= 6.365
GIN = 1.517 TE = 1.367 SOL = 0.197 NE = 0.123E+21 NDT= 0.104E+21

MIRNOV SKALIERUNG - ACCESSIBILITY CHARTS TIBER II
EINGABEDATEN
GT = 1.4585 THETA= 1.9400 C = 0.8880 BMBMO= 1.0190 EE0 = 1.5000 QQ0 = 1.0370 GG0 = 0.4790
CN = 1.0230 CP = 0.8770 CF = 1.3280 F1 = 0.2720 F2 = 0.1370 F3 = 0.2510 F4 = 0.0390
AUSGABEDATEN RELATIV
EM = 3.8228 TM = 0.6118 TMX = 0.6338 DEL = 1.0592 RHO = 0.5658 AA0 = 0.8193
BB0 = 1.0102 X = 1.0000 SS0 = 1.5590 ETA = 0.5057 BETA = 1.0705 DBET = 2.0973
BPBPO= 0.4070 AKAKO= 0.6905 BKBKO= 1.0358 COST = 0.6295 MK = 0.3267 MI = 1.5084
MIKG = 1.1356 MIJG = 0.7476 MIGH = 2.9342 MIAX = 2.4451 MIMV = 1.6219 TETEO= 1.3185
SIGMA= 1.0770 JJO = 2.0113 NNDTO= 0.5702 NENEO= 0.5833 ETARO= 0.2861 BBDTO= 0.9506
AUSGABEDATEN ABSOLUT
R = 2.999 A = 3.619 B = 5.556 S = 9.978 P = 313.6 PW = 1.377 BET = 5.995 E = 2.400
G = 2.766 Q = 2.155 TS = 0.519 TOH = 1.000 TTF = 0.561 AKW = 0.919 PR = 0.000 FOH = 2.373
R1 = 1.561 R2 = 4.956 AK = 0.829 QS = 3.750 BTUDA=10.704 BBERN=10.908 BKINK= 6.873 BYAMA= 8.234
GIN = 2.167 TE = 1.226 SOL = 0.090 NE = 0.106E+21 NDT= 0.798E+20

MIRNOV SKALIERUNG - ACCESSIBILITY CHARTS OTR
EINGABEDATEN
GT = 1.2080 THETA= 0.8000 C = 1.1540 BMBMO= 0.9830 EE0 = 0.9380 QQ0 = 1.0140 GG0 = 0.6030
CN = 0.9230 CP = 0.9170 CF = 0.8590 F1 = 0.4760 F2 = 0.2690 F3 = 0.2720 F4 = 0.0900
AUSGABEDATEN RELATIV
EM = 1.4942 TM = 0.7161 TMX = 0.8318 DEL = 0.5896 RHO = 1.1885 AA0 = 0.9514
BB0 = 1.0551 X = 1.0000 SS0 = 1.2481 ETA = 0.8042 BETA = 0.5710 DBET = 0.4960
BPBPO= 0.5818 AKAKO= 1.2492 BKBKO= 1.1717 COST = 1.2424 MK = 1.0397 MI = 1.0981
MIKG = 0.9391 MIJG = 0.6598 MIGH = 3.1368 MIAX = 2.6140 MIMV = 1.1807 TETEO= 1.5100
SIGMA= 0.8656 JJO = 0.8150 NNDTO= 1.0000 NENEO= 0.9230 ETARO= 0.9558 BBDTO= 0.6590
AUSGABEDATEN ABSOLUT
R = 6.299 A = 4.202 B = 5.803 S = 7.988 P = 498.6 PW = 0.766 BET = 3.198 E = 1.501
G = 3.482 Q = 2.107 TS = 0.949 TOH = 2.197 TTF = 1.353 AKW = 1.801 PR = 0.000 FOH = 0.827
R1 = 3.550 R2 = 9.997 AK = 1.499 QS = 2.912 BTUDA= 4.318 BBERN= 5.241 BKINK= 2.695 BYAMA= 3.989
GIN = 0.918 TE = 1.404 SOL = 0.302 NE = 0.168E+21 NDT= 0.140E+21

MIRNOV SKALIERUNG - ACCESSIBILITY CHARTS "S"
EINGABEDATEN
GT = 1.9494 THETA= 1.0000 C = 1.1300 BMBMO= 0.9500 EE0 = 1.3000 QQ0 = 1.0000 GG0 = 0.5500
CN = 0.9230 CP = 0.9000 CF = 0.8970 F1 = 0.3800 F2 = 0.2400 F3 = 0.2500 F4 = 0.0600
AUSGABEDATEN RELATIV
EM = 2.7203 TM = 0.8256 TMX = 0.9568 DEL = 1.0179 RHO = 0.9597 AA0 = 0.9516
BB0 = 0.9947 X = 1.0001 SS0 = 1.5776 ETA = 1.0646 BETA = 0.8648 DBET = 0.8363
BPBPO= 0.5234 AKAKO= 1.0086 BKBKO= 1.3112 COST = 1.1638 MK = 0.9568 MI = 1.7783
MIKG = 1.8899 MIJG = 1.1113 MIGH = 4.3154 MIAX = 3.5962 MIMV = 1.9121 TETEO= 1.8142
SIGMA= 0.8956 JJO = 1.0618 NNDTO= 1.0744 NENEO= 0.9917 ETARO= 1.0217 BBDTO= 0.9772
AUSGABEDATEN ABSOLUT
R = 5.087 A = 4.203 B = 5.471 S = 10.096 P = 660.1 PW = 1.323 BET = 4.843 E = 2.080
G = 3.176 Q = 2.078 TS = 0.954 TOH = 1.810 TTF = 0.986 AKW = 1.336 PR = 0.000 FOH = 1.243
R1 = 2.796 R2 = 8.331 AK = 1.210 QS = 3.228 BTUDA= 7.647 BBERN= 7.872 BKINK= 4.982 BYAMA= 6.126
GIN = 1.525 TE = 1.687 SOL = 0.126 NE = 0.180E+21 NDT= 0.150E+21